TÉCNICO LISBOA

On the Propagation and Attenuation of Sound in a Two-phase Dissipative Medium

Inês Filipa de Castro Machado Sales d'Ávila

Thesis to obtain the Master of Science Degree in

Aerospace Engineering

Supervisor: Prof. Luiz Manuel Braga da Costa Campos

Examination Committee

Chairperson: Prof. José Fernando Alves da Silva
Supervisor: Prof. Luiz Manuel Braga da Costa Campos
Member of the Committee: Prof. Pedro Da Graça Tavares Álvares Serrão

November 2019

To my parents, who made everything possible.

Per aspera ad astra

Acknowledgements

First of all I would like to thank my supervisor, Professor Luiz Braga Campos, for giving me the opportunity of embrace this project and for all the guidance given to me throughout this journey.

My biggest thank you goes without a doubt to my parents. To my mother, for showing me what unconditional love is, for always supporting me, even in the darkest times, remaining confident, calm, hopeful and always proud of me. For allowing me to grow with the example of what a true woman means. I can not thank you enough for all you have given me and taught. To my father, that always pushed me to fly high and be strong, that taught me to never give up of my dreams because with hard work everything is conquered and you are the biggest example of that. If I am here today is because you made all of this possible while always supporting me, a simple thank you is not enough.

To my brother, for being my role model, for pushing me beyond my limits teaching me how to overcome the struggles in life, I'm so proud of you. Thanks to you and Cátia, for my biggest gifts, Carlos and Martim, with a special thanks to Cátia for showing me how to be a "woman of arms".

I cannot go on without expressing my gratefulness to Isabel, thank you for listening and supporting me as if I were one of yours.

To all my friends, thank you so much for making these years so much better with your presence, for always being there when I needed, whether it was to talk, to decompress or just to be present. And specially, thank you, for making me laugh and live great and memorable moments. You know how you all are important to me.

Finally, a special and heartfelt gratitude to my grandma, one of the most important persons in my early development as a human being, thank you for being a developer of character, for teaching me so many things and for all the love you have given to me. And if you were still here I hope you were proud of what I became because I know that not even in your wildest dream you would imagine this.

Resumo

Com a evolução da exploração espacial o avanço tecnológico torna-se necessário. Esta tese aborda a atenuação do som em um meio dissipativo de duas fases tendo por objectivo modelar a redução do ruído e vibrações dos lançadores e satélites, durante a descolagem. Com o estabelecimento da teoria, baseada nas seis equações fundamentais da mecânica de fluidos, são considerados os principais efeitos dos fluxos de massa e calor. A atenuação acústica obtida é devida a três efeitos, térmico, viscoso e de difusão de massa, que se combinam na atenuação global do som. A condutividade, difusão de massa e os coeficientes de acoplamento cruzado são extrapolados e calculados para um escoamento de dupla fase, com base nas relações de Onsager para processos irreversíveis. A influência da viscosidade de volume na atenuação acústica é também analisada como parte da atenuação viscosa; embora a maioria dos trabalhos teóricos desprezem esta componente, na realidade representa a maior quota da atenuação viscosa. Os resultados obtidos demonstram que a maioria do efeito de atenuação é devido à atenuação térmica, relacionada com a condutividade térmica, o menor impacto na atenuação geral é o da atenuação viscosa, que quando comparada com as restantes é desprezável. A componente de difusão de massa tem o efeito de ampliação do som, com grandeza intermédia, pelo que reduz a atenuação.

Palavras-chave: propagação do som, atenuação acústica, ondas dissipativas, fluxo bifásico.

Abstract

With the advances of space exploration further steps in technological progress become necessary. This thesis addresses the attenuation of sound in a two-phase dissipative medium that is used to reduce the vibrations of the launch vehicles and satellites, during lift-off. In this theory, based on the six fundamental equations of fluid mechanics, the main effects of mass and heat fluxes are included. The acoustic damping has three components; thermal, viscous and mass diffusion, that combine in the global attenuation of sound. The thermal conductivity, mass diffusion and cross-coupling coefficients are extrapolated and calculated for a two-phase flow, based on the Onsager relations for irreversible processes. The influence of bulk viscosity in acoustic attenuation is also analysed as part of the viscous damping, whereas most theoretical works ignore this component, it is shown that actually it represents the biggest share in the viscous attenuation. The results obtained will demonstrate that the majority of the attenuation effect is induced by the thermal damping, related to the thermal conductivity, the smallest impact in the overall attenuation is due to the viscous damping, that when compared to the remaining terms is negligible. The mass diffusion is intermediate in magnitude, and causes a sound amplification, that reduces the dominant effect of thermal attenuation.

Keywords: propagation of sound, acoustic attenuation, dissipative waves, two-phase flow.

Contents

List of Tables

List of Figures

Nomenclature

Greek symbols

α	Thermal cross-coupling coefficient; sound absorption coefficient.
β	Mass diffusion cross-coupling coefficient.
$\Box^2$	Acoustic wave operator.
χ	Thermal conductivity.
δ	Damping of the decaying mode.
η	Shear viscosity.
γ	Ratio of the specific heats.
Γ_{nl}	Kinetic coefficients.
κ	Water thermal conductivity.
μ	Chemical potential.
ν	Kinematic viscosity.
ω	Frequency.
$\overline{\epsilon}$	Damping of the acoustic modes.
$\overline{\omega}$	Doppler shifted frequency.
ψ	Barodiffusion coefficient.
ρ	Mass density.
θ	Non-adiabatic coefficient.
υ	Specific volume.
ε	Total damping of the acoustic modes.
ε_1	Thermal acoustic dissipation coefficient.
ε_2	Viscous acoustic dissipation coefficient.

ε_3 Mass diffusion acoustic dissipation coefficient.

φ Barodiffusion coefficient.

ς Bulk viscosity.

ϑ Total acoustic damping divided by Doppler shifted frequency squared.

ϑ_1 Thermal damping divided by Doppler shifted frequency squared.

ϑ_2 Viscous damping divided by Doppler shifted frequency squared.

ϑ_3 Mass diffusion damping divided by Doppler shifted frequency squared.

ξ Concentration.

Roman symbols

A Exponential amplitude; arbitrary constant.

$a_\pm$ Phase velocity.

B Arbitrary constant.

C Arbitrary constant.

c Adiabatic sound speed.

c_1 Isothermal sound speed.

C_p Specific heat at constant pressure.

C_V Specific heat at constant volume.

G Free enthalpy.

C Arbitrary constant.

D Mass diffusion coefficient.

E Energy density; arbitrary constant.

e Fractional error.

e_{RMS} Root mean square error.

$\vec{F}$ Convective energy flux.

H Enthalpy.

i Imaginary number.

$\vec{j}$ Diffusion mass flux.

$\vec{k}$ Normal wavevector.

k Wave-number

m Molecular mass.

$\vec{n}$ Normal unit vector.

N Moles number.

p Pressure.

$\vec{Q}$ Diffusive energy flux.

$\vec{q}$ Heat flux.

R Gas constant.

$\dot{S}$ Entropy's rate of change.

S Sutherland's coefficient.

s Entropy.

T Temperature; mean temperature.

t Time.

U Internal energy.

v velocity.

$\vec{w}_{\pm}$ Group velocity.

$\dot{x}_n$ Fluxes.

$\vec{x}$ Position vector.

x Mass quality.

X_l Entropy production gradient.

X_n Entropy production gradient.

$\vec{y}$ Position vector.

Subscripts

0 Uniform state; reference state under standard conditions.

$*$ Diffusive mode related.

$\pm$ Acoustic modes related.

g Gas related.

H_2O Water related.

j Mass related.

jq Mass and heat coupling related.

l Liquid related.

m Medium related.

q Heat related.

qj Heat and mass coupling related.

1 First constituent of the mixture; heat related.

12 Heat and mass coupling related.

2 Second constituent of the mixture; mass related.

exterior Exterior related.

system System related.

Superscripts

$*$ Reduced parameter.

$\dot{}$ Flux.

$'$ Non-uniform perturbation.

Glossary

MATLAB MATrix LABoratory is a programming platform used for numerical calculus.

NASA National Aeronautics and Space Administration.

NaN Not a Number.

SLS Space Launch System.

l.h.s Left-hand side.

r.h.s Right-hand side.

Chapter 1

Introduction

In this first chapter the motivation for the thesis is explained and an overview of the subject is given. The objectives expected to be fulfilled are stated as well as an outline of the work to be presented in the next chapters.

1.1 Motivation

One of the most intense man made sources of noise, short of an explosion, is the launch phase of a large rocket. A large rocket motor or cluster with a lift-off thrust of over one meganewton can produce noise levels of 150-170 dB affecting the first stage rocket structures. Also of concern are the noise levels of 130-140 dB in the payload shroud at the nose of the rocket that houses the satellite(s). Thus satellite payloads have to be certified against acoustic fatigue at in-flight noise levels, unless the lift-off noise levels are higher, and drive the requirements. One tried and tested means of reducing lift-off noise levels is to use a water spray: the vaporization of water reduces the high exhaust gas temperature and also absorbs sound. The design of water spray systems for use at rocket launch pads is a costly empirical process of trial and error due to the lack of a suitable theoretical predictive framework, hence this work is expected to be an attempt to develop a theory of sound propagation and attenuation in a two-phase medium including thermal and mass diffusion.

1.2 Topic Overview

Nowadays space exploration aims on missions like returning to the moon, send humans to Mars and increasingly more and more long distance space travel, requiring bigger and more powerful rockets than ever. However, with this necessity and achievements also comes complications, as usual. This new space era revolves around more affordable launches, implying cheaper vehicle production, reusable launchers and simpler systems. While many of the targets are being achieved, as it is being the case of SpaceX, Arianespace and other rocket companies, some problems still remain unsolved or at least without a full functional solution. One of the remaining obstacles on accomplishing the current targets

is the noise produced during lift-off. Actually the first time that this was considered was for the Saturn V rocket, one of the biggest and most powerful launchers ever made.

During lift-off the launcher faces the most severe dynamic environment in its flight cycle due to the high acoustic loads generated. The primary source of the generated noise and vibrations comes from the high jet exhaust velocity required to boost the launch vehicle, where shock waves are formed, the intensity of these shock waves depends, not only, but also on the size of the rocket, which represents a challenge for the vehicles proposed for future missions to Mars for example [1]. This represents a problem because the extremely high acoustic loads create structural vibration affecting the operation of the rocket launch vehicle, its components, payload and supporting structures leading to system failures and the necessity of a more robust equipment to be included in the missions [1]. Hence, these problems negatively affect the accomplishment of the targets already stated, making it crucial to come up with a solution. One of the easiest solutions that help to mitigate part of the problem is to perforate the launch pad. The majority of the launch pads are composed by flat concrete surfaces that are highly reflective of sound waves reaching the launcher. More typical techniques include flame deflection, a proper choice of nozzle configuration and water injection systems, also know as acoustic suppression systems, these are the systems studied throughout this work.

It all started with Saturn V, the first ever water-based acoustic suppression system that can be seen during a test performance in fig. 1.1.

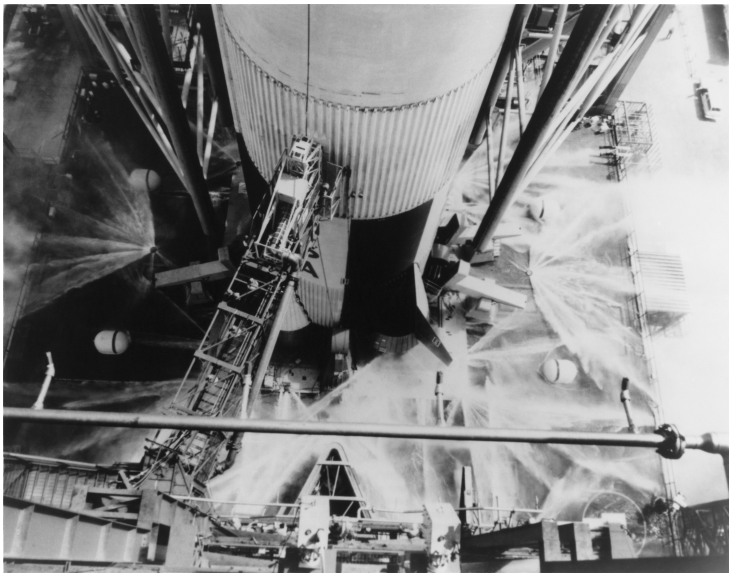

Figure 1.1: Saturn V water suppression system captured during a test. [2]

Since then the systems used have evolved and NASA has been at the leading edge of the advances having developed two more sophisticated systems since Saturn V, one used during the Space Shuttle era and the other designed very recently, with its first test in the beginning of 2018 that is being developed for their upcoming rocket, the SLS - Space Launch System. The acoustic suppression system built for the Space Shuttle (fig. 1.2) was able to deliver approximately 57000 kg/s of water at the peak flow rate [3]. Their new system during testing was able to flow 1.7 million litters of water (fig. 1.3) and it is expected to reach a peak flow rate of approximately 70000 kg/s at full capacity [4].

Figure 1.2: Space Shuttle water acoustic suppression system. [3]

Figure 1.3: SLS water acoustic suppression system. [3]

During this work, some of the calculations were made based on these systems, more specifically in the mass flow rate parameter, but since NASA's new system is not yet fully operational and so there is not a real awareness on the exact value it will be able to achieve, the calculations hereafter are based on the Space Shuttle system, with a mass flow rate of 57000 kg/s being implemented when necessary.

1.3 Objectives

The main goal of this thesis is to test the new theory presented here on the attenuation of sound in a two-phase dissipative medium, creating in this way a theoretical approach on the subject. The way of testing the theory, and check its applicability, is to calculate the acoustic damping. To do so, intermediate data is required, including the calculation of thermal conductivity, mass diffusion and cross-coupling coefficients for a two-phase medium. On the other hand, to perform these intermediate calculations it is necessary to do research on a theoretical implementation model of the chemical potential as a function of temperature and concentration; kinetic coefficients governed by the Onsager principle; shear and bulk viscosity, all of them for a two-phase flow. Basically, in order to achieve the main goal it is first necessary to achieve the intermediate objectives of obtaining the required data. The objectives of this work can be divided into three steps, where each one needs to be fulfilled in sequence, from the base to the top as illustrated in fig. 1.4.

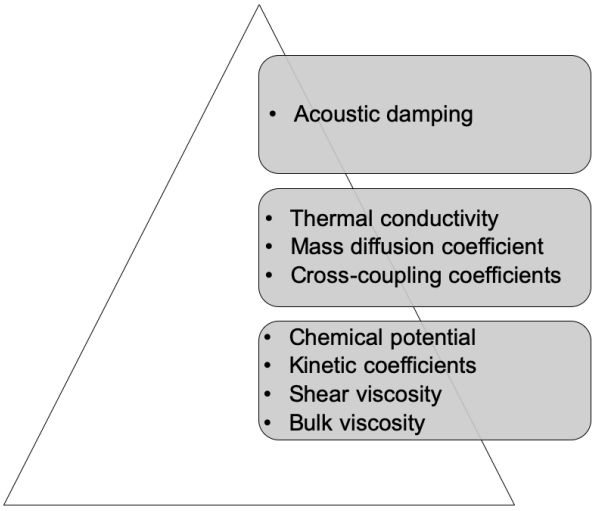

Figure 1.4: Thesis objectives.

In conclusion, the first objective to be achieved is the calculation of the chemical potential, kinetic coefficients, shear and bulk viscosity for a two-phase flow. The second one, is the calculation of the thermal conductivity, mass diffusion and cross-coupling coefficients. The third objective, considered the main goal, is the calculation of the total acoustic damping whose results will act as a test in regard to the accuracy of the proposed theory.

1.4 Thesis Outline

Chapter 2 Establishment of the starting point as the six fundamental equations of fluid mechanics, namely continuity, mass diffusion, heat and momentum, plus the equations of state for a perfect gas and entropy for an ideal gas. The essential effects of mass and heat fluxes are considered, comparatively less important are omitted, including viscosity, vaporization and chemical reactions. The six fundamental equations are linearised (section 2.1) around a constant state of uniform motion, and eliminated leading to a doubly diffusive acoustic wave equation of order 4 in space and time. The corresponding quartic dispersion relation (section 2.2) drops to a cubic neglecting the products of diffusivities, that are assumed to be small. This specifies two damping coefficients (section 2.3), one for acoustic-waves propagating in opposite directions and the other for a third mode, that also decays in time and is a non-propagating diffusion mode (section 2.4). The thermal conductivity, mass diffusion and cross-coupling coefficients play an essential role, the cross-coupling coefficients are related by the Onsager reciprocity principle (section 2.6) and must satisfy the second principle of thermodynamics by ensuring entropy growth (section 2.5).

Chapter 3 Dedicated to both theoretical (section 3.1) and computational (section 3.2) implementations of the previously formulated theory. Presentation of the research on theoretical and empirical models for chemical potential (section 3.1.1), kinetic coefficients (section 3.1.2), thermal conductivity (section 3.1.3), shear viscosity (section 3.1.4) and bulk viscosity (section 3.1.5). Comparison of the var-

ious models, calculation of the error percentage by comparison with theoretical and experimental data, when available, as a measure of performance and decision on which the most adjusted one. Description of the program developed in MATLAB with the purpose of being a mathematical tool for the necessary theoretical calculations (section 3.2).

Chapter 4 Presentation and discussion of the results obtained after implementing the theory described in chapter 2 with the theoretical models selected in chapter 3.

Chapter 5 Final remarks about the work performed compared with the defined objectives and notes on what to change in order to attain improved results in subsequent studies on the subject.

Chapter 2

Theoretical Formulation

In this chapter it is explained step-by-step the theoretical formulation of a new theory, concerning the propagation and attenuation of sound in a two-phase dissipative medium.

2.1 Fundamental Equations for a Two-phase Dissipative Flow

The equation of continuity states the conservation of mass:

$$\frac{\partial \rho}{\partial t} + \nabla \cdot (\rho \vec{v}) = 0, \tag{2.1}$$

where ρ is the mass density and $\vec{v}$ the velocity. The mass diffusion equation:

$$\frac{\partial \xi}{\partial t} + \nabla \cdot (\xi \vec{v}) = -\nabla \cdot \vec{j}, \tag{2.2}$$

is similar for the concentration ξ on the l.h.s of eq. (2.2) balanced on the r.h.s by minus the divergence of the diffusive mass flux $\vec{j}$. The heat equation:

$$\rho T \left(\frac{\partial s}{\partial t} + \vec{v} \cdot \nabla s \right) = -\nabla \cdot \vec{q}, \tag{2.3}$$

involves the temperature T and material derivative of the entropy s on the l.h.s balanced against minus the divergence of the heat flux $\vec{q}$ that includes mass diffusion effects. The effect of viscosity was omitted in the heat equation (2.3), and hence the inviscid momentum equation is used.

$$\frac{\partial \vec{v}}{\partial t} + (\vec{v} \cdot \nabla)\, \vec{v} = -\rho^{-1} \nabla p, \tag{2.4}$$

where p is the pressure. The medium is assumed to be a perfect gas with equation of state:

$$p = \rho R T, \tag{2.5}$$

where R is the gas constant. The entropy for an ideal gas, that is a perfect gas with constant specific heats at constant volume C_V and pressure C_p is given by:

$$s = s_0 + C_V \log p - C_p \log \rho. \tag{2.6}$$

The set of five scalar (2.1, 2.2, 2.3, 2.5, 2.6) and one vector (2.4) equations involves five scalar and one vector variable namely the density ρ, pressure p, temperature T, entropy s, concentration ξ and velocity $\vec{v}$.

To close the system (2.1)–(2.6) the heat $\vec{q}$ and mass $\vec{j}$ fluxes are specified in terms of the gradients of temperature ∇T and concentration $\nabla \xi$ by:

$$\vec{q} = -\chi \nabla T - \beta \nabla \xi, \quad \vec{j} = -D \nabla \xi - \alpha \nabla T, \tag{2.7a,b}$$

where:

(i) the first term on the r.h.s of eq. (2.7a) is the Fourier's law involving the thermal conductivity χ;

(ii) the first term on the r.h.s of eq. (2.7b) is the Fick's law involving the mass diffusion coefficient D;

(iii) the second terms on the r.h.s are the diffusive cross-coupling coefficients α, β that are related by the Onsager reciprocity principle [5].

Substitution of eqs.(2.7a) and (2.7b) respectively in eqs.(2.3) and (2.2) lead to the heat (2.8) and mass (2.9) diffusion equations.

$$\rho T \left(\frac{\partial s}{\partial t} + \vec{v} \cdot \nabla s \right) = \chi \nabla^2 T + \beta \nabla^2 \xi, \tag{2.8}$$

$$\frac{\partial \xi}{\partial t} + \nabla \cdot (\xi \vec{v}) = D \nabla^2 \xi + \alpha \nabla^2 T. \tag{2.9}$$

For the purpose of elimination among the fundamental equations (2.1, 2.4, 2.5, 2.8, 2.9) it is convenient to put the entropy equation (2.6) in a differential form (2.10b) using the material derivative (2.10a).

$$\frac{\mathsf{D}}{\mathsf{D}t} \equiv \frac{\partial}{\partial t} + \vec{v} \cdot \nabla : \quad \frac{\mathsf{D}s}{\mathsf{D}t} = \frac{C_V}{p} \frac{\mathsf{D}p}{\mathsf{D}t} - \frac{C_p}{\rho} \frac{\mathsf{D}\rho}{\mathsf{D}t}. \tag{2.10a,b}$$

Solving eq. (2.10b) for the pressure leads to eq. (2.11a):

$$\frac{\mathsf{D}p}{\mathsf{D}t} = \frac{C_p}{C_V} \frac{p}{\rho} \frac{\mathsf{D}\rho}{\mathsf{D}t} + \frac{p}{C_V} \frac{\mathsf{D}s}{\mathsf{D}t} = c^2 \frac{\mathsf{D}\rho}{\mathsf{D}t} + \theta \frac{\mathsf{D}s}{\mathsf{D}t} \tag{2.11a,b}$$

where eq. (2.11b) appears:

(i) the adiabatic sound speed (2.12a) involving the adiabatic exponent:

$$c^2 \equiv \left(\frac{\partial p}{\partial \rho} \right)_s = \frac{C_p}{C_V} \frac{p}{\rho} = \gamma R T, \quad \theta = \left(\frac{\partial p}{\partial s} \right)_\rho = \frac{p}{C_V} = p \, \frac{\gamma - 1}{R}, \tag{2.12a,b}$$

(ii) the non-adiabatic coefficient (2.12b) that is needed because heat and mass diffusion are associated with entropy production.

The total state of the fluid is assumed to consist of an uniform mean state with subscript "0" and an unsteady non-uniform perturbation with prime:

$$\{p, \rho, T, s, \xi, \vec{v}\}(\vec{x}, t) = \{p_0, \rho_0, T_0, s_0, \xi_0, \vec{v}_0\} + \{p', \rho', T', s', \xi', \vec{v}'\}(\vec{x}, t). \quad (2.13a\text{-}f)$$

The linearisation of the material derivative (2.10a) for the mean flow leads to (2.14a), and the linearisation of the fundamental equations (2.1, 2.4, 2.5, 2.11b, 2.8, 2.9) leads respectively to eqs.(2.14b)$-$(2.19):

$$\frac{\mathsf{d}}{\mathsf{d}t} \equiv \frac{\partial}{\partial t} + \vec{v}_0 \cdot \nabla : \quad \frac{\mathsf{d}\rho'}{\mathsf{d}t} + \rho_0 (\nabla \cdot \vec{v}') = 0, \quad (2.14a,b)$$

$$\rho_0 \frac{\mathsf{d}\vec{v}'}{\mathsf{d}t} + \nabla p' = 0, \quad (2.15)$$

$$p' = R(\rho_0 T' + T_0 \rho'), \quad (2.16)$$

$$\frac{\mathsf{d}p'}{\mathsf{d}t} = c_0^2 \frac{\mathsf{d}\rho'}{\mathsf{d}t} + \theta_0 \frac{\mathsf{d}s'}{\mathsf{d}t}, \quad (2.17)$$

$$\rho_0 T_0 \frac{\mathsf{d}s'}{\mathsf{d}t} = \chi \nabla^2 T' + \beta \nabla^2 \xi', \quad (2.18)$$

$$\frac{\mathsf{d}\xi'}{\mathsf{d}t} + \xi_0 (\nabla \cdot \vec{v}') = D \nabla^2 \xi' + \alpha \nabla^2 T'. \quad (2.19)$$

The elimination among these 6 perturbation equations leads to the doubly diffusive acoustic wave equation (section 2.2).

2.2 Doubly Diffusive Acoustic Wave Equation

Applying the linearised material derivative (2.14a) to eqs.(2.14b) and (2.19) leads respectively to eqs.(2.20a,b) and (2.21) after elimination of the velocity perturbation from the momentum equation (2.15):

$$\frac{\mathsf{d}^2\rho'}{\mathsf{d}t^2} = -\rho_0 \nabla \cdot \left(\frac{\mathsf{d}\vec{v}'}{\mathsf{d}t} \right) = \nabla^2 p', \quad (2.20a,b)$$

$$\frac{\mathsf{d}^2\xi'}{\mathsf{d}t^2} - \frac{\xi_0}{\rho_0} \nabla^2 p' = D \nabla^2 \left(\frac{\mathsf{d}\xi'}{\mathsf{d}t} \right) + \alpha \nabla^2 \left(\frac{\mathsf{d}T'}{\mathsf{d}t} \right). \quad (2.21)$$

The system of five scalar equations (2.20b, 2.21, 2.16, 2.17, 2.18) now has five scalar variables (p', ρ', T', s', ξ'). The entropy perturbation s' appears only in eq. (2.18), and is eliminated using eq. (2.17) or equivalently the linearisation of eq. (2.10b):

$$\chi \nabla^2 T' + \beta \nabla^2 \xi' = \rho_0 T_0 \left(\frac{C_V}{p_0} \frac{\mathsf{d}p'}{\mathsf{d}t} - \frac{C_p}{\rho_0} \frac{\mathsf{d}\rho'}{\mathsf{d}t} \right) = \frac{C_V}{R} \left(\frac{\mathsf{d}p'}{\mathsf{d}t} - \frac{C_p}{C_V} R T_0 \frac{\mathsf{d}\rho'}{\mathsf{d}t} \right). \quad (2.22a,b)$$

Applying $\frac{\mathrm{d}}{\mathrm{d}t}$ to eq. (2.22b) leads to:

$$(\gamma-1)\left[\chi\,\nabla^2\left(\frac{\mathrm{d}T'}{\mathrm{d}t}\right)+\beta\,\nabla^2\left(\frac{\mathrm{d}\xi'}{\mathrm{d}t}\right)\right]=\frac{\mathrm{d}^2p'}{\mathrm{d}t^2}-c_0^2\,\frac{\mathrm{d}^2\rho'}{\mathrm{d}t^2}$$
$$=\frac{\mathrm{d}^2p'}{\mathrm{d}t^2}-c_0^2\,\nabla^2p'. \tag{2.23a,b}$$

The r.h.s of eq. (2.23b) is the classical wave equation involving the adiabatic sound speed (2.12a), that is valid when the l.h.s of eq. (2.23b) vanishes, that is, for constant entropy.

The system of four scalar equations (2.16, 2.20b, 2.21, 2.23b) involves four variables $(p',\,\rho',\,T',\,\xi')$. The mass density perturbation ρ' appears only in eq. (2.16) and is eliminated applying $\frac{\mathrm{d}^2}{\mathrm{d}t^2}$ leading to:

$$R\rho_0\frac{\mathrm{d}^2T'}{\mathrm{d}t^2}=\frac{\mathrm{d}^2p'}{\mathrm{d}t^2}-RT_0\frac{\mathrm{d}^2\rho'}{\mathrm{d}t^2}=\frac{\mathrm{d}^2p'}{\mathrm{d}t^2}-RT_0\,\nabla^2p'$$
$$=\frac{\mathrm{d}^2p'}{\mathrm{d}t^2}-c_1^2\,\nabla^2p'; \tag{2.24a-c}$$

the r.h.s of eq. (2.24c) is the classical wave equation involving the isothermal sound speed (2.25) because it holds when the l.h.s of eq. (2.24c) vanishes, that is in isothermal conditions.

$$c_1^2=RT_0=\frac{c_0^2}{\gamma}. \tag{2.25}$$

The system of three scalar equations (2.24c, 2.23b, 2.21) involves only three variables $(p',\,\xi',\,T')$. The temperature perturbation T' appears in eq. (2.21) and after application of $\frac{\mathrm{d}}{\mathrm{d}t}$ is eliminated using eq. (2.24c).

$$\frac{\mathrm{d}^2}{\mathrm{d}t^2}\left(\frac{\mathrm{d}\xi'}{\mathrm{d}t}-D\,\nabla^2\xi'\right)=\frac{\xi_0}{\rho_0}\,\nabla^2\left(\frac{\mathrm{d}p'}{\mathrm{d}t}\right)+\alpha\,\nabla^2\left(\frac{\mathrm{d}^2T'}{\mathrm{d}t^2}\right)$$
$$=\nabla^2\left(\frac{\xi_0}{\rho_0}\frac{\mathrm{d}p'}{\mathrm{d}t}+\frac{\alpha}{\rho_0R}\frac{\mathrm{d}^2p'}{\mathrm{d}t^2}-\frac{\alpha T_0}{\rho_0}\,\nabla^2p'\right), \tag{2.26a,b}$$

implying (2.27).

$$\nabla^2\left(\frac{\mathrm{d}^2T'}{\mathrm{d}t^2}\right)=\frac{1}{\rho_0R}\,\nabla^2\left(\frac{\mathrm{d}^2p'}{\mathrm{d}t^2}-\frac{T_0}{\rho_0}\,\nabla^2p'\right). \tag{2.27}$$

The term in curved brackets on the l.h.s of eq. (2.26a) is the mass diffusion equation that holds at constant pressure, when the r.h.s of eq. (2.26a,b) vanishes.

The two equations (2.23b) and (2.26b) have two variables $(p',\,\xi')$. Solving eq. (2.23b) for ξ' and applying $\frac{\mathrm{d}}{\mathrm{d}t}$ and using eq. (2.27) leads to:

$$\beta\,\nabla^2\left(\frac{\mathrm{d}^2\xi'}{\mathrm{d}t^2}\right)-\frac{1}{\gamma-1}\left[\frac{\mathrm{d}^3p'}{\mathrm{d}t^3}-c_0^2\,\nabla^2\left(\frac{\mathrm{d}p'}{\mathrm{d}t}\right)\right]=-\chi\,\nabla^2\left(\frac{\mathrm{d}^2T'}{\mathrm{d}t^2}\right)$$
$$=-\frac{\chi}{\rho_0R}\,\nabla^2\left(\frac{\mathrm{d}^2p'}{\mathrm{d}t^2}\right)+\chi\frac{T_0}{\rho_0}\,\nabla^4p'. \tag{2.28a,b}$$

The two equations (2.28b) and (2.26b) involve only two variables $(\xi',\, p')$. Applying $\beta\,\nabla^2$ to eq. (2.26b) and substituting eq. (2.28b) leads to:

$$\beta\,\nabla^4\left(\frac{\xi_0}{\rho_0}\frac{\mathrm{d}p'}{\mathrm{d}t}+\frac{\alpha}{\rho_0 R}\frac{\mathrm{d}^2p'}{\mathrm{d}t^2}-\alpha\frac{T_0}{\rho_0}\,\nabla^2p'\right)=\beta\,\frac{\mathrm{d}}{\mathrm{d}t}\left[\nabla^2\left(\frac{\mathrm{d}^2\xi'}{\mathrm{d}t^2}\right)\right]-\beta D\,\nabla^4\left(\frac{\mathrm{d}^2\xi'}{\mathrm{d}t^2}\right)$$
$$=\frac{1}{\gamma-1}\left[\frac{\mathrm{d}^4p'}{\mathrm{d}t^4}-c_0^2\,\nabla^2\left(\frac{\mathrm{d}^2p'}{\mathrm{d}t^2}\right)\right]-\frac{\chi}{\rho_0 R}\,\nabla^2\left(\frac{\mathrm{d}^3p'}{\mathrm{d}t^3}\right)+\chi\frac{T_0}{\rho_0}\,\nabla^4\left(\frac{\mathrm{d}p'}{\mathrm{d}t}\right)$$
$$-\frac{D}{\gamma-1}\left[\nabla^2\left(\frac{\mathrm{d}^3p'}{\mathrm{d}t^3}\right)-c_0^2\,\nabla^4\left(\frac{\mathrm{d}p'}{\mathrm{d}t}\right)\right]+\frac{\chi D}{\rho_0 R}\,\nabla^4\left(\frac{\mathrm{d}^2p'}{\mathrm{d}t^2}\right)-\chi D\frac{T_0}{\rho_0}\,\nabla^6p'. \tag{2.29a,b}$$

This can be re-arranged as the acoustic wave operator with double, thermal and mass, diffusion:

$$\Box^2=\frac{1}{\gamma-1}\frac{\mathrm{d}^2}{\mathrm{d}t^2}\left(\frac{\mathrm{d}^2}{\mathrm{d}t^2}-c_0^2\,\nabla^2\right)-\left(\frac{D}{\gamma-1}+\frac{\chi}{\rho_0 R}\right)\nabla^2\frac{\mathrm{d}^3}{\mathrm{d}t^3}$$
$$+\left(\frac{c_0^2 D}{\gamma-1}+\chi\frac{T_0}{\rho_0}-\beta\frac{\xi_0}{\rho_0}\right)\nabla^4\frac{\mathrm{d}}{\mathrm{d}t}+\frac{\chi D-\alpha\beta}{\rho_0 R}\,\nabla^4\left(\frac{\mathrm{d}^2}{\mathrm{d}t^2}-\frac{c_0^2}{\gamma}\,\nabla^2\right), \tag{2.30}$$

that is of the fourth-order in time and sixth-order in space; it applies to all scalar wave variables, namely the pressure, density, temperature, entropy and concentration perturbations (2.31a-e):

$$\Box^2\left\{p',\rho',T',s',\xi',\nabla\cdot\vec{v}\,'\right\}(\vec{x},t)=0, \tag{2.31a-f}$$

because the linearised system has constant coefficients. The divergence of the velocity perturbation satisfies the same wave equation (2.31f) and the curl is conserved as follows from eq. (2.15). In the absence of diffusivities (2.30) it reduces to the adiabatic wave equation in the first brackets of (2.30); the last brackets in (2.30) is the isothermal wave equation multiplied by the determinant of the diffusion coefficients in eq. (2.7a,b). The wave operator (2.30) leads to the dispersion relation and wave modes (section 2.3).

2.3 Dispersion Relation and Decay of the Three Modes

The solution of the wave equation (2.30) is sought in the form of plane waves (2.32a) with frequency ω and wave vector $\vec{k}$ leading to:

$$p'\,(\vec{x},t)=A\exp\left[i\left(\vec{k}\cdot\vec{x}-\omega t\right)\right]:\left\{\frac{\partial}{\partial t},\nabla,\nabla^2\right\}\rightarrow\left\{-i\omega,i\vec{k},-k^2\right\}. \tag{2.32a-d}$$

The spatial dependence in the wave equation (2.30) appears only through Laplacians, so only the modulus of the wave vector (2.32d) appears; this dependence on the wave-number implies isotropic waves, since there is no preferred direction. The isotropy is in a frame convected with the mean flow velocity $\vec{v}_0$, since the linearised material derivative (2.14a)≡(2.33a) leads to the Doppler shifted frequency (2.33b):

$$\frac{\mathrm{d}}{\mathrm{d}t}=\frac{\partial}{\partial t}+\vec{v}_0\cdot\nabla\rightarrow-i\overline{\omega},\quad\overline{\omega}=\omega-\vec{k}\cdot\vec{v}_0. \tag{2.33a,b}$$

Substituting the plane wave solution (2.32a) in the doubly-diffusive acoustic wave equation (2.30, 2.31a-f) and using eqs.(2.32b,d) and (2.33b) leads to the dispersion relation that is of fourth-order in frequency and sixth-order in wave-number:

$$0 = \frac{\overline{\omega}^4}{\gamma-1} + i\overline{\omega}^3 k^2 \left(\frac{D}{\gamma-1} + \frac{\chi}{\rho_0 R}\right) - \overline{\omega}^2 k^2 \left(\frac{c_0^2}{\gamma-1} + k^2 \frac{\chi D - \alpha\beta}{\rho_0 R}\right)$$
$$-i\overline{\omega} k^4 \left(\frac{c_0^2 D}{\gamma-1} + \chi\frac{T_0}{\rho_0} - \beta\frac{\xi_0}{\rho_0}\right) + (\chi D - \alpha\beta)\frac{T_0}{\rho_0} k^6. \tag{2.34}$$

The four modes may be expected to be two damped acoustic waves propagating in opposite directions plus two decaying fields , one thermal and one diffusive.

The diffusivities are usually small, and neglecting their determinant (2.35a) simplifies the dispersion relation (2.34) from a quartic to a cubic (2.35b).

$$\chi D - \alpha\beta \ll \rho_0 R c_0^2 : \quad \overline{\omega}^3 + i\overline{\omega}^2 k^2 \left[D + (\gamma-1)\frac{\chi}{\rho_0 R}\right]$$
$$-\overline{\omega} k^2 c_0^2 - i k^4 \left[c_0^2 D + (\gamma-1)\frac{T_0\chi - \xi_0\beta}{\rho_0}\right] = 0. \tag{2.35a,b}$$

In the absence of dissipation (2.36a) the dispersion relation (2.35b) reduces to eq. (2.36b) for purely acoustic waves (2.36c).

$$\chi = D = \beta = 0 : \quad \overline{\omega}^2 - c_0^2 k^2 = 0, \quad \overline{\omega} = \pm c_0 k. \tag{2.36a-c}$$

In the presence of weak dissipation (2.35a) it may be expected that the cubic dispersion relation (2.35b) leads to three modes:

(i/ii) two sound waves propagating in opposite directions (2.36c) with weak dampings $\varepsilon_\pm$ in eq. (2.37a);

(iii) a purely decaying mode with damping δ in eq. (2.37b).

$$\omega - \vec{k}\cdot\vec{v}_0 = \overline{\omega} = \begin{cases} \pm c_0 k - i\varepsilon_\pm = \overline{\omega}_\pm & (2.37a) \\ -i\delta = \overline{\omega}_* & (2.37b) \end{cases}$$

The dispersion relation with roots (2.37a,b) must be of the form:

$$0 = (\overline{\omega} - c_0 k + i\varepsilon_+)(\overline{\omega} + c_0 k + i\varepsilon_-)(\overline{\omega} + i\delta). \tag{2.38}$$

Since the product of diffusivities was neglected (2.35a) in the cubic dispersion relation (2.35b) the product of dampings is also neglected (2.39a) in eq. (2.38) leading to eq. (2.39b):

$$\varepsilon_+\varepsilon_-, \varepsilon_+\delta, \varepsilon_-\delta \ll \overline{\omega}^2 :$$
$$\overline{\omega}^3 + i\overline{\omega}^2(\varepsilon_+ + \varepsilon_- + \delta) - \overline{\omega} c_0 k [c_0 k + i(\varepsilon_- - \varepsilon_+)] - i\delta c_0^2 k^2 = 0. \tag{2.39a,b}$$

Thus eqs.(2.39b) and (2.35b) must coincide. The coincidence of eqs.(2.39b)≡(2.35b) proves that:

(i) the ”guess” about the modes (2.37a,b) was correct;

(ii) the coefficients of $\overline{\omega}$ show that the damping is the same for sound waves propagating in opposite directions (2.40a) as should be expected;

(iii) the independent term specifies the decay of the non-acoustic mode (2.40b),

$$\varepsilon_+ = \varepsilon_- \equiv \overline{\varepsilon}, \quad \delta = k^2 D + \frac{\gamma-1}{\rho_0}\frac{k^2}{c_0^2}\left(T_0\chi - \xi_0\beta\right); \tag{2.40a,b}$$

(iv) the coefficient of $\overline{\omega}^2$ determines the total damping (2.41a) leading to the damping (2.41b) for the acoustic modes:

$$2\overline{\varepsilon} + \delta = k^2\left(D + \frac{\gamma-1}{\rho_0}\frac{\chi}{R}\right) \quad \overline{\varepsilon} = \frac{k^2\left(\gamma-1\right)^2\chi}{2\rho_0 R\gamma} + \frac{\gamma-1}{2\rho_0}\frac{k^2}{c_0^2}\xi_0\beta. \tag{2.41a,b}$$

The thermal part of the thermoviscous acoustic dissipation coefficient [6] per unit time is eq. (2.42a):

$$\varepsilon_1 \equiv \frac{\overline{\omega}^2}{2\rho_0 c_0^2}\chi\left(\frac{1}{C_V} - \frac{1}{C_p}\right) = \frac{k^2\chi}{2\rho_0 C_p}\left(\frac{C_p}{C_V} - 1\right) = \frac{k^2\chi}{2\rho_0}\frac{\gamma-1}{C_p} = \frac{k^2\chi\left(\gamma-1\right)^2}{2\rho_0 R\gamma} \tag{2.42a-d}$$

which is in agreement (2.42d) with the first term on the r.h.s of eq. (2.41b). In the passage from eq. (2.42a) to eq. (2.42b) it was used eq. (2.36c) that is valid to the next order, that was neglected, in the diffusion (2.35a) and damping (2.39a) coefficients. These dampings and frequencies apply (section 2.4) to all wave variables (2.13a-f).

2.4 Amplitude, Phase and Decay of Six Wave Variables

The thermoviscous dissipation coefficient for acoustic waves [6] adds to eq. (2.42a) a term (2.43a) involving the shear η and bulk ζ viscosities:

$$\varepsilon_2 = \frac{\overline{\omega}^2}{2\rho_0 c_0^2}\left(\frac{4}{3}\eta + \zeta\right); \quad \varepsilon_3 = \frac{\gamma-1}{2\rho_0 c_0^2}\frac{\overline{\omega}^2}{c_0^2}\xi_0\beta, \tag{2.43a,b}$$

the mass diffusion coefficient D appears in the damping of the diffusive mode (2.40b) but drops out of the acoustic mode (2.41b) where appears (2.43b) the thermal-mass diffusion cross-coupling coefficient in eq. (2.7a). Thus the total dissipation coefficient for acoustic waves, including thermal (2.42a-d) and mass diffusion (2.43b) considered before, and adding the viscous diffusion (2.43a) omitted before is:

$$\varepsilon = \overline{\varepsilon} + \varepsilon_2 = \varepsilon_1 + \varepsilon_2 + \varepsilon_3 = \frac{\overline{\omega}^2}{2\rho_0 c_0^2}\left[\frac{4}{3}\eta + \zeta + \chi\left(\frac{1}{C_V} - \frac{1}{C_p}\right) + \frac{\xi_0\beta}{c_0^2}\left(\gamma-1\right)\right]. \tag{2.44}$$

The damping (2.44) applies to the acoustic modes propagating in opposite directions (2.37a) of the acoustic pressure perturbation (2.32a), leading to:

$$\begin{aligned} p'_\pm\left(\vec{x},t\right) &= A\exp\left\{i\left[\vec{k}\cdot\vec{x} - \left(\overline{\omega}_\pm + \vec{k}\cdot\vec{v}_0\right)t\right]\right\} \\ &= A\exp\left\{i\vec{k}\cdot\left[\vec{x} - \left(\vec{v}_0 \pm c_0\vec{n}\right)t\right]\right\}\exp\left(-\varepsilon t\right), \end{aligned} \tag{2.45a,b}$$

where eq. (2.46a) is the wave normal and eq. (2.46b) the group velocity corresponding to the phase speed of propagation (2.46c) in opposite directions along the wave normal:

$$\vec{k} = k\vec{n}: \quad \vec{w}_\pm = \vec{v}_0 \pm c_0\vec{n}, \quad a_\pm \equiv \vec{w}_\pm \cdot \vec{n} = \pm c_0 + \vec{v}_0 \cdot \vec{n}. \tag{2.46a-c}$$

The third mode (2.37b) is a purely decaying mode (2.47b,c):

$$\begin{aligned} \vec{y} = \vec{x} - \vec{v}_0 t: \quad p'_* (\vec{x}, t) &= A \exp\left\{ i \left[\vec{k} \cdot \vec{x} - \left(\overline{\omega}_* + \vec{k} \cdot \vec{v}_0 \right) t \right] \right\} \\ &= A \exp\left[i\vec{k} \cdot (\vec{x} - \vec{v}_0 t) \right] \exp(-\delta t) \\ &= A \exp\left(i\vec{k} \cdot \vec{y} \right) \exp(-\delta t), \end{aligned} \tag{2.47a-d}$$

relative (2.47d) to a reference frame (2.47a) convected with the uniform mean flow.

The total acoustic pressure perturbation is a superposition of the acoustic (2.45a,b) and diffusive (2.47a-d) modes:

$$p'(\vec{x}, t) = A\, p'_+ (\vec{x}, t) + B\, p'_- (\vec{x}, t) + C\, p'_* (\vec{x}, t), \tag{2.48}$$

with the arbitrary constants (A, B, C) determined by initial conditions. The five remaining wave variables (2.13b-f) are a similar linear combination of two acoustic and one diffusive mode:

$$\begin{bmatrix} p'(\vec{x}, t) \\ \rho'(\vec{x}, t) \\ T'(\vec{x}, t) \\ s'(\vec{x}, t) \\ \xi'(\vec{x}, t) \\ \vec{v}\,'(\vec{x}, t) \end{bmatrix} = \begin{bmatrix} p'_+ (\vec{x}, t) & p'_- (\vec{x}, t) & p'_* (\vec{x}, t) \\ \rho'_+ (\vec{x}, t) & \rho'_- (\vec{x}, t) & \rho'_* (\vec{x}, t) \\ T'_+ (\vec{x}, t) & T'_- (\vec{x}, t) & T'_* (\vec{x}, t) \\ s'_+ (\vec{x}, t) & s'_- (\vec{x}, t) & s'_* (\vec{x}, t) \\ \xi'_+ (\vec{x}, t) & \xi'_- (\vec{x}, t) & \xi'_* (\vec{x}, t) \\ \vec{v}\,'_+ (\vec{x}, t) & \vec{v}\,'_- (\vec{x}, t) & \vec{v}\,'_* (\vec{x}, t) \end{bmatrix} \begin{bmatrix} A \\ B \\ C \end{bmatrix} \tag{2.49}$$

with the modes related by polarization relations that are obtained next. Substituting eqs.(2.45a,b) and (2.47a-d) in eq. (2.15) specifies respectively the acoustic (2.50a,b) and diffusive (2.51a,b) modes of the velocity perturbation:

$$\vec{v}\,'_\pm (\vec{x}, t) = \frac{\vec{k}}{\rho_0 \overline{\omega}_\pm} p'_\pm (\vec{x}, t) = \pm \frac{\vec{n}}{\rho_0 \left(c_0 \pm i \dfrac{\varepsilon}{k} \right)} p'_\pm (\vec{x}, t), \tag{2.50a,b}$$

$$\vec{v}\,'_* (\vec{x}, t) = \frac{\vec{k}}{\rho_0 \overline{\omega}_*} p'_* (\vec{x}, t) = i \frac{k}{\rho_0 \delta} \vec{n}\, p'_* (\vec{x}, t). \tag{2.51a,b}$$

The modes for the mass density perturbation follow similarly from eq. (2.20b):

$$\rho'_{\pm}(\vec{x},t) = \left(\frac{k}{\overline{\omega}_{\pm}}\right)^2 p'_{\pm}(\vec{x},t) = \left(c_0 \pm i\frac{\varepsilon}{k}\right)^{-2} p'_{\pm}(\vec{x},t)\,, \tag{2.52a,b}$$

$$\rho'_{*}(\vec{x},t) = \left(\frac{k}{\overline{\omega}_{*}}\right)^2 p'_{*}(\vec{x},t) = -\frac{k^2}{\delta^2}\, p'_{*}(\vec{x},t)\,. \tag{2.53a,b}$$

The modes for the temperature perturbation follow from eq. (2.24b):

$$T'_{\pm}(\vec{x},t) = \frac{1}{\rho_0}\left[\frac{1}{R} - \frac{T_0}{\left(c_0 \pm i\frac{\varepsilon}{k}\right)^2}\right] p'_{\pm}(\vec{x},t)\,, \tag{2.54}$$

$$T'_{*}(\vec{x},t) = \left[\frac{1}{\rho_0 R} - \frac{T_0}{\rho_0}\left(\frac{k}{\overline{\omega}_{*}}\right)^2\right] p'_{*}(\vec{x},t) = \left(\frac{1}{\rho_0 R} + \frac{T_0\, k^2}{\rho_0\, \delta^2}\right) p'_{*}(\vec{x},t) \tag{2.55a,b}$$

Besides the polarization relations, relating the velocity, density and temperature to the pressure perturbation, there are two more for the entropy and concentration.

The modes for the entropy perturbation follow from eqs.(2.18) and (2.23b).

$$\rho_0 T_0 \frac{\mathsf{d}^2 s'}{\mathsf{d}t^2} = \frac{1}{\gamma - 1}\left(\frac{\mathsf{d}^2 p'}{\mathsf{d}t^2} - c_0^2\, \nabla^2 p'\right), \tag{2.56}$$

that on substitution of eqs.(2.45a,b) and (2.47a-c) lead respectively to eqs.(2.57) and (2.58).

$$s'_{\pm}(\vec{x},t) = \frac{1}{\rho_0 T_0}\frac{1}{\gamma - 1}\left[1 + \left(1 \pm \frac{i\varepsilon}{c_0 k}\right)^{-2}\right] p'_{\pm}(\vec{x},t)\,, \tag{2.57}$$

$$s'_{*}(\vec{x},t) = \frac{1}{\rho_0 T_0}\frac{1}{\gamma - 1}\left[1 - \left(\frac{c_0 k}{\delta}\right)^2\right] p'_{*}(\vec{x},t)\,. \tag{2.58}$$

The modes for the perturbation of concentration follow from eq. (2.28b).

$$\beta\, \xi'(\vec{x},t) = \left[-\frac{\chi}{\rho_0 R}\left(1 - R T_0\, \frac{k^2}{\overline{\omega}^2}\right) + \frac{i}{\gamma - 1}\left(\frac{\overline{\omega}}{k^2} - \frac{c_0^2}{\overline{\omega}}\right)\right] p'(\vec{x},t)\,, \tag{2.59}$$

leading to:

$$\xi'_{\pm}(\vec{x},t) = \left\{-\frac{\chi}{\rho_0 R\beta}\left[1 - \frac{\frac{c_0^2}{\gamma}}{\left(c_0 \pm i\frac{\varepsilon}{k}\right)^2}\right] - \frac{1}{\gamma - 1}\,\frac{1}{\varepsilon \mp i\, c_0 k}\left[\left(c_0 \pm i\frac{\varepsilon}{k}\right)^2 - c_0^2\right]\right\} p'_{\pm}(\vec{x},t)\,, \tag{2.60}$$

$$\xi'_{*}(\vec{x},t) = \left\{-\frac{\chi}{\rho_0 R\beta}\left(1 + \frac{c_0^2 k^2}{\gamma \delta^2}\right) - \frac{1}{\gamma - 1}\,\frac{1}{\beta\delta}\left(c_0^2 - \frac{\delta^2}{k^2}\right)\right] p'_{*}(\vec{x},t)\,. \tag{2.61}$$

The dampings (2.40b) and (2.44) that appear in the wave fields (2.50b)–(2.55b), (2.57), (2.58), (2.60) and (2.61) are specified by the thermodynamic and kinetic properties of the fluid mixture, that relate to the first and second principles of thermodynamics and hence to the energy and entropy equations (section 2.5).

2.5 Energy Density and Convective and Diffusive Fluxes

The energy density per unit volume in a fluid is the stagnation internal energy (2.62a) that is the sum of the kinetic energy and internal energy (2.62b) specified per unit mass by the first principle of thermodynamics

$$E = \rho\left(\frac{v^2}{2} + U\right), \quad \mathrm{d}U = T\,\mathrm{d}s - p\,\mathrm{d}\upsilon + \mu_1\,\mathrm{d}N_1 + \mu_2\,\mathrm{d}N_2, \tag{2.62a,b}$$

where υ is the specific volume or the inverse of the mass density (2.63a) and $(\mu_1,\, \mu_2)$ the chemical potentials and $(N_1,\, N_2)$ the mole numbers of the two constituents of the two-phase flow; the mass conservation requires eq. (2.63b) where $(m_1,\, m_2)$ are the molecular masses of the two constituents:

$$\upsilon = \frac{1}{\rho}; \quad m_1 N_1 + m_2 N_2 = 0. \tag{2.63a,b}$$

Using eq. (2.63b) the two chemical terms last on the r.h.s of eq. (2.62b) can be rewritten (2.64a):

$$\mu_1\,\mathrm{d}N_1 + \mu_2\,\mathrm{d}N_2 = \left(\mu_1 - \frac{\mu_2}{m_2}m_1\right)\mathrm{d}N_1 = \mu\,\mathrm{d}\xi, \tag{2.64a,b}$$

where eq. (2.65a) is the concentration of the first species and (2.65b) the relative chemical potential:

$$\xi = m_1 N_1, \quad \mu = \frac{\mu_1}{m_1} - \frac{\mu_2}{m_2}. \tag{2.65a,b}$$

Substituting eqs.(2.63a) and (2.64b) specifies (2.62b) the internal energy:

$$\mathrm{d}U = T\,\mathrm{d}s + \frac{p}{\rho^2}\,\mathrm{d}\rho + \mu\,\mathrm{d}\xi, \tag{2.66}$$

as the sum of the heat, isotropic mechanical work and chemical energy of the two phases.

The equation of energy (2.67) specifies the rate of change with time of the total energy density (2.62a), specified in a convected frame by the exact material derivative (2.10a):

$$\frac{\mathrm{D}E}{\mathrm{D}t} = \left(\frac{v^2}{2} + U\right)\frac{\mathrm{D}\rho}{\mathrm{D}t} + \rho\vec{v}\cdot\frac{\mathrm{D}\vec{v}}{\mathrm{D}t} + \rho\,\frac{\mathrm{D}U}{\mathrm{D}t}. \tag{2.67}$$

Using in the three terms of the r.h.s of eq. (2.67) respectively the equations of continuity (2.1), inviscid momentum (2.4) and internal energy (2.66) leads to:

$$\frac{\mathrm{D}E}{\mathrm{D}t} = -\rho\left(\frac{v^2}{2} + U\right)(\nabla\cdot\vec{v}) - \vec{v}\cdot\nabla p + \rho T\,\frac{\mathrm{D}s}{\mathrm{D}t} + \frac{p}{\rho}\,\frac{\mathrm{D}\rho}{\mathrm{D}t} + \mu\,\frac{\mathrm{D}\xi}{\mathrm{D}t}. \tag{2.68}$$

The diffusive terms involving the concentration (2.2) and entropy (2.4) are separated from the rest in:

$$-\nabla\cdot\vec{q}-\mu\,\nabla\cdot\vec{j}=\frac{\partial E}{\partial t}+\vec{v}\cdot\nabla E+E\left(\nabla\cdot\vec{v}\right)+\vec{v}\cdot\nabla p+p\left(\nabla\cdot\vec{v}\right)$$
$$=\frac{\partial E}{\partial t}+\nabla\cdot\left[\left(E+p\right)\vec{v}\right]. \tag{2.69}$$

The term in square brackets is the convective energy flux (2.70b) involving the enthalpy (2.70a) plus kinetic energy that is the stagnation enthalpy times the velocity and mass density in eq. (2.70c).

$$H=U+\frac{p}{\rho}:\quad \vec{F}=\left(E+p\right)\vec{v}$$
$$=\left(\rho U+\frac{\rho}{2}v^2+p\right)\vec{v}=\rho\left(H+\frac{v^2}{2}\right)\vec{v}. \tag{2.70a-d}$$

The energy equation (2.69) thus involves (2.71a) the energy density (2.62a) and convective flux (2.70b-d):

$$\frac{\partial E}{\partial t}+\nabla\cdot\vec{F}=-\nabla\cdot\vec{Q},\quad \nabla\cdot\vec{Q}=\nabla\cdot\vec{q}+\mu\,\nabla\cdot\vec{j}, \tag{2.71a,b}$$

and the diffusive energy flux is given by eq. (2.71b), involving the heat (2.3) and mass (2.2) fluxes.

Substitution of eq. (2.71b) in eq. (2.3) leads to the equation of entropy.

$$\rho T\,\frac{\mathsf{D}s}{\mathsf{D}t}=-\nabla\cdot\vec{Q}+\mu\,\nabla\cdot\vec{j}=-\nabla\cdot\left(\vec{Q}-\mu\vec{j}\right)-\vec{j}\cdot\nabla\mu. \tag{2.72a,b}$$

The first principle of thermodynamics concerns the internal energy (2.62b), and the second the entropy production given locally by eq. (2.73a), where is used the equation of continuity (2.1) leading to eq. (2.73c):

$$\frac{\partial}{\partial t}\left(\rho s\right)=\frac{\mathsf{D}}{\mathsf{D}t}\left(\rho s\right)-\vec{v}\cdot\nabla\left(\rho s\right)=\rho\,\frac{\mathsf{D}s}{\mathsf{D}t}+s\,\frac{\mathsf{D}\rho}{\mathsf{D}t}-\vec{v}\cdot\nabla\left(\rho s\right)$$
$$=\rho\,\frac{\mathsf{D}s}{\mathsf{D}t}-s\rho\left(\nabla\cdot\vec{v}\right)-\vec{v}\cdot\nabla\left(\rho s\right)=\rho\,\frac{\mathsf{D}s}{\mathsf{D}t}-\nabla\cdot\left(\rho s\vec{v}\right). \tag{2.73a-d}$$

The second term on the r.h.s of eq. (2.73d) is the divergence of the convective entropy flux, and hence unrelated to diffusion, that is specified by the first term (2.74a) where may be substituted (2.72b) leading to eq. (2.74b):

$$\frac{\partial}{\partial t}\left(\rho s\right)=\rho\,\frac{\mathsf{D}s}{\mathsf{D}t}=-\frac{1}{T}\left[\nabla\cdot\left(\vec{Q}-\mu\vec{j}\right)+\vec{j}\cdot\nabla\mu\right]. \tag{2.74a,b}$$

The first term on the r.h.s of eq. (2.74b) may be re-written,

$$-\frac{\nabla\cdot\left(\vec{Q}-\mu\vec{j}\right)}{T}=-\nabla\cdot\left(\frac{\vec{Q}-\mu\vec{j}}{T}\right)+\left(\vec{Q}-\mu\vec{j}\right)\cdot\nabla\left(\frac{1}{T}\right); \tag{2.75}$$

the first term on the r.h.s of eq. (2.75) is the divergence of a flux, hence non-local, and only the second

term contributes in eq. (2.74b) to the local entropy production:

$$0 < \dot{S} \equiv \frac{\partial}{\partial t}(\rho s) = -\frac{1}{T^2}\left(\vec{Q} - \mu\vec{j}\right) \cdot \nabla T - \frac{\vec{j} \cdot \nabla \mu}{T}. \tag{2.76a,b}$$

The heat (2.7a) and mass (2.7b) diffusion relations have kinetic coefficients that must satisfy (section 2.6) the condition (2.76b) of entropy growth.

2.6 Thermal, Mass and Pressure Kinetic Coefficients

The entropy production per unit time is a linear function (2.77a) of the fluxes $\dot{x}_n$ whose coefficients are the gradients (2.77b):

$$\dot{S} = \sum_n X_n \dot{x}_n > 0, \quad X_n = \frac{\partial \dot{S}}{\partial \dot{x}_n}. \tag{2.77a,b}$$

For small gradients the fluxes are linear functions with kinetic coefficients (2.78a) that appear also in the entropy production (2.78b):

$$\dot{x}_n = \sum_l \Gamma_{nl} X_l, \quad \dot{S} = \sum_{n,l} \Gamma_{nl} X_n X_l > 0. \tag{2.78a,b}$$

Since the entropy production (2.78b) is a quadratic form, the kinetic coefficients may be taken as symmetric (2.79a); also since it must be positive-definite, in the case of a 2×2 matrix of kinetic coefficients the Cayley-Hamilton conditions (2.79b,c) must be satisfied [5]:

$$\Gamma_{nl} = \Gamma_{ln}; \quad \Gamma_{11} > 0, \quad \Gamma_{22} > \frac{\Gamma_{12}\Gamma_{21}}{\Gamma_{11}} = \frac{(\Gamma_{12})^2}{\Gamma_{11}} > 0. \tag{2.79a-c}$$

In the present case (2.76b) the fluxes are eq. (2.80a) and hence the gradients eq. (2.80b):

$$\dot{x}_n = \left\{\vec{Q} - \mu\vec{j}, \vec{j}\right\}, \quad X_n = \left\{-\frac{\nabla T}{T^2}, -\frac{\nabla \mu}{T}\right\}. \tag{2.80a,b}$$

Thus the diffusion relations (2.78a) are:

$$\vec{Q} - \mu\vec{j} = -\Gamma_{11}\frac{\nabla T}{T^2} - \Gamma_{12}\frac{\nabla \mu}{T}, \quad \vec{j} = -\Gamma_{12}\frac{\nabla T}{T^2} - \Gamma_{22}\frac{\nabla \mu}{T}, \tag{2.81a,b}$$

where the kinetic coefficients satisfy eq. (2.79b,c).

Solving eq. (2.81b) for the gradient of the chemical potential $\nabla\mu$ and substituting in eq. (2.81a) it is eliminated from the energy flux:

$$\vec{Q} = -\left[\Gamma_{11} - \frac{(\Gamma_{12})^2}{\Gamma_{22}}\right]\frac{\nabla T}{T^2} + \left(\mu + \frac{\Gamma_{12}}{\Gamma_{22}}\right)\vec{j}. \tag{2.82}$$

In the absence of mass flux (2.83a) the energy flux coincides with the heat flux that is specified by the

Fourier's Law (2.83b) where the thermal conductivity (2.83c) is positive by eq. (2.79c),

$$\vec{j}=0: \quad \vec{Q}=-\overline{\chi}\,\nabla T, \quad \overline{\chi}=\frac{1}{T^2}\left[\Gamma_{11}-\frac{(\Gamma_{12})^2}{\Gamma_{22}}\right]>0; \tag{2.83a-c}$$

thus heat flows from the higher to the lower temperatures. The energy flux in the presence of mass flux is given by:

$$\vec{Q}=-\overline{\chi}\,\nabla T+\left(\mu+\frac{\Gamma_{12}}{\Gamma_{22}}\right)\vec{j}. \tag{2.84}$$

The mass flux appears in eq. (2.81b) in terms of the gradient of temperature ∇T and chemical potential $\nabla\mu$ instead of the concentration in eq. (2.7b). The free enthalpy is related to the internal energy (2.66) by eq. (2.85a) leading to eq. (2.85b)

$$G=U-Ts+\frac{p}{\rho}: \quad \mathsf{d}G=-s\,\mathsf{d}T+\frac{1}{\rho}\,\mathsf{d}p+\mu\,\mathsf{d}\xi. \tag{2.85a,b}$$

Thus the chemical potential is (2.86a) the derivative of the free enthalpy with regard to the concentration, and is a function of the same variables:

$$\mu=\left(\frac{\partial G}{\partial \xi}\right)_{T,p}:$$
$$\nabla\mu=\left(\frac{\partial \mu}{\partial T}\right)_{p,\xi}\nabla T+\left(\frac{\partial \mu}{\partial p}\right)_{T,\xi}\nabla p+\left(\frac{\partial \mu}{\partial \xi}\right)_{T,p}\nabla\xi, \tag{2.86a,b}$$

leading to eq. (2.86b).

Substituting (2.86a,b) specifies the mass (2.81b) and energy (2.84) fluxes respectively as:

$$-\vec{j}=D\,\nabla\xi+\alpha\,\nabla T+\varphi\,\nabla p, \quad -\vec{Q}=\overline{\overline{\chi}}\,\nabla T+\overline{\beta}\,\nabla\xi+\psi\,\nabla p, \tag{2.87a,b}$$

where:

(i) the barodiffusion coefficients

$$\varphi\equiv\frac{\Gamma_{22}}{T}\left(\frac{\partial\mu}{\partial p}\right)_{T,\xi}=0, \quad \psi\equiv\left(\mu+\frac{\Gamma_{12}}{\Gamma_{22}}\right)\varphi=0, \tag{2.88a,b}$$

can be omitted from eq. (2.87a,b), because they must be zero, otherwise the entropy production (2.76a,b) would have terms $\nabla p\cdot\nabla T$ and $\nabla p\cdot\nabla\mu$ without fixed sign, contradicting the second principle of thermodynamics that it must be positive in all cases;

(ii) the mass flux (2.81b) is thus given by eqs.(2.87a)≡(2.7b)≡(2.89a) with mass diffusion coefficient (2.89b) and thermal cross-coefficient (2.89c).

$$\vec{j}=-D\,\nabla\xi-\alpha\,\nabla T: \quad D\equiv\frac{\Gamma_{22}}{T}\left(\frac{\partial\mu}{\partial\xi}\right)_{T},$$
$$\alpha\equiv\frac{\Gamma_{12}}{T^2}+\frac{\Gamma_{22}}{T}\left(\frac{\partial\mu}{\partial T}\right)_{\xi}; \tag{2.89a-c}$$

(iii) using eq. (2.89a) the energy flux (2.84) is given by eqs.(2.90a)≡(2.87b) with coefficients (2.90b,c):

$$\vec{Q} = -\overline{\overline{\chi}}\,\nabla T - \overline{\beta}\,\nabla\xi: \quad \overline{\overline{\chi}} = \overline{\chi} + \alpha\left(\mu + \frac{\Gamma_{12}}{\Gamma_{22}}\right),$$
$$\overline{\beta} = \left(\mu + \frac{\Gamma_{12}}{\Gamma_{22}}\right) D; \tag{2.90a-c}$$

(iv) rewriting eq. (2.71b) in the form of eq. (2.91a) and neglecting the second non-linear term on the r.h.s. leads to eq. (2.91b)

$$\nabla\cdot\vec{Q} = \nabla\cdot\left(\vec{q} + \mu\vec{j}\right) - \vec{j}\cdot\nabla\mu: \quad \vec{Q} = \vec{q} + \mu\vec{j}, \tag{2.91a,b}$$

and substitution of eqs.(2.89a) and (2.90a) specifies the heat flux (2.7a)≡(2.92a):

$$\vec{q} = -\chi\,\nabla T - \beta\,\nabla\xi: \quad \chi = \overline{\chi} + \alpha\,\frac{\Gamma_{12}}{\Gamma_{22}}, \quad \beta = D\,\frac{\Gamma_{12}}{\Gamma_{22}}, \tag{2.92a-c}$$

where eq. (2.92b) is the thermal conductivity and eq. (2.92c) the mass diffusion cross-coefficient.

The diffusion relations (2.7a,b) are valid with coefficients (2.89b,c; 2.92b,c) whereas the damping (2.40b) of the decaying mode (2.47a-d) and the damping (2.44) of the acoustic modes (2.45a,b) are specified in terms of the thermodynamic properties and diffusion coefficients of the binary mixture.

Chapter 3

Implementation

The main objective of this work, as stated before, is to obtain an approach of a theory for sound attenuation by a two-phase dissipative medium. In the previous chapter (2) the theoretical foundation of the theory was built and next it is implemented to verify its validity. This chapter is divided into two parts: the theoretical implementation, where the mathematical relations necessary to obtain the total dissipation coefficient for acoustic waves are tested and chosen; and the computational implementation with the description of a tool developed in MATLAB which applied the relations of the first part leading to the results to be discussed in the next chapter.

3.1 Theoretical Implementation

The coefficients in eqs. (2.89b,c) and (2.92b,c) appear in the diffusion relations (2.7a,b) as well as in the damping of the decaying (2.40b) and acoustic (2.44) modes, and hence it is important the dependence of the relative chemical potential on both these coefficients and on the kinetic coefficients. Concerning the viscous dissipation coefficient (2.43a) for acoustic waves it is necessary to perform a mathematical extrapolation of the shear and bulk viscosities.

3.1.1 Chemical Potential

The chemical potential, also known as Gibbs free energy, is the tendency of a substance: to decompose itself or to react with other substances; to suffer a change of state or to redistribute in space [7]. In a very simple and generalized physical point-of-view it can be seen as the tendency to give particles, where the particles tend to flow from the highest potential to the lowest one until it achieves equilibrium [8]. As seen in sections 2.5 and 2.6 this property is strictly necessary to perform the main goal of this work. With this, it is important to recall the definition of the relative chemical potential (2.65b):

$$\mu = \frac{\mu_1}{m_1} - \frac{\mu_2}{m_2}, \tag{3.1}$$

where (μ_1, μ_2) are the chemical potentials of the two constituents of the two-phase flow, respectively water and air. However, the air has no chemical potential due to the fact that its main components, O_2 and N_2, have a chemical potential of value equal to 0. The potential value 0 does not mean that the substances have no tendency to transform, it is a matter of simplicity, where a zero value is assigned to the most stable and usual form of an element as a base level for other element-containing substances [7]. Reducing eq. (3.1) to

$$\mu = \frac{\mu_1}{m_1} = \frac{\mu_{H_2O}}{m_{H_2O}}. \tag{3.2}$$

The relative chemical potential now depends exclusively of the water properties, respectively the chemical potential and molecular mass. There are many derivations of chemical potential formulas, to choose the most appropriate one it has to be taken into account eq. (2.89b,c), dependent on both the temperature and concentration, which means that eq. (3.3) [7, 8], also known as mass action equation, has to depend on these two variables.

$$\mu_{H_2O}\left(T, \xi\right) = \mu_0 + RT \ln\left(\frac{\xi}{\xi_0}\right). \tag{3.3}$$

Eq. (3.3) determines the difference between a specified state and a reference state calculated under standard conditions, referenced by the subscript 0. It is noteworthy that eq. (3.3) is only valid for values of $\xi \ll \xi_0$. Substituting eq. (3.3) in eq. (3.2) it is obtained the relative chemical potential equation (3.4).

$$\mu = \left[\mu_0 + RT \ln\left(\frac{\xi}{\xi_0}\right)\right] \frac{1}{m_{H_2O}}. \tag{3.4}$$

In table (3.1) are presented the data corresponding to the reference state [9], standard conditions [9] and respective properties of eq. (3.4).

Table 3.1: Water chemical potential data

μ_0 [kJ/mol]	ξ_0 [mol/m^3]	T_0 [K]	p_0 [Pa]	R [kJ/kmol.K]	m_{H_2O} [kg/mol]
-237.18	1000	298	101130	8.314	0.01802

As it can be seen from table 3.1 the reference value of the water chemical potential is negative, as a matter of fact, most of the chemical potential values are negative. This represents the stability of a substance, being negative means it is not propitious to decomposition, it will not decompose into their elements, instead it will spontaneously be produced from them [7].

The chemical potential of a substance varies with changes in temperature and concentration, it decreases with increasing temperature and increases with increasing concentration [7]. This means that in warmer environments the substance has less tendency to transform, whereas regarding to the concentration, the more concentrated a substance is, the more is the tendency to decompose into their elements. In figure 3.1 it is possible to observe this behaviour using the relation from eq. (3.4), it is important to note that for higher concentrations the values depart quite noticeable from this relation, hence it is recommended to maintain the concentration values between the range of validity ($\xi \ll \xi_0$), in the case of liquids this value is approximately 100 mol/m^3 which is at the limit of $\xi \leq 100$ mol/m^3 [7].

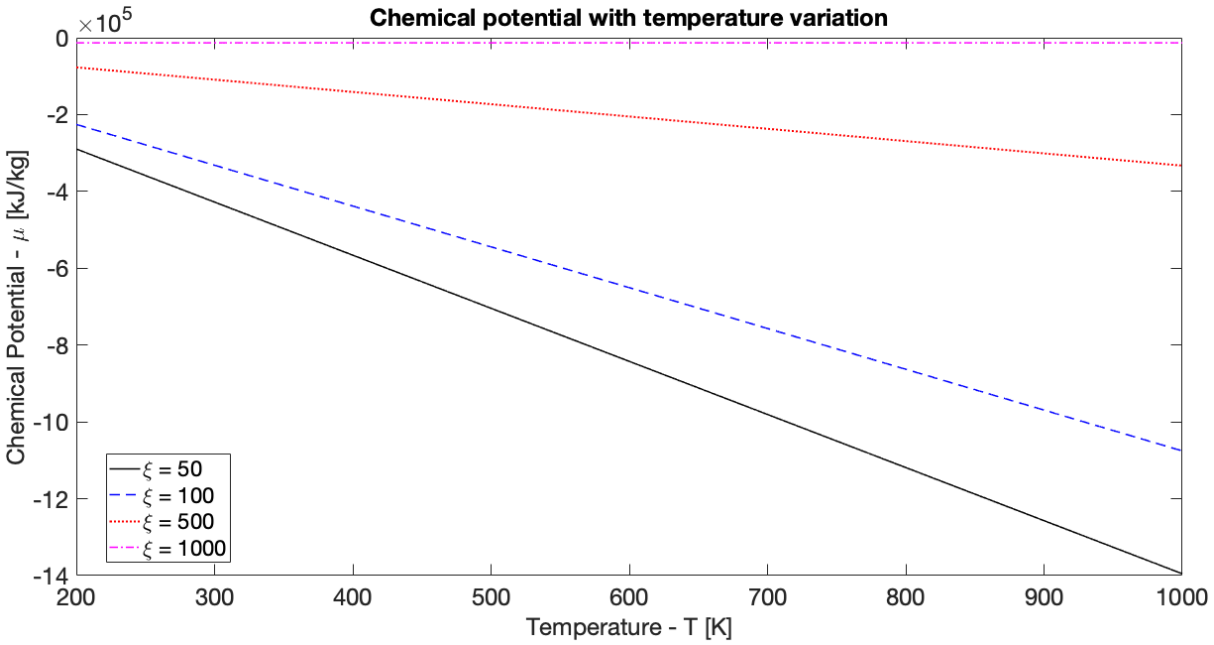

(a) Temperature variation for different concentrations in [mol/m^3].

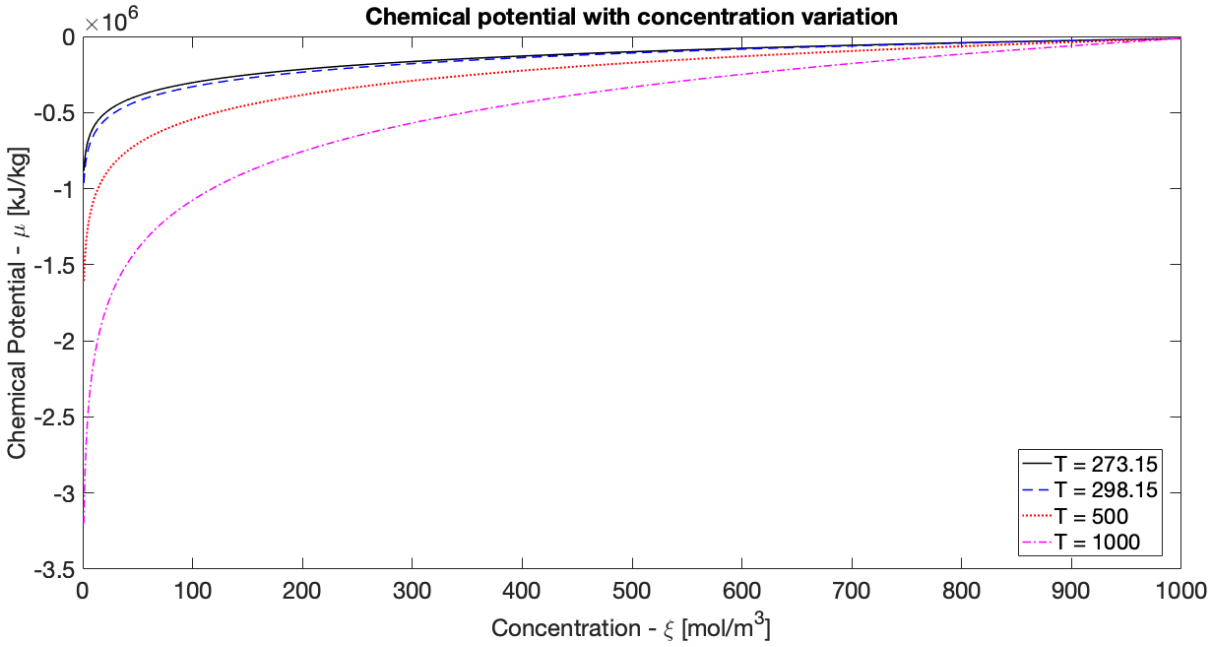

(b) Concentration variation for different temperatures in [K].

Figure 3.1: Variation of the relative chemical potential with temperature and concentration.

In chapter 2 the mass diffusion coefficient (2.89b) and the thermal cross-coupling (2.89c) rely on the derivative of the relative chemical potential, in eq. (3.5a,b) both of the derivatives are presented as well as their graphic representation (figs. 3.2 and 3.3) with temperature and concentration variations.

$$\frac{\partial \mu}{\partial \xi} = \frac{RT}{\xi}\frac{1}{m_{H_2O}}, \quad \frac{\partial \mu}{\partial T} = R\ln\left(\frac{\xi}{\xi_0}\right)\frac{1}{m_{H_2O}}. \tag{3.5a,b}$$

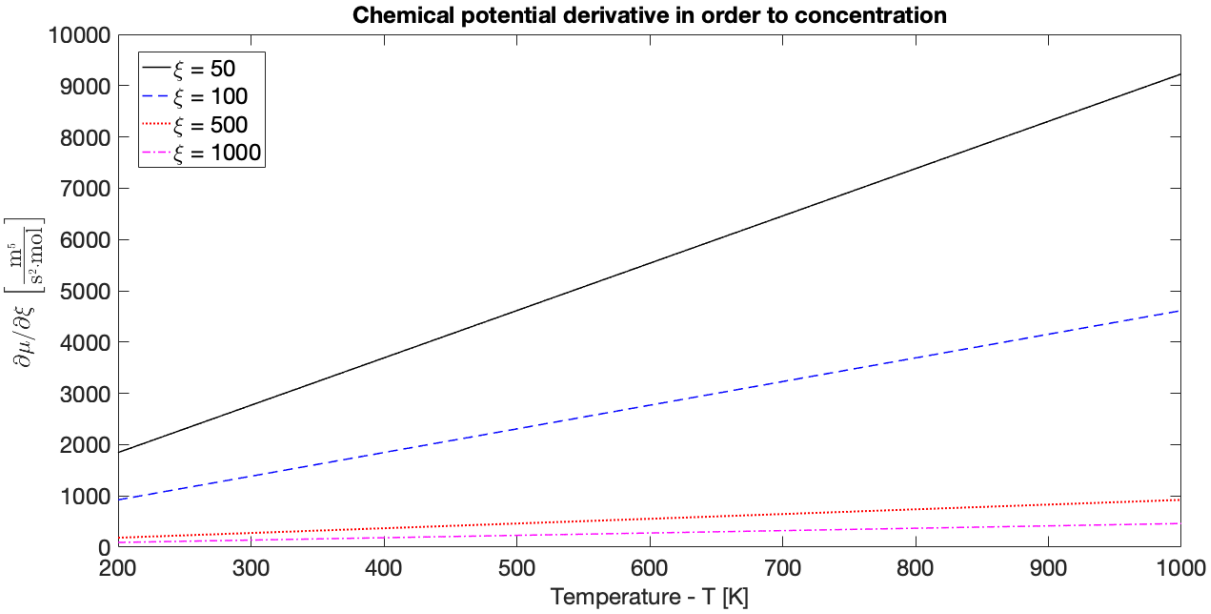

(a) Temperature variation of the derivative for different concentrations in [mol/m^3].

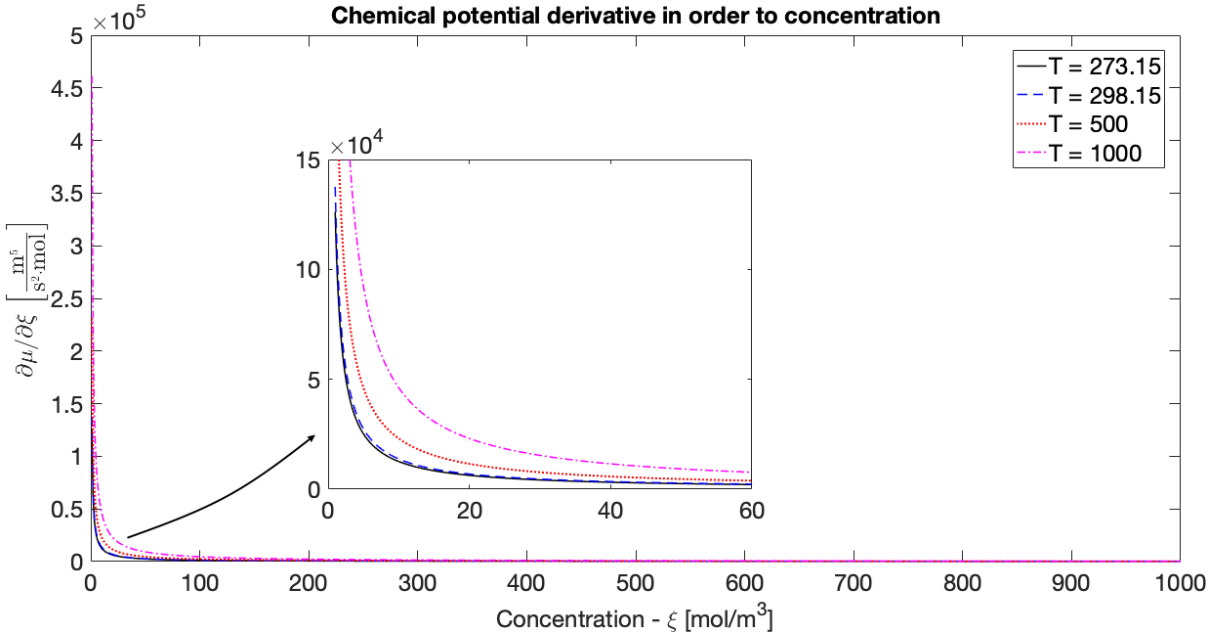

(b) Concentration variation of the derivative for different temperatures in [K].

Figure 3.2: Derivative of the relative chemical potential with regard to concentration - $\partial\mu/\partial\xi$.

Since the derivative regarding to temperature reduces eq. (3.4) to one parameter in eq. (3.5b), the concentration, there is only one representation depending on this parameter in fig. 3.3.

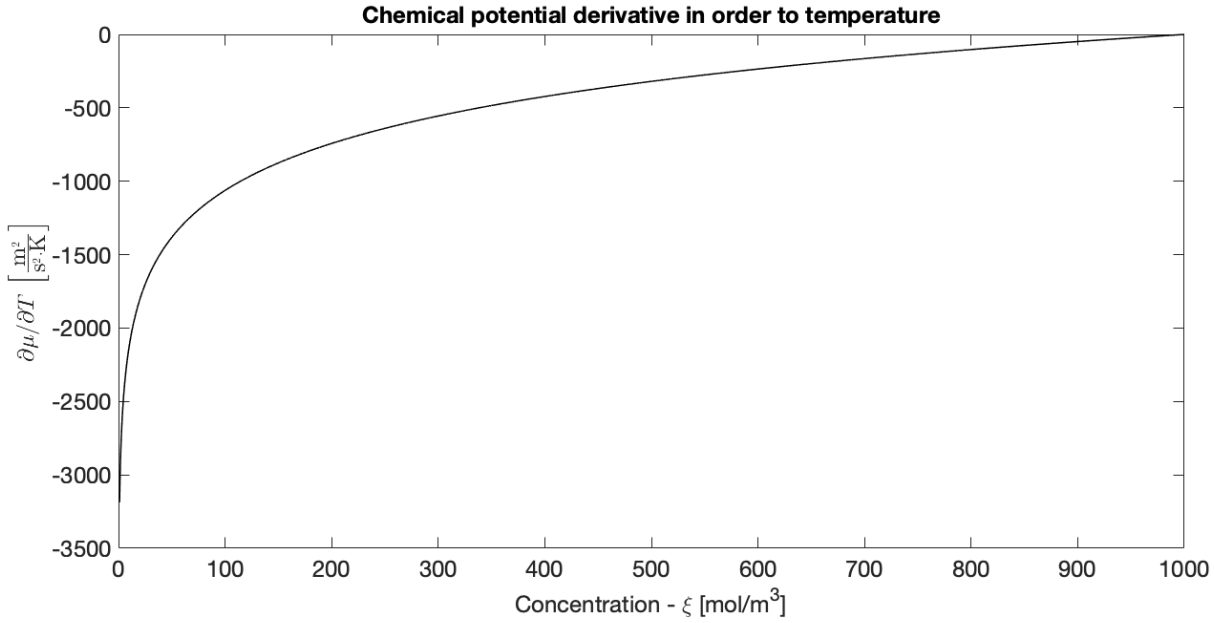

Figure 3.3: Derivative of the relative chemical potential with regard to temperature - $\partial\mu/\partial T$.

3.1.2 Kinetic Coefficients

This work involves a thermodynamic system where both heat conduction and mass diffusion coexist and when two or more irreversible transport processes occur simultaneously they may interfere with each other. Besides prior work, Lars Onsager described in the most detailed form, the reciprocal relations in irreversible processes [5, 10] by means of phenomenological relations and associated coefficients, the kinetic coefficients, better known as phenomenological coefficients (Γ_{nl}). These relations consist of appropriate flux-force pairs (3.7a,b), already obtained in section 2.6, where the fluxes (3.7a) include heat and mass while the forces (3.8a,b) involve finite gradients in temperature, T, and chemical potential, μ. The kinetic coefficients are the link between the fluxes and the forces (2.78a). In an attempt to simplify the visualization of the following equations the subscripts q and j are used, corresponding to heat and mass with the relation between nomenclatures being expressed in eq. (3.6).

$$\begin{bmatrix} \Gamma_{qq} & \Gamma_{qj} \\ \Gamma_{jq} & \Gamma_{jj} \end{bmatrix} = \begin{bmatrix} \Gamma_{11} & \Gamma_{12} \\ \Gamma_{21} & \Gamma_{22} \end{bmatrix} \tag{3.6}$$

$$\dot{x}_n = \{\dot{x}_q, \dot{x}_j\}, \quad X_n = \{X_q, X_j\}. \tag{3.7a,b}$$

$$X_q = -\frac{\nabla T}{T^2}, \quad X_j = -\frac{\nabla \mu}{T}. \tag{3.8a,b}$$

In this section the equations concerning the phenomenological coefficients relate to gradients but

what matters the most for this analysis is the difference between the variable values and not so much the position or distance between them. Therefore to simplify the calculations it is assumed that the reference position is the beginning of the water jet, referenced as 0 meters, $x_1 = 0$, and the second position is the peak of the jet, considered in this case to have 1 meter, $x_2 = 1$. Using the temperature as example, this means $\nabla T = \dfrac{\Delta T}{\Delta x} = \dfrac{\Delta T}{x_2 - x_1} = \dfrac{\Delta T}{1 - 0} = \Delta T$. All units presented are relative to the gradients, the only purpose is to better observe the effect generated by the variation of the variables, in this case temperature and chemical potential.

Since the two processes (3.8a,b), heat conduction and mass diffusion, interfere with each other it is necessary to use the phenomenological relations (3.9a,b) [5].

$$\dot{x}_q = \Gamma_{qq} X_q + \Gamma_{qj} X_j, \tag{3.9a}$$

$$\dot{x}_j = \Gamma_{jq} X_q + \Gamma_{jj} X_j. \tag{3.9b}$$

The phenomenological coefficients Γ_{qq} and Γ_{jj} are due to the heat and mass uncoupled case whereas Γ_{qj} and Γ_{jq} result from the coupling between the heat flux and the chemical potential difference and the mass flux and temperature difference. It is possible to write the previous relations relating the heat flow (3.10a) and mass flow (3.10b) substituting eq. (3.8a,b) in eqs. (3.9a,b), which was also already defined previously in eq. (2.81a,b),

$$\dot{x}_q = -\Gamma_{qq} \frac{\nabla T}{T^2} - \Gamma_{qj} \frac{\nabla \mu}{T}, \tag{3.10a}$$

$$\dot{x}_j = -\Gamma_{jq} \frac{\nabla T}{T^2} - \Gamma_{jj} \frac{\nabla \mu}{T}. \tag{3.10b}$$

The objective is to obtain the values for the phenomenological coefficients, and literature on this subject is scarce and even scarcer when the subject involves two-phase flows. The only method available to calculate such values for this kind of flows is through the use of the kinetic theory of condensation and evaporation [11–13], yet this method features some constraints that makes it unfeasible to the present approach. In first place, as already stated in section 1.4 the vaporization effect being a less important effect is to be omitted, and since the kinetic theory is based on this same effect it would disregard this approximation. Even when deciding to use evaporation as a way of calculating the coefficients this is a very slow process compared with the kind of process dealt here which would result in much smaller values. Besides, the kinetic theory of condensation and evaporation deals with two-phase flows only of the same fluid, this means water and water-vapour and not a water-air mixture as it is the case here. With this in mind, the chosen approach is the direct use of the phenomenological equations, where the heat related flow, $\dot{x}_q$, can not be assumed, but the mass flow, $\dot{x}_j$, is going to be treated as the water flow of the deluge system, in this way trying to obtain the phenomenological coefficients for different system configurations.

When $\Delta T = 0$, eq. (3.10b) reduces to [11, 14, 15],

$$\dot{x}_j = -\Gamma_{jj} \frac{\nabla \mu}{T}, \tag{3.11}$$

where T is the mean temperature.

Similarly, when $\Delta\mu = 0$, from eq. (3.10b) [11, 14, 15],

$$\dot{x}_j = -\Gamma_{qj}\,\frac{\nabla T}{T^2}. \tag{3.12}$$

Recalling eq. (2.82), when there is no mass flux (2.83a), $\vec{j} = 0$, it is obtained [11, 14, 15],

$$\dot{x}_Q = -\left[\Gamma_{qq} - \frac{(\Gamma_{qj})^2}{\Gamma_{jj}}\right]\frac{\nabla T}{T^2}. \tag{3.13}$$

As already mentioned, in the absence of mass flux the energy flux coincides with the heat flux that is specified by Fourier's law (2.83b) [14, 16]. It was stated in the beginning of this section that this method is an approximation since it only takes into account the water phase instead of the two-phase flow, therefore, the conductivity here will be different from the one considered in eq. (2.83c) which combines both phases.

$$\dot{x}_Q = -\kappa\,\nabla T, \tag{3.14}$$

where, κ is the water thermal conductivity in the spray system. Thus, substituting eq. (3.14) in eq. (3.13) leads to an equation for Γqq,

$$\kappa T^2 = \Gamma_{qq} - \frac{(\Gamma_{qj})^2}{\Gamma_{jj}}. \tag{3.15}$$

Through the Onsager's reciprocal relations it is finally obtained the following eqs. (3.16)–(3.18) for the phenomenological coefficients,

$$\Gamma_{jj} = -\dot{x}_j\,\frac{T}{\nabla\mu}, \tag{3.16}$$

$$\Gamma_{qj} = -\dot{x}_j\,\frac{T^2}{\nabla T}, \tag{3.17}$$

$$\Gamma_{qq} = \kappa T^2 + \frac{(\Gamma_{qj})^2}{\Gamma_{jj}}, \tag{3.18}$$

with

$$\Delta T = T_2 - T_1 = T_{exterior} - T_{system}, \quad \Delta\mu = \mu_2 - \mu_1 = \mu_{exterior} - \mu_{system},$$
$$T = \frac{T_1 + T_2}{2} = \frac{T_{system} + T_{exterior}}{2}. \tag{3.19a-c}$$

The demonstration and calculation of the conductivity of water can be analysed in the next section (3.1.3).

The results obtained for the kinetic coefficients are presented in the following figures. Since eqs. (3.16)–(3.18) depend on the variation or the mean temperature what is important is the difference between the two temperatures and not their individual values, so it is possible to assume a fixed system temperature while varying the exterior one, for all the following cases it was chosen a system temperature of 23° C. For the cases not dependent of temperature variation it was assumed an exterior temperature of 25° C.

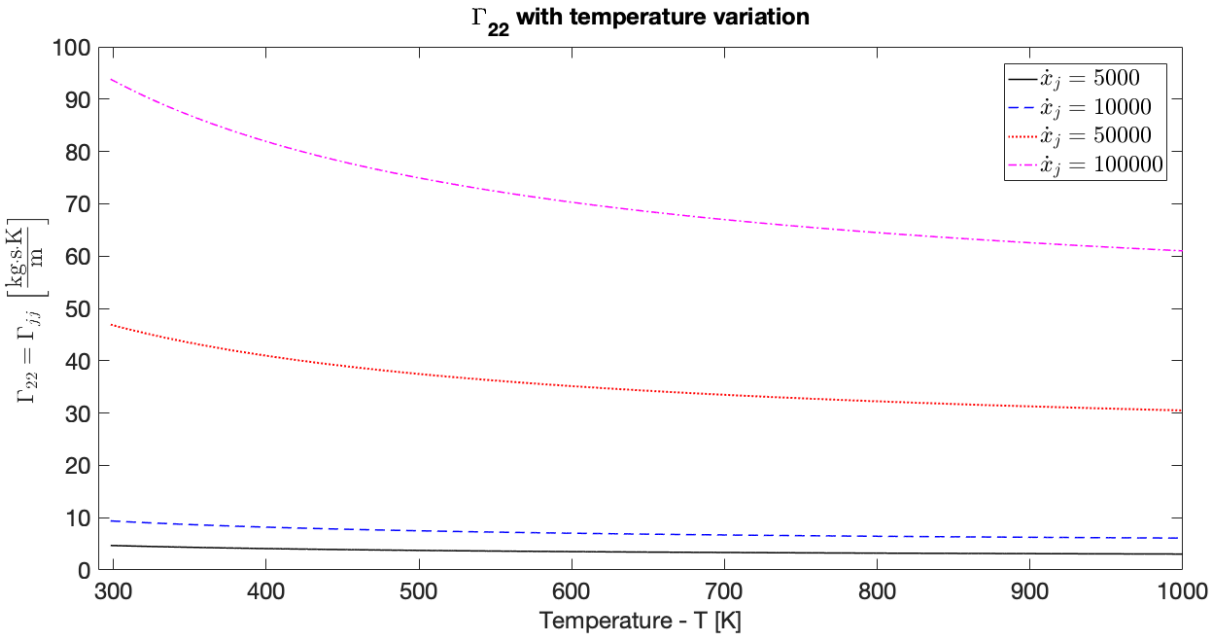

(a) Γ_{22} for different mass flows in [kg/s] with $\xi = 100\,[\text{mol/m}^3]$ and $T_{system} = 23°$ C.

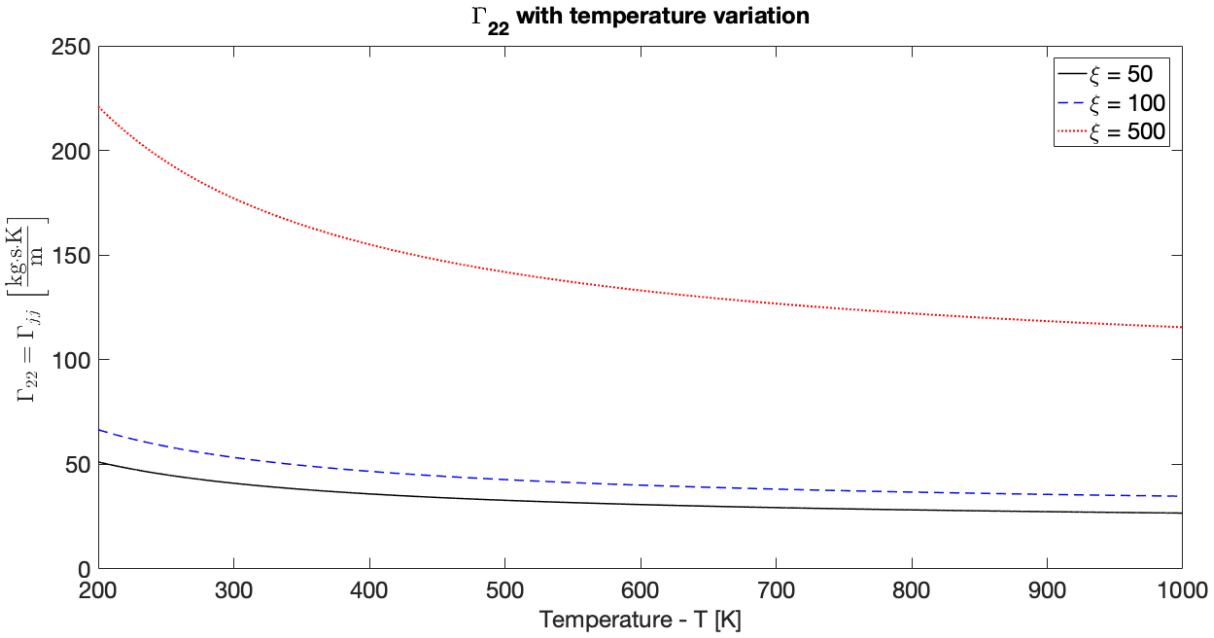

(b) Γ_{22} for different concentrations in [mol/m^3] with $\dot{x}_j = 57000$ [kg/s] and $T_{system} = 23°$ C.

Figure 3.4: Γ_{22} with exterior temperature variation.

Regarding the concentration, when needed a constant value it was used 100 mol/m^3 because as seen in the previous section it is the limiting value for the good functioning of the chemical potential equation (3.4). When testing the effects of the variation in concentration were used higher values comparatively to the limiting one to observe the consequences when the domain of validity of eq. (3.4) is not respected. For the water flow variation four very different values were chosen in an attempt to examine the impact of this parameter. For the constant mass flow was used 57000 kg/s based on NASA's deluge system. In fig. 3.4 it is presented the coefficient Γ_{jj} from eq. (3.16) dependence on the temperature variation for the two possible alternatives, water flow alteration with fixed concentration and vice-versa; for both

cases, Γ_{jj} decreases with increasing temperature and increases with water flow and concentration.

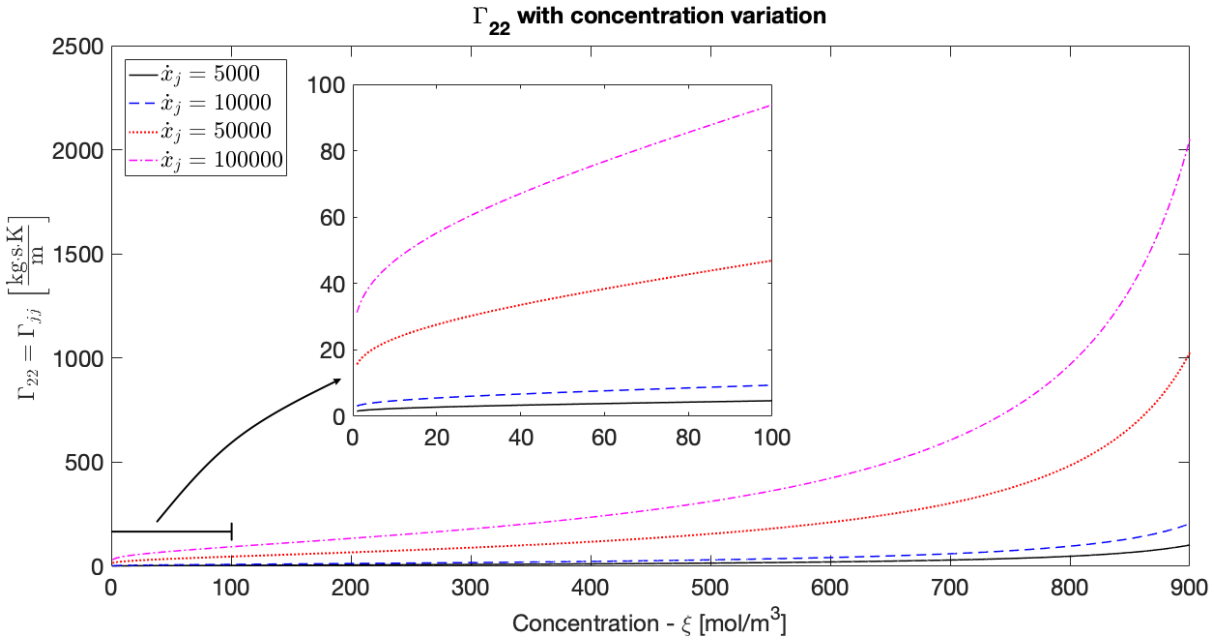

(a) Γ_{22} for different mass flows in [kg/s] with $T_{system} = 23°$ C and $T_{exterior} = 25°$ C.

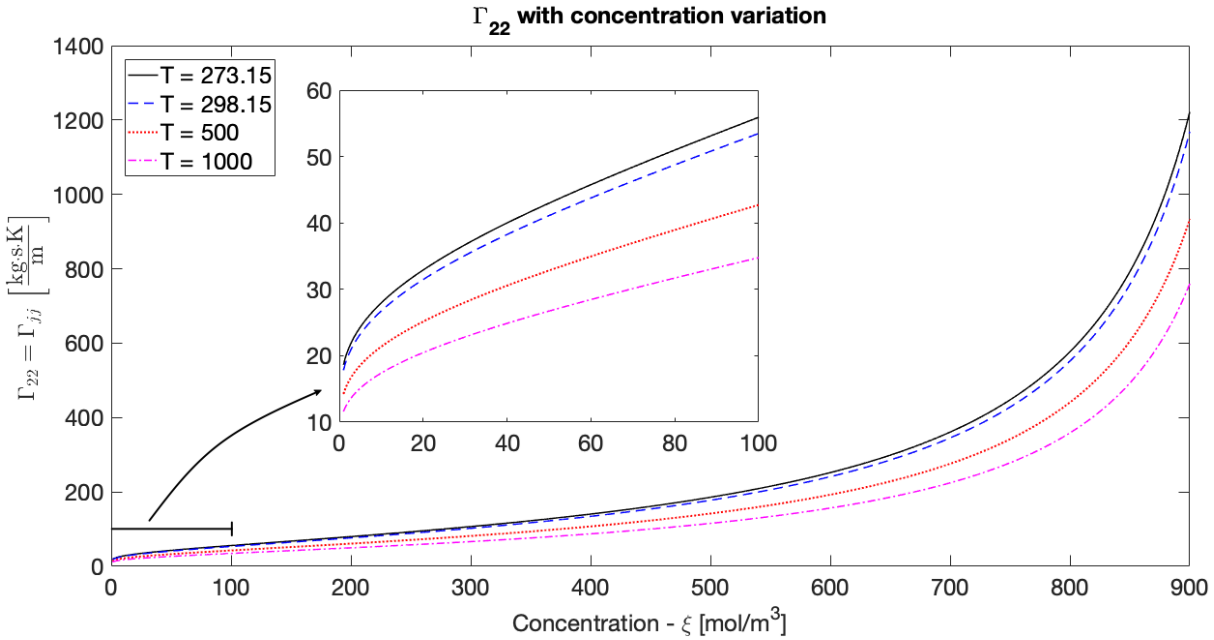

(b) Γ_{22} for different $T_{exterior}$ in [K] with $T_{system} = 23°$ C and $\dot{x}_j = 57000$ [kg/s].

Figure 3.5: Γ_{22} with concentration variation.

When subject to concentration variation (fig. 3.5), Γ_{jj} increases with it, it also increases with increasing mass flow (fig. 3.5a) but decreases with increasing temperature (fig. 3.5b) which reassures what was stated before, done with the simple purpose of observing the progress of the function (3.16) in both strands. The Cayley-Hamilton condition in eq. (2.79c) is satisfied as it was mandatory.

While analysing Γ_{qj} from eq. (3.17) in fig. 3.6 it is important to state two points: the negative value of this coefficient is due to the fact that the exterior temperature is higher than the one from the system, causing the temperature variation, ΔT, in the gradient to be positive and since eq. (3.17) has a negative

sign the final value is also negative; the exterior and system temperatures must not be the same as this would turn out in a null temperature variation and successively a null gradient and with this parameter in the denominator of eq. (3.17) it would tend to infinity making it a discontinuous function. Γ_{qj} depends on the temperature, the mean and the gradient, and on the water flow, it decreases, in negative value, with increasing temperature and increases with the mass flow.

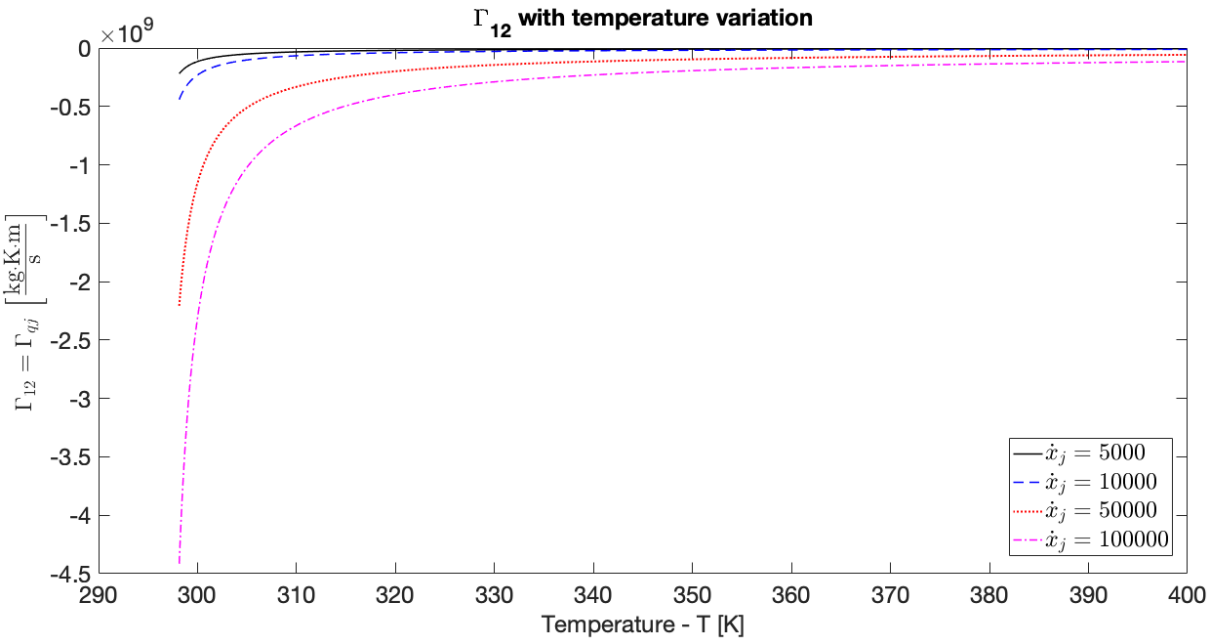

Figure 3.6: Γ_{12} with exterior temperature variation for different mass flows in [kg/s] and $T_{system} = 23°$ C.

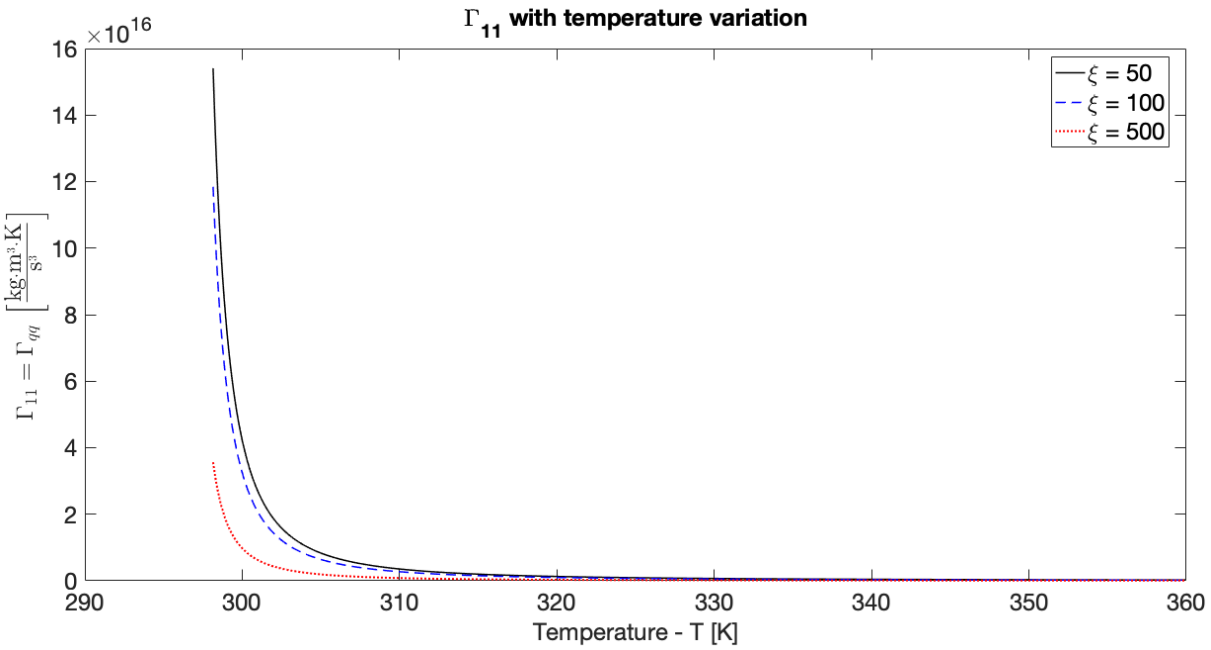

Figure 3.7: Γ_{11} with exterior temperature variation for different concentrations in [mol/m^3] and $T_{system} = 23°$ C.

Γ_{qq} from eq. (3.18) depends not only on the water conductivity but also on the values of Γ_{qj} and Γ_{jj}, being derived from the other phenomenological coefficients. In the presence of temperature variation

(fig. 3.7), Γ_{qq} decreases with increasing temperature and the same happens regarding to the concentration. In fig. 3.8 it is possible to observe the same behaviour, increasing concentration leads to smaller values and higher temperatures leads to smaller values as well. The required condition from eq. (2.79b), is achieved, as it is easily observed in figs. 3.7 and 3.8 .

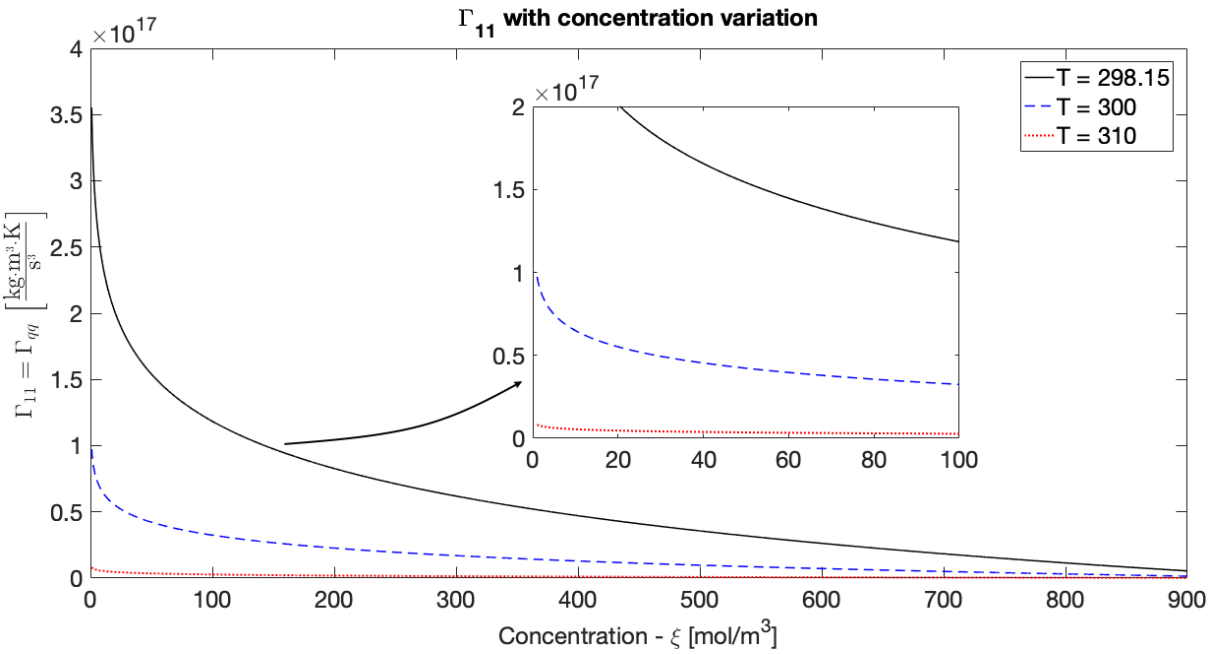

Figure 3.8: Γ_{11} with concentration variation for different $T_{exterior}$ in [K] and $T_{system} = 23°$ C.

3.1.3 Water Thermal Conductivity

The thermal conductivity, κ, is the parameter responsible for measuring a material's ability to conduct heat, in this case the material in question is water, flowing from the spray system. The temperature is one of the most important variables when defining the phenomenological coefficients and thus, research was made with the goal of defining the water thermal conductivity dependent on this variable. Furthermore since the coefficients from eqs. (3.16)–(3.18) are defined using a specific temperature, the mean temperature T, the thermal conductivity will also be defined for this variable to maintain the consistency in the equations. In this section various formulas from different authors are going to be presented and compared with theoretical [17] and experimental [18] data calculating the error percentage between them choosing the most fitted.

The constants in eq. (3.20a,b) from [19] are determined for a temperature range from 0 to 150° C, it

is noteworthy that this is the only formula whose coefficients are calculated for degree Celsius.

$$\kappa = A + BT + CT^{1.5} + DT^2 + ET^{0.5}; \quad \begin{cases} A = 0.5650285, \\ B = 0.0026363895, \\ C = -0.00012516934, \\ D = -1.5154918 \times 10^{-6}, \\ E = -0.0009412945. \end{cases} \tag{3.20a,b}$$

Equation (3.21) was obtained from [20] with temperature expressed in kelvin,

$$\kappa = -8.354 \times 10^{-6}\, T^2 + 6.53 \times 10^{-3}\, T - 0.5981. \tag{3.21}$$

The following equation (3.22) from [21] has a domain of validity of [273; 633 K],

$$\kappa = -0.2758 + 4.6120 \times 10^{-3}\, T - 5.5391 \times 10^{-6}\, T^2. \tag{3.22}$$

The eq. (3.23a) is expressed in terms of the dimensionless variables, reduced temperature (3.23b) and reduced conductivity (3.23c), and has a range of validity of [274; 370 K] [22],

$$\kappa^* = -1.48445 + 4.12292T^* - 1.63866{T^*}^2; \quad T^* = \frac{T}{298.15}, \quad \kappa^* = \frac{\kappa\,(T)}{\kappa\,(298.15)}, \tag{3.23a-c}$$

with κ (298.15) = 0.6065 W/mK as the standard value of the thermal conductivity of water at 298.15 K.

In fig. 3.9 are represented the results obtained from eqs. (3.20a,b)–(3.23a-c) compared with the theoretical [17] and experimental data [18].

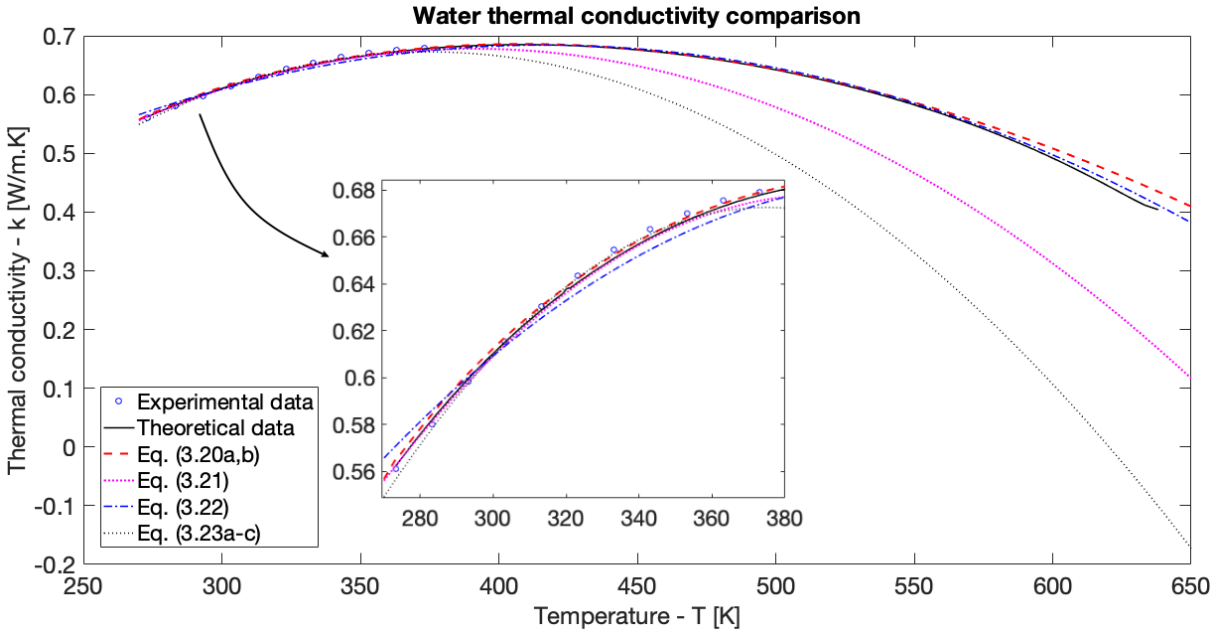

Figure 3.9: Comparison between the different formulas of the thermal conductivity and theoretical and experimental data.

To choose the most fitted formula two types of errors were used, eq. (3.24), the fractional error applied to each available data point and the root mean square error, eq. (3.25), for groups of data.

$$e = \left| \frac{\text{Predicted} - \text{Available}}{\text{Available}} \right| \times 100 \tag{3.24}$$

$$e_{\text{RMS}} = \left[\frac{1}{N} \sum_{K=1}^{N} e_K^2 \right]^{1/2} \times 100 \tag{3.25}$$

Table 3.2: Errors between thermal conductivity formulas and theoretical data [17].

Temperature interval [°C]	**e_{RMS} [%]**			
	Eq.(3.20a,b) [19]	**Eq.(3.21) [20]**	**Eq.(3.22) [21]**	**Eq.(3.23a-c) [22]**
[0,50]	0.36013	0.16553	0.65289	0.46701
[0,100]	0.29497	0.16784	0.68021	0.40763
[0,150]	0.27364	0.57054	0.62558	1.4581
[0,200]	0.25676	1.8123	0.58353	4.3735
[0,250]	0.25036	4.1934	0.57368	9.5544
[0,300]	0.37329	8.1687	0.56473	17.92
[0,365]	1.3031	13.1	0.69912	28.371

Table 3.3: Errors between thermal conductivity formulas and experimental data [18].

Temperature [°C]	**Error [%]**			
	Eq. (3.20a,b) [19]	**Eq. (3.21) [20]**	**Eq. (3.22) [21]**	**Eq. (3.23a-c) [22]**
0	0.7181	0.2264	1.7274	0.8211
10	0.7424	0.1891	1.0339	0.3332
20	0.5590	0.0247	0.2999	0.1496
30	0.2654	0.2701	0.3437	0.1128
40	0.0095	0.4676	0.8299	0.1315
50	0.2099	0.5912	1.1434	0.1709
60	0.3070	0.6315	1.2824	0.2150
70	0.3216	0.6228	1.2867	0.2940
80	0.2601	0.5819	1.1762	0.4221
90	0.1589	0.5536	0.9977	0.6432
100	0.0250	0.5521	0.7660	0.9710
e_{RMS} [%]	**0.4028**	**0.4734**	**1.0670**	**0.4799**

Since the theoretical data is very extensive and precise regarding the temperature interval measurements (consult appendix A to the complete data set) and each formula has its own domain of validity the root mean square error was computed for different incremented temperature intervals. The experimen-

tal data is the opposite therefore both errors were calculated. The results are presented in tables 3.2 and 3.3 respectively. When analysing table 3.2, eq. (3.23a-c) is easily excluded since it is the one with the highest error percentages reaching 28%, the same happens with eq. (3.21), besides the lowest values obtained in the first intervals, as of 200ºC it presents the second highest errors and it is noteworthy that even the lowest values have only approximately 0.2% of difference from the second lowest (3.20a,b). The choice is clearly between eq. (3.20a,b) and eq. (3.22) and even then it is easy to see an overall better performance in the first one. Regarding the experimental values (table 3.3) the errors by data point, e, are so inconsistent that the choice will come down to the mean error, in which eq. (3.20a,b) is once again the one with the lowest error percentage. Hence, the formula of the water thermal conductivity to be implemented in eq. (3.18) for the calculation of Γ_{qq} is set as eq. (3.20a,b).

3.1.4 Shear Viscosity

Shear viscosity, η, also very well known as dynamic viscosity, as mentioned before is crucial for the evaluation of the dissipation coefficient more specifically to the viscous dissipation coefficient in eq. (2.43a). It is thus necessary to obtain a formula for the two-phase flow shear viscosity and apply it to an air-water system. In this section, various formulas regarding the two-phase flow [23] are explored and a choice is be made. To implement the chosen formula arises the necessity of air and water viscosities, thus formulas for these parameters are studied, examining the most suitable one.

In the following equations the two-phase viscosity, η_m, satisfies an important limiting condition (3.26) related to the mass quality [23],

$$\begin{cases} x = 0, \eta_m = \eta_g \\ x = 1, \eta_m = \eta_l \end{cases} \tag{3.26}$$

where x is the mass-quality and the subscripts l and g correspond to liquid and gas, respectively. McAdams et al. [24] introduced

$$\eta_m = \left(\frac{x}{\eta_l} + \frac{1-x}{\eta_g} \right)^{-1}. \tag{3.27}$$

Based on the mass averaged value Cicchitti et al. [25] presented

$$\eta_m = x\,\eta_l + (1-x)\,\eta_g. \tag{3.28}$$

Dukler et al. [26] introduced an expression based on the kinematic viscosity,

$$\eta_m = \rho_m \left[x \left(\frac{\eta_l}{\rho_l} \right) + (1-x) \left(\frac{\eta_g}{\rho_g} \right) \right], \quad \rho_m = \left(\frac{x}{\rho_l} + \frac{1-x}{\rho_g} \right)^{-1}, \tag{3.29a,b}$$

where ρ_m is the density of two-phase gas-liquid flow [23]. Beattie and Whalley [27] proposed

$$\eta_m = \eta_g - 2.5\eta_g \left(\frac{x\rho_g}{x\rho_g + (1-x)\rho_l} \right)^2 + \left(\frac{x\rho_g\,(1.5\eta_g + \eta_l)}{x\rho_g + (1-x)\rho_l} \right). \tag{3.30}$$

Lin et al. [28] presented the following definition of two-phase viscosity

$$\eta_m = \frac{\eta_g \eta_l}{\eta_l + x^{1.4}\left(\eta_g - \eta_l\right)}. \tag{3.31}$$

Fourar and Bories [29] introduced eq. (3.32),

$$\eta_m = \rho_m \left(\sqrt{x\nu_l} + \sqrt{(1-x)\nu_g}\right)^2, \quad \nu_l = \frac{\eta_l}{\rho_l}, \quad \nu_g = \frac{\eta_g}{\rho_g}, \tag{3.32a-c}$$

where ν_l and ν_g are the kinematic viscosities of liquid and gas, respectively. Lastly, in [23] is described a new expression derived by analogy with Maxwell-Eucken thermal conductivity formula.

$$\eta_m = \eta_l \frac{2\eta_l + \eta_g - 2\left(\eta_l - \eta_g\right)(1-x)}{2\eta_l + \eta_g + \left(\eta_l - \eta_g\right)(1-x)}. \tag{3.33}$$

In similarity to what was done for the water thermal conductivity, the assessment of the best definition of two-phase flow viscosity should rely on errors formulations, however in this case there is no direct experimental data on the two-phase viscosity, hence other method has to be applied.

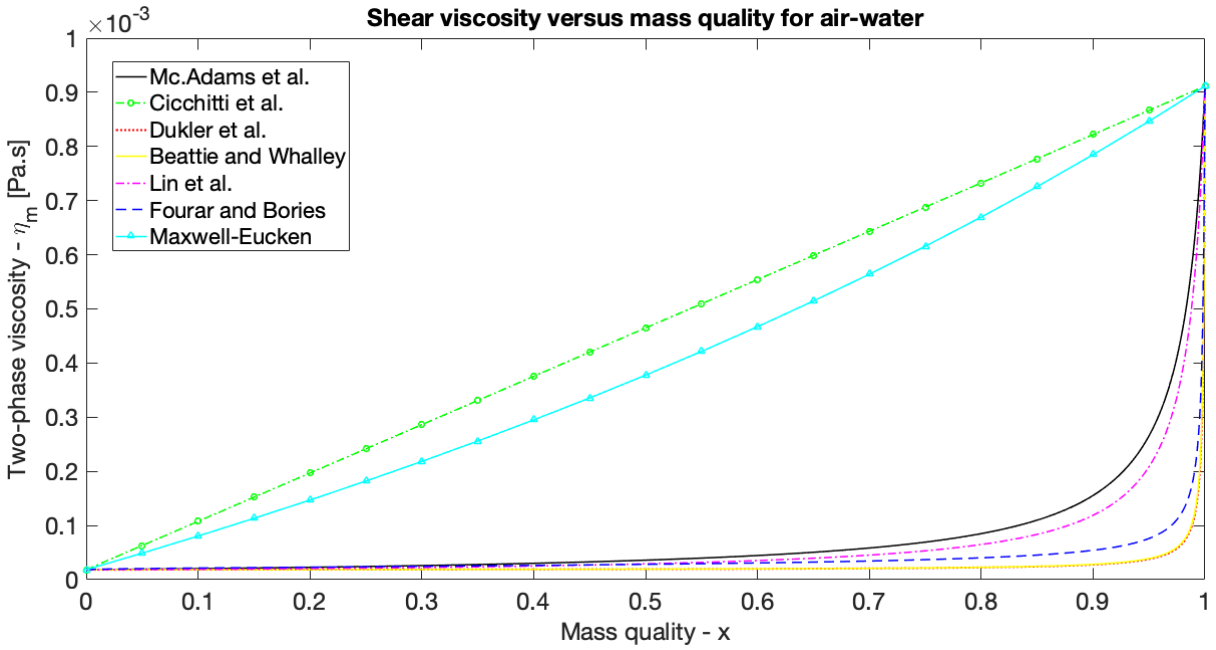

Figure 3.10: Two-phase shear viscosity formulas in order to mass quality for air-water system.

In fig. 3.10 it is presented a comparison between eqs. (3.27)–(3.33) as a function of the mass quality. While analysing the comparison it is possible to divide the viscosity formulas into two groups, one composed by eqs. (3.28) and (3.33), approximately linear and the remaining ones, approximately with an exponential form. It is important to understand this separation and what it means in terms of viscosity, eq. (3.33), proposed in [23] is suitable for materials in which the thermal conductivity of the continuous phase is higher than the thermal conductivity of the dispersed phase, this means that the heat flow avoid the dispersed phase and the dominant phase is the liquid one [23]. The second group of formulas ex-

press the opposite, where the dominant phase is the gas and the heat flow involves this phase as much as possible, with lower thermal conductivities for the continuous phases and higher for the dispersed ones [23]. With this explanation in mind it is possible to relate the first group of viscosities as being the most suitable group for this specific flow resuming the choice to eqs. (3.28) and (3.33).

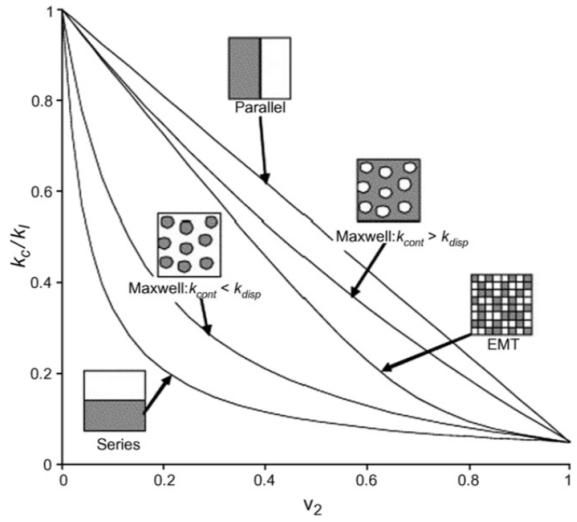

Figure 3.11: Two-phase conductivities [23].

Figure 3.11 besides working as a mirror in comparison to our results in fig. 3.10 it is a good decision tool, it presents the division of the two viscosity groups as well as their explanation in terms of conductivity that is defined as analogous to the viscosity. In the case of water spray systems implemented on launch pads the flow it is not a simple kind of spray jet, it is instead a system able to inject thousands of litres in just a few seconds, thus from the interpretation of fig. 3.11 these systems are more likely to behave as a parallel conductivity, linked to eq. (3.28).

In fig. 3.12 there is a demonstration of the behaviour of the chosen formula regarding temperature and concentration. The last step to define the two-phase flow viscosity is the computation of water and air shear viscosities.

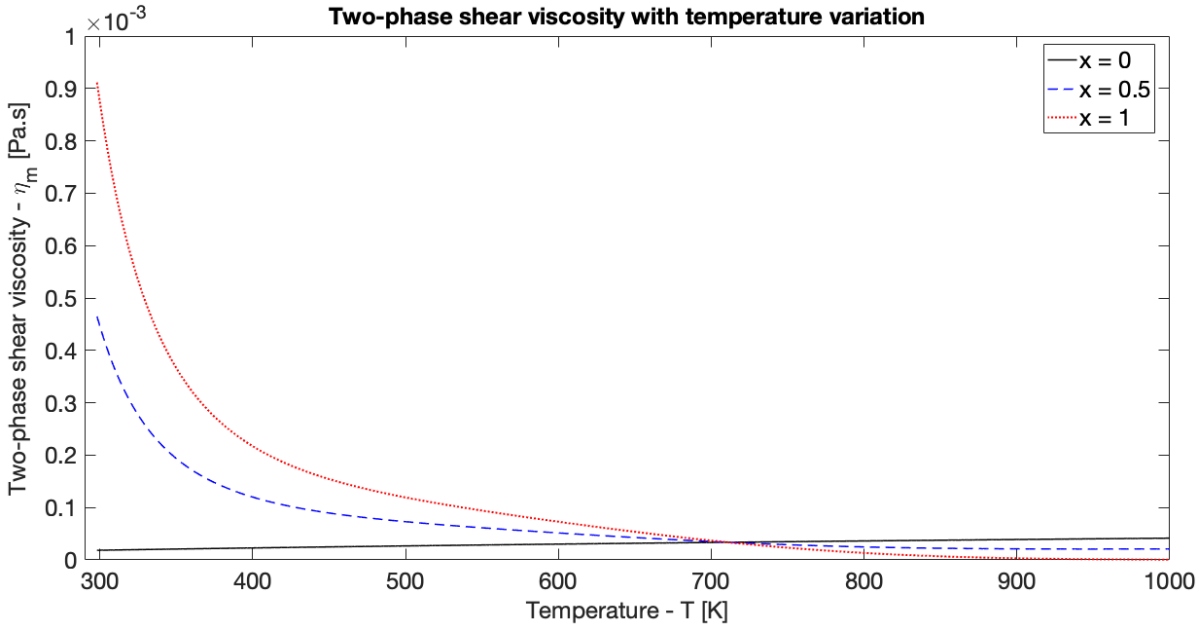

(a) η_m with temperature variation for multiple values of mass quality.

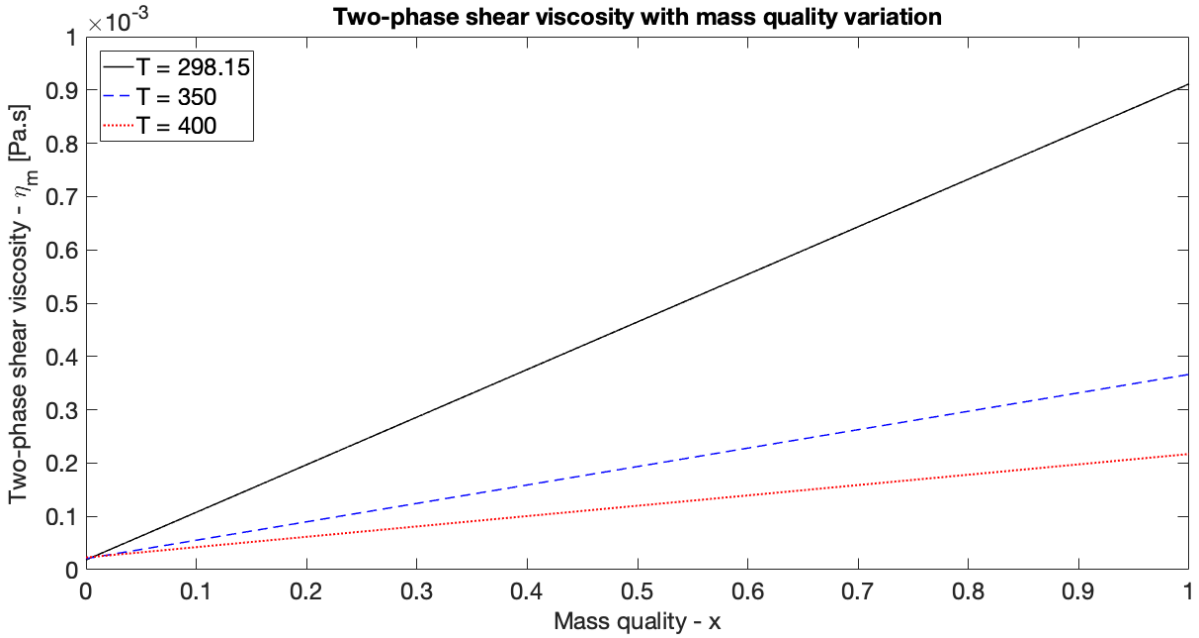

(b) η_m with temperature variation for multiple values of temperature in [K].

Figure 3.12: Temperature and concentration dependence of the two-phase shear viscosity, η_m.

Gas viscosity

With respect to air viscosity there are undoubtedly two main formulas for its calculation, therefore only those are subject to discussion. The commonly used eq. (3.34a,b) refers to Sutherland's Law [30, 31] proposed by Sutherland [30] in which η_0 is a known viscosity at a known temperature T_0.

$$\eta_g = \eta_{0_g} \left(\frac{T}{T_0} \right)^{3/2} \frac{T_0 + S}{T + S}; \quad \begin{cases} \eta_{0_g} = 1.716 \times 10^{-5}\,[\text{Pa} \cdot \text{s}], \\ T_0 = 273\ \text{K}, \\ S = 110.4\ \text{K}. \end{cases} \tag{3.34a,b}$$

Equation (3.35) known as Power Law [31], also a very common approximation, has the same reference temperature and viscosity values of eq. (3.34b).

$$\eta_g = \eta_{0_g} \left(\frac{T}{T_0} \right)^{2/3}, \tag{3.35}$$

In both formulas (3.34a,b) and (3.35) there is no mention to the pressure due to the fact that viscosity is strongly affected by temperature changes but pressure only has a moderate effect on it. The viscosity in both gases and liquids has a slow increase with pressure, but this effect is only felt upon 101.325 $\times 10^5$ Pa, being possible to neglect it [31]. Gas viscosity increases with temperature as is possible to observe from fig. 3.13, comparing both equations (3.34a,b) and (3.35) with known values (available in appendix B). In table 3.4 are presented the errors regarding these values.

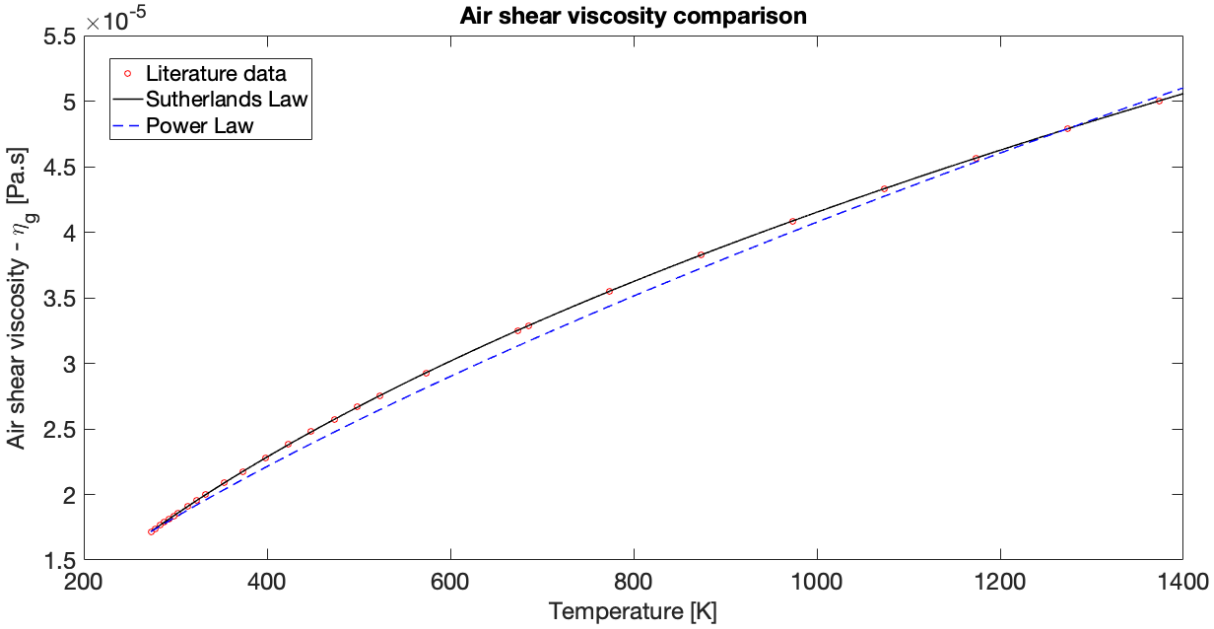

Figure 3.13: Air shear viscosity comparison.

After analysing the results the choice is obvious, Sutherland's Law (3.34a,b) is the one with the lowest percentage of error in all the intervals studied.

Table 3.4: Air shear viscosity error

Temperature Interval [°C]	e_{RMS} [%]	
	Eq. (3.34a,b)	**Eq. (3.35)**
[0,50]	0.0471	0.9525
[0,100]	0.0418	1.4742
[0,200]	0.0448	2.1802
[0,500]	0.0520	2.6758
[0,1100]	0.0466	2.4735

Liquid viscosity

The calculation of water viscosity is not so clear from the literature as that of air, hence some more formulas need to be analysed in order to find the one most suitable for this work purpose. The first to be studied is (3.36a,b) where the constants are determined for a temperature domain between 0 and 150° C [19],

$$\eta_l = \frac{1}{A + BT + CT^2 + DT^3} \text{ [Pa} \cdot \text{s]}; \quad \begin{cases} A = 557.825, \\ B = 19.409, \\ C = 0.136, \\ D = -3.116 \times 10^{-4}. \end{cases} \tag{3.36a,b}$$

Poiseuille [32] presented the following early formula for pure water shear viscosity in millipoise[1] [33],

$$\eta_l = \frac{17.8}{1 + 0.0377T + 0.00022T^2} \text{ [mP]}. \tag{3.37}$$

It should be pointed out that eqs. (3.36a,b) and (3.37) must be calculated in degree Celsius since their constants have been computed using this unit. Equation (3.38a,b) is derived from experimental values, it is valid within the 273.15 and 643 K temperature range and is given in centipoise[2] [21],

$$\log_{10} \eta_l = A + \frac{B}{T} + CT + DT^2 \text{ [cP]}, \quad \begin{cases} A = -10.2158, \\ B = 1.7925 \times 10^3, \\ C = 1.7730 \times 10^{-2}, \\ D = -1.2631 \times 10^{-5}. \end{cases} \tag{3.38a,b}$$

[1] 1 mP = 1×10^{-4} Pa·s
[2] 1 cP = 1×10^{-3} Pa·s

From White [31] appears the following logarithmic function,

$$\ln \frac{\eta_l}{\eta_{0l}} = A + B\left(\frac{T_0}{T}\right) + C\left(\frac{T_0}{T}\right)^2 \text{ [Pa} \cdot \text{s]}, \quad \begin{cases} \eta_{0l} = 1.792 \times 10^{-3} \text{ [Pa} \cdot \text{s]}, \\ T_0 = 273.16 \text{ [K]}, \\ A = -1.94, \\ B = -4.80, \\ C = 6.74. \end{cases} \tag{3.39a,b}$$

Once again, similarly to air viscosity, the pressure was not considered for the same reasons, only above 1 MPa does the pressure affects viscosity, below that its effect does not exceed $\pm$0.2% [19]. A comparison between the different formulas (3.36a,b)–(3.39a,b) relatively to water shear viscosity data (appendix A) is found in fig. 3.14 where as expected the liquid viscosity decreases with temperature in an exponential way. It is also possible to find the resulting errors for the same comparison in tables 3.5 and 3.6.

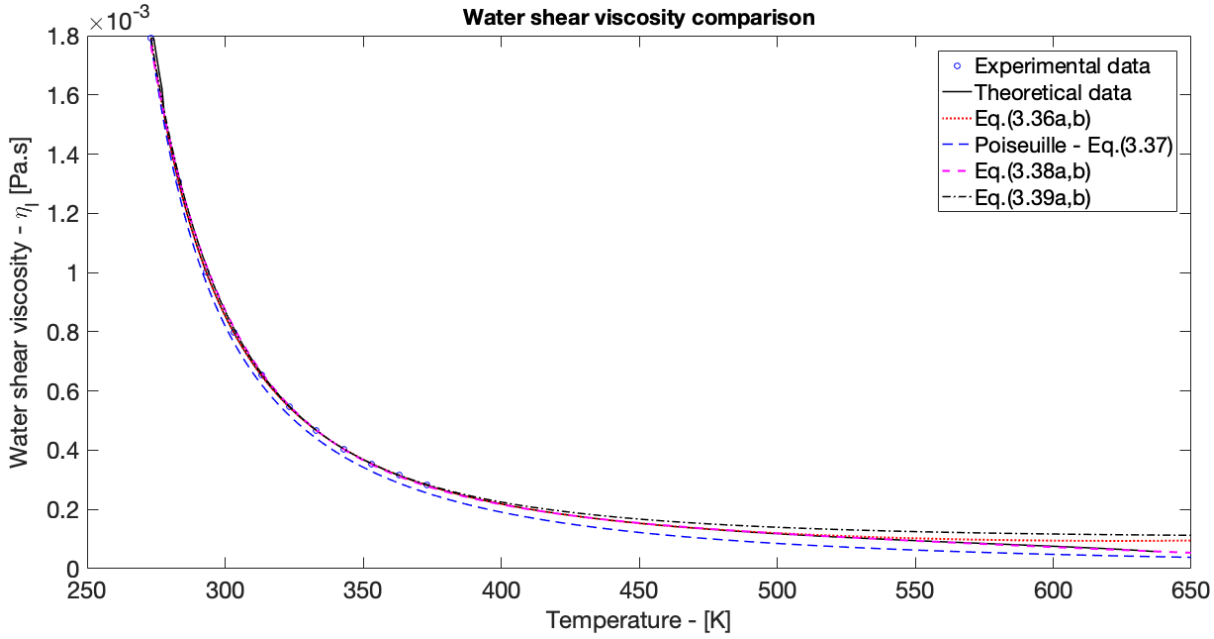

Figure 3.14: Water shear viscosity comparison.

Table 3.5: Water shear viscosity error regarding theoretical data [17].

Temperature Interval [°C]	e_{RMS} **[%]**			
	Eq. (3.36a,b)	**Eq. (3.37)**	**Eq. (3.38a,b)**	**Eq. (3.39a,b)**
[0,50]	0.9067	3.9638	2.0695	1.7320
[0,100]	0.6472	5.7644	1.5487	1.2589
[0,200]	0.5380	10.789	1.3346	4.2435
[0,250]	0.9826	14.417	1.2990	8.1124
[0,300]	3.2871	17.925	1.2718	13.732
[0,365]	9.6630	19.362	1.4528	21.084

Table 3.6: Water shear viscosity error regarding experimental data [18].

Temperature [°C]	**Error [%]**			
	Eq. (3.36a,b)	**Eq. (3.37)**	**Eq. (3.38a,b)**	**Eq. (3.39a,b)**
0	0.0180	0.7250	1.4885	0.0240
10	0.0124	2.6521	1.4061	1.7901
20	0.0078	3.5588	2.3363	2.1000
30	0.0408	4.1900	2.1731	1.6762
40	0.0641	4.7187	1.5698	1.0720
50	0.0696	5.2660	0.8366	0.5185
60	0.0553	5.8794	0.1512	0.1375
70	0.0378	6.5944	0.4121	0.0376
80	0.0003	7.4009	0.7962	0.0394
90	0.0071	8.3437	1.0409	0.3052
100	0.0299	9.3754	1.1095	0.7968
e_{RMS} **[%]**	**0.0388**	**5.863**	**1.3711**	**1.0699**

In regard to table 3.5, Poiseuille (3.37) and White (3.39a,b) formulas are the first ones to be discarded due to the very high percentage of error, mainly for higher temperatures. While eq. (3.36a,b) has the lowest error values until 250°C, above this the errors become larger, whereas eq. (3.38a,b) has some larger errors yet above the same limit the error does not increase as much. Relative to the data presented in table 3.6, eq. (3.36a,b) has by far the best results with the smallest error percentage; however when analysing it outside its scope of validity it was found a deficiency, pictured in fig. 3.15.

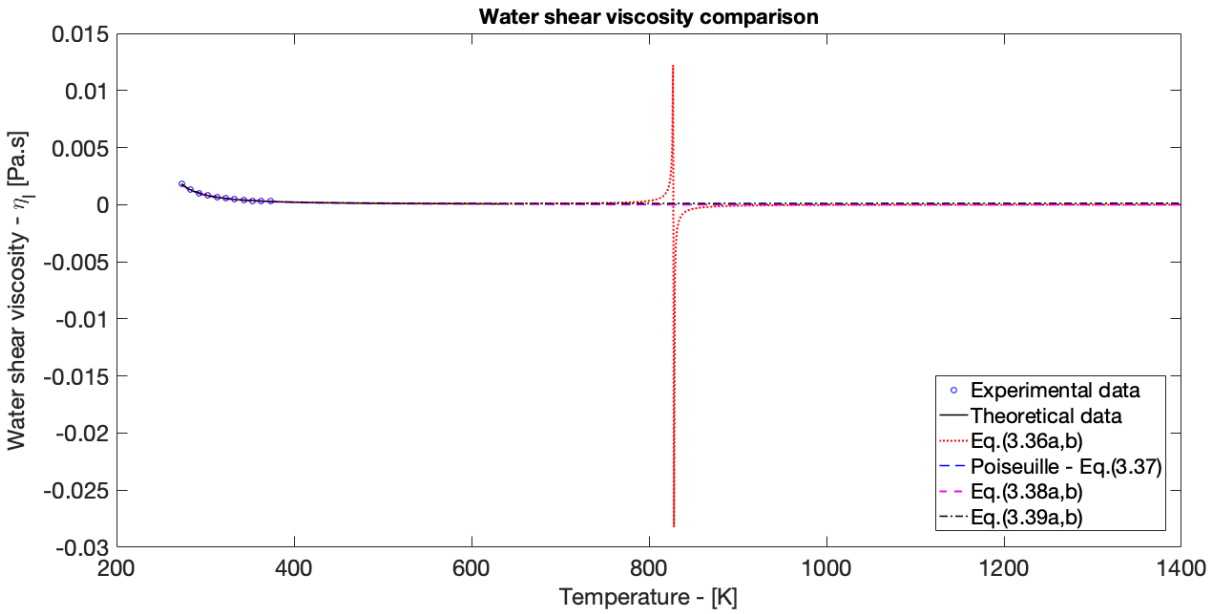

Figure 3.15: Water shear viscosity.

Equation (3.36a,b) represented by the red dotted line presents an unexpected peak at approximately 827 K, the use of this formula would compromise all the following calculations for temperatures in a range of validity of values containing this peak. Despite eq. (3.39a,b) having the second best results, the experimental values in table 3.6 are much lower than the theoretical ones that were tested in table 3.5 where this formula was immediately discarded, it is actually possible to notice that until 100°C the percentage of error is very reliable and the problem happens for higher temperatures and it is necessary to have this in account when choosing a feasible formula. In this way, eq. (3.38a,b) is chosen as the most fit for the purpose.

3.1.5 Bulk Viscosity

In liquids and gases, molecules have translational, rotational and vibrational degrees of freedom. Whilst the shear viscosity is associated with the translational motion, the bulk viscosity ζ, also known as volume viscosity among many other names, it concerns to the relaxation of both rotational and vibrational degrees of freedom [34]. The two viscosities combined control sound attenuation. Its existence was first assumed as a possibility by Stokes in 1845 but at that time there was no method for measuring it, and during many years it was completely discarded from theoretical calculations. However, despite its fundamental role, even today no consistent and widely accepted method has yet been developed, with sparse experiments based on different methods there is a paucity of data in the literature regarding this topic. One of the biggest issues in testing theories is not only the already mentioned scarcity of experimental measurements but also the lack of precision from the existing ones due to the fact that the bulk viscosity cannot be measured directly, in fact it must be derived from other quantities measurements such as the

sound absorption coefficient, α, based on Stokes' law of sound attenuation [35–37],

$$\alpha = \frac{\omega^2}{2\rho v^3}\left(\frac{4}{3}\eta + \frac{\gamma - 1}{c_P}\kappa + \zeta\right). \tag{3.40}$$

The calculation of bulk viscosity is important in this specific work because as stated in section 3.1.4 it is necessary in eq. (2.43a) to obtain the viscous dissipation coefficient, meaning that in order to calculate it, the bulk viscosity is needed but to obtain this viscosity the absorption coefficient is required, leading to a contradiction. In this way, formulas like the one in eq. (3.40) are not what is needed, instead it would be advantageous to have a formula in which the bulk viscosity depends on temperature.

There are three possible experimental techniques that can be used to measure the bulk viscosity, the Brillouin spectroscopy, laser transient grating spectroscopy and acoustic spectroscopy. As shown by Dukhin et al [34] the acoustic spectroscopy is the most suitable method and since it depends directly on the acoustic attenuation is the only one to have a validation procedure for the measured parameter while using the theoretical definition (3.40). Similarly to the phenomenological coefficients in section 3.1.2 with the scarcity of theoretical formulas and experimental results for fluids in general it is expected not to have data or even a theoretical equation describing the behaviour of a two-phase flow when there is still not a full comprehension for most of the molecular flows. Hence, in this section it is defined a bulk viscosity formula for water, present in the spray system. Later on, the values obtained for water are compared with the experimental values of air bulk viscosity to relate their order of magnitude.

Holmes et al [36] made an experiment using acoustic spectroscopy, the most qualified method, to study the water bulk viscosity temperature dependence. With the results obtained it were determined two possible equations (3.41a,b) and (3.42a,b) to fit the data,

$$\zeta = A\exp\left(-BT\right), \quad \begin{cases} A = 5.091712 \times 10^{-3}, \\ B = 2.545425 \times 10^{-2} \end{cases} \tag{3.41a,b}$$

$$\zeta = A + BT + CT^2 + DT^3, \quad \begin{cases} A = 5.94068 \times 10^{-3}, \\ B = -2.37073 \times 10^{-4}, \\ C = 4.94789 \times 10^{-6}, \\ D = -3.97502 \times 10^{-8} \end{cases} \tag{3.42a,b}$$

The first one (3.41a,b), is based on a common exponential model for shear viscosity where the results obtained closely follow the model, while eq. (3.42a,b) is a cubic expression better fitting to the data [36]. The results obtained are presented in fig. 3.16 comparing with some of the existing data on literature. In what concerns the experimental data, all the values used for this comparison and calculations are contained in appendix A. Leonard Hall [38] computed this kind of values in 1947 but they can not be considered experimental values since the absorption coefficient was calculated by means of theoretical formulas and then implemented in eq. (3.40), thus the Hall data is here used as a base of comparison

for the more recent experimental values regarding the older theoretical ones. After careful analysis of fig. 3.16 there are some facts worth mentioning, eq. (3.42a,b) does in fact adjust better to the data than eq. (3.41a,b) as can be seen in table 3.7 by the error percentage obtained. Nonetheless Holmes experiment has a temperature range from 7 to 50°C and it is well known that the temperatures during this work achieve a much higher value, when analysing the curve for Holmes cubic expression (3.42a,b) is easily observed that the curve is well adjusted to the measurements but upon that it decays rapidly, tending to infinity, turning it unfeasible for usage as it would compromise all the calculations in need of this parameter. With eq. (3.41a,b) there is not this problem any more, the error is bigger but the difference relatively to eq. (3.42a,b) is just of 4.31% having a total error of 4.77% which is acceptable, even more so having in mind that there are not many experimental values that can be used for comparison and even the existing ones have some differences between them. Xu et al [39] is an example, in their experiment the Brillouin scattering method was implemented and a temperature range of 2 to 35°C was tested, the results in similarity with the ones from Litovitz et al [37] and Dukhin et al [34] are not quite the same as the ones from Holmes experiment, however it is important to note that all experimental values are very close to each other and so the existing data, although being sparse, it is very consistent.

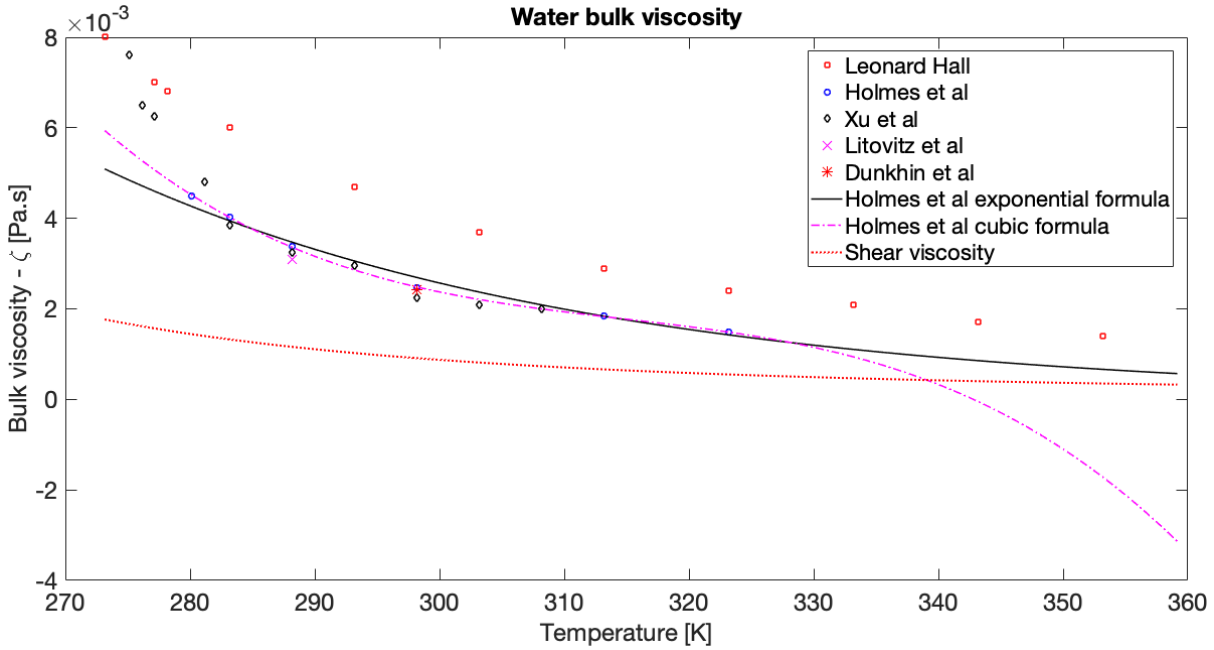

Figure 3.16: Bulk viscosity comparison.

The shear viscosity, the red doted curve, is present in fig. 3.16 as a comparison tool between both viscosities. Bulk viscosity was neglected during many years and its value assumed as zero in most of the calculations, yet it is clear that this parameter cannot be neglected and instead has a bigger value than the dynamic viscosity. In fact it is approximately three times larger than its shear counterpart throughout the experimental temperature range. With increasing temperature the exponential formula for the bulk viscosity leads to a decrease in a monotonic form, as for the shear viscosity; however in the experimental data it tends to the same values as the dynamic viscosity. More data would be needed over a wider temperature range to study this behaviour. Thus, eq. (3.41a,b) is considered to have the best fit

and it is implemented throughout the following work, mainly based in the fact that acoustic spectroscopy achieve better results than Brillouin scattering [34].

Table 3.7: Bulk viscosity error.

Available data	e_{RMS} **[%]**	
	Holmes exponential - Eq. (3.41a,b)	**Holmes cubic - Eq. (3.42a,b)**
Leonard Hall [38]	40.202	81.019
Holmes et al [36]	4.770	0.455
Xu et al [39]	18.970	13.255

Table B.1, included in appendix B, contains experimental values on the air bulk viscosity that allows a comparison with the values obtained for water. While the water takes values on the order of 10^{-3} as seen in fig. 3.16, the air bulk viscosity is on the order of magnitude of 10^{-5} [40]. There is still a large difference between the two orders of magnitude, with air having the lowest value; the initial assumption of considering water, instead of air, as the predominant phase for viscosity it is now substantiated. It is known, nonetheless, that the bulk viscosity of air should be considered at a later stage since it will always influence the two-phase bulk viscosity.

3.2 Computational Implementation

After the theoretical implementation it is necessary to implement the formulas derived in the previous section (3.1) and perform the respective calculations, obtaining the desired results. In order to do that with the highest degree of confidence a mathematical tool, was developed on the MATLAB software. It is important to emphasize that the code implemented is used only as a tool developed with the intent of perform the calculations without the common human errors that come with more complicated and extensive calculations. The computational tool is used to compare the results obtained with the existing data in the literature, calculate the error between them and hence validate the formulas implemented and obtain a graphic representation of the various results and equations. In this section is given an overview on how the computational tool was developed, works and which results it leads to.

Multiple MATLAB functions were developed, each one responsible for a specific area of calculation; next is given an explanation on each of the functions as well as some caution that must be taken into account. It is noteworthy that the majority of the functions have one common feature, namely all of them apply over a set of temperature and concentration intervals as well as for a specific point in temperature and concentration, showing the variation with the two most important variables in study.

chemical_potential Definition and calculation of the chemical potential and the relative chemical potential from eqs. (3.3) and (3.4). Incorporation of the following two functions also related with chemical potential to maintain the subject in only one global equation. The functions related to the chemical potential and hence, with eq. (3.3) have to be used with a certain caution since it is a logarithmic expres-

sion. In particular it is necessary to be careful with the concentration, ξ, present in the numerator of the logarithm, that can not have a zero value as that would create a NaN response.

chemical_potential_temperature Obtaining of the formula for the derivative of the relative chemical potential in order to temperature and posterior calculation. In this case, since the derivative only depends on the concentration (3.5b) the calculation for a temperature interval is not available. This derivative is the only that maintains the logarithmic expression thus maintaining the necessity of the previously described caution.

chemical_potential_concentration Obtaining of the formula for the derivative of the chemical potential in order to temperature (3.5a), its calculation and graphical representation.

shear_viscosity_water Implementation of eqs. (3.36a,b)–(3.39), call of the theoretical and experimental data, from Excel files previously created, these files contain temperature and viscosity values. The data is stored into vectors and through the use of for cycles the viscosity values, for each of the equations implemented, is calculated for the respective theoretical and experimental temperatures. The results obtained are compared with those from the files calculating the error from eq. (3.24). The fractional error is written in table format and it is transferred to a text document that is posteriorly saved on the computer. The process is repeated for the root mean square error (3.25). Plot of the multiple equations and data available for a graphical comparison. Definition of eq. (3.38) as the liquid viscosity.

shear_viscosity_air The exact same process implemented before for water shear viscosity but this time with eqs. (3.34a,b) and (3.35). Both viscosities depend only on the temperature as can be seen by their equations, so once again it is not possible to apply concentration variation.

shear_viscosity_two_phase This function acts as a mother function for viscosity calling the two last described and viscosity related functions. Definition of the two-phase density and kinematic viscosities from eqs. (3.29b) and (3.32b,c) and all the two-phase viscosity models to be studied, eqs. (3.27)–(3.33). Graphical comparison of the multiple models and definition of the chosen one as the two-phase shear viscosity. In this case, it remains the calculations for temperature intervals and the mass quality on which the viscosity depends acts as a concentration variation.

bulk_viscosity Reading of the Excel file with theoretical and experimental data and storage of the values in vector format. Call of the water shear viscosity function only for graphical comparison purposes. Definition of the exponential bulk viscosity equation (3.41a,b) and the cubic expression (3.42). Calculation and writing of the errors in the exact same form as in water and air shear viscosity. Graphical comparison between Holmes et al expressions, water shear viscosity and the data from the file. Definition of the exponential expression as the bulk viscosity, dependent only on the temperature.

thermal_conductivity_water Definition of the temperature as mean temperature, as already explained on section 3.1.3 and definition also of the multiple formulas for water thermal conductivity (3.20a,b)–(3.23). Reading of the Excel file with theoretical and experimental data with posterior error calculation, once again as calculated in the viscosities. Graphical comparison of the models studied and data available, definition of the chosen formula as the water thermal conductivity.

onsager_coefficients Definition of exterior and mean temperature as well as temperature variation; exterior chemical potential as the relative chemical potential previously calculated; system chemical potential and chemical potential variation, regarding temperature and concentration. Call of the water thermal conductivity. Implementation and calculation of eqs. (3.16)–(3.18). In this case, Γ_{12} does not depend on the concentration thus, only being calculated for intervals of temperature. During the calculation of the coefficients it is necessary to have some caution: $\Gamma_{22} = \Gamma_{jj}$ (3.16) depends on the variation of the chemical potential, so once again the concentration can not be equal to zero, besides that since this variation is in the denominator of the coefficient it can not have a zero value, this means that the exterior chemical potential can not be equal to the one from the system, considered as the standard chemical potential of water thus, the concentration must not achieve the 1000 mol/m^3 since it would return the logarithm as zero; $\Gamma_{12} = \Gamma_{qj}$ (3.17) has the temperature variation in the denominator, which means that if there is no temperature difference, the variation will have a zero value and the expression will be undefined hence, the exterior temperature must be higher that the one from the system; Since $\Gamma_{11} = \Gamma_{qq}$ depends on both the previous coefficients the same previously cautions must be taken into account.

conductivity_overbar Definition and calculation of the conductivity defined in eq. (2.83c). This conductivity depends on Γ_{11}, Γ_{12} and Γ_{22} the already mentioned precautionary measures are applied here as well.

coupling_alpha Definition and calculation of the thermal cross-coupling coefficient from eq. (2.89c). The α coefficient, depends on Γ_{12}, Γ_{22} and $\frac{\partial \mu}{\partial T}$ so both temperature variation and chemical potential logarithmic cautions apply.

conductivity Definition and calculation of the thermal conductivity described in eq. (2.92b). Once again, dependence on Γ_{12} and Γ_{22} requires the same careful.

mass_diffusion Definition and calculation of the mass diffusion coefficient defined in eq. (2.89c). This coefficient depends on $\frac{\partial \mu}{\partial \xi}$, that is not a logarithmic expression, however it depends on Γ_{22} that presents the variation in temperature and in chemical potential.

coupling_beta Definition and calculation of the mass diffusion cross-coefficient from eq. (2.92c). The β coefficient will also depend on temperature and chemical potential variation.

dampings Definition of the acoustic damping, ε, normalized by the Doppler shifted frequency squared ($\overline{\omega}^2$). The total damping is divided into three more specific dampings that are firstly defined and calculated and only then combined to obtain the total acoustic damping, the final result. The thermal damping (2.42d) is defined and calculated, secondly the viscous damping (2.43a) and thirdly the mass diffusion damping (2.43b). Lastly, it adds up the three dampings obtaining the total acoustic damping in order to temperature, concentration, mass quality and pressure. The thermal damping, depends on the conductivity and its mathematical restrictions as well as the mass diffusion damping that depends on the mass diffusion cross-coefficient, β. The only one that does not have any restrictions regarding temperature or concentration is the viscous damping.

Thesis_main This is the main file, the one that generates all the calculations described until now. In this function it must be inserted the manual inputs with all the values for which it is necessary to perform the calculations: exterior temperature, system temperature, concentration, pressure, mass quality and water flux specific points and temperature, concentration, pressure and mass quality intervals. This file contains also the standard values necessary, specifically chemical potential, water and air density, adiabatic exponent, molecular mass of water, ideal gas constant, reference temperature, pressure and concentration, these values must not be changed since they are specified accordingly to literature and the demands of the theoretical models used throughout all the calculations.

As it could be seen, there are some mathematical constraints in the calculations derived from the models used that can not be bypassed. Besides, in section 3.1 was defined the domain of validity of each of the formulas used, that should always be respected in order to obtain the best results possible from the equations.

All of the above functions have the option to display a graphical representation concerning the dependence on the temperature and concentration variation, if dependent of both parameters; otherwise it has only the representation for the one dependent parameter. However, since the acoustic damping is the main result, and the most important to study and analyse it is the only one to be displayed, for each of the damping components and the total damping, as plots for temperature and concentration intervals, and as a numerical value for a specific point in temperature and concentration. The remaining graphical representations are disabled and can be enabled, removing the comments, whenever one desires to analyse that specific calculation/result. Figure 3.17 depicts a flowchart of the mathematical tool in its final form where only the acoustic damping results are displayed.

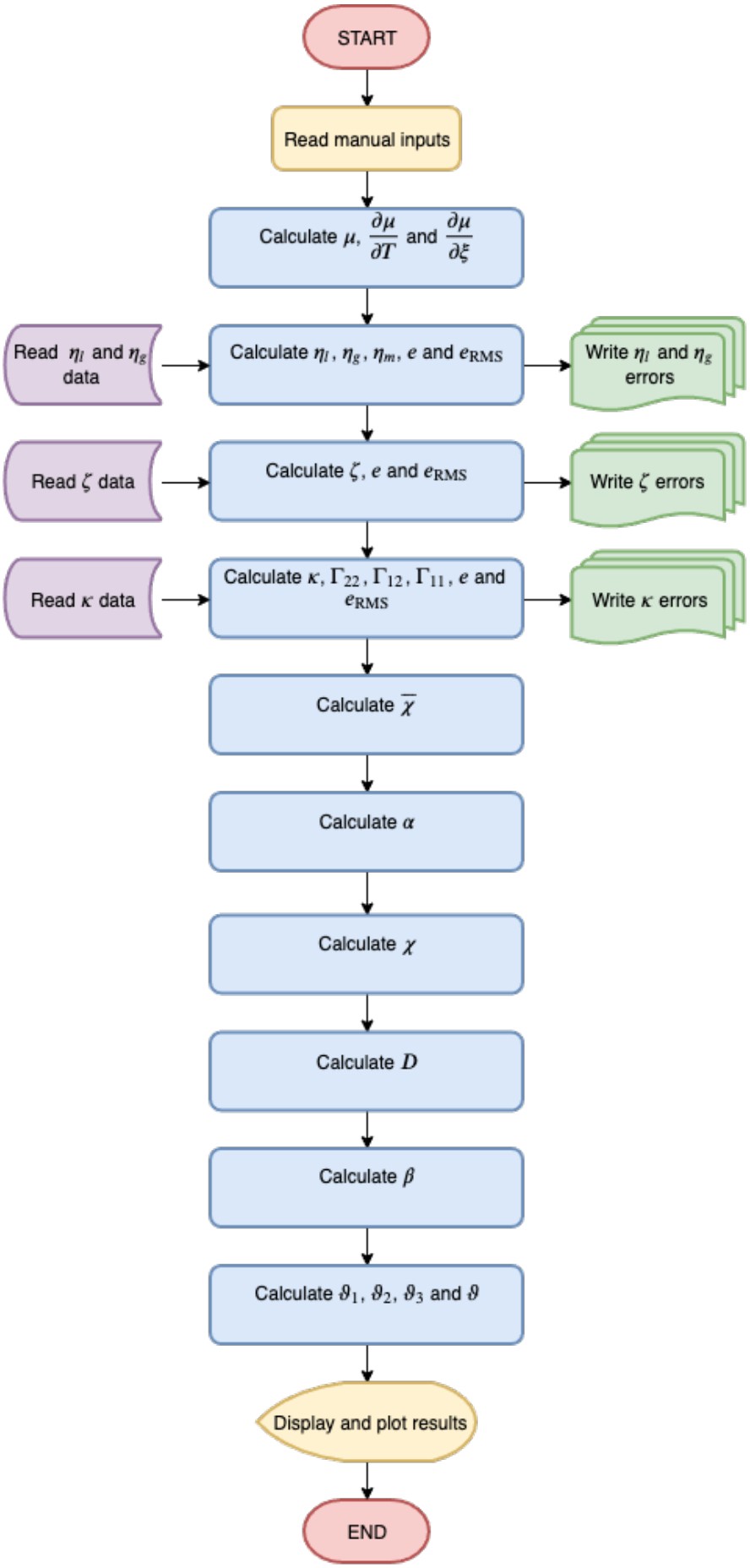

Figure 3.17: Flowchart of the mathematical tool.

Chapter 4

Results

While in chapter 3 was developed the first step of the objectives proposed in section 1.3, in this section is presented and discussed the results obtained regarding the fulfilment of the second (section 4.1) and third (section 4.2) steps represented in fig. 1.4. It is important to state that in the results presented in this chapter when a parameter is not varying it has a fixed and standard value that is used throughout the calculations; those reference values, are presented in the next table (table 4.1).

Table 4.1: reference values used during the results calculation.

Parameter	Reference value
Exterior temperature	25ºC
System temperature	23ºC
Concentration	100 mol/m^3
Pressure	101325 Pa
Mass quality	0.5
Water flow	57000 kg/s

4.1 Thermal and Mass Kinetic Coefficients

4.1.1 Conductivity - $\overline{\chi}$

The first coefficient from chapter 2 to be obtained is the thermal conductivity expressed in eq. (2.83c) and recalled next.

$$\overline{\chi} = \frac{1}{T^2}\left[\Gamma_{11} - \frac{(\Gamma_{12})^2}{\Gamma_{22}}\right] > 0. \tag{4.1}$$

The first detail to pay attention to from figs. 4.1 and 4.2 is that both feature a positive conductivity value as it is imposed by eq. (4.1). With regard to temperature variation (fig. 4.1) the result is as expected for a liquid: a decreasing value with increasing temperature. However, it is important to note that the formula in eq. (4.1), for $\overline{\chi}$, does not coincide with the conductivity χ, that is discussed subsequently in

section 4.1.4. The concentration does not have a significant impact in the variation of the conductivity, in fact it is negligible, as can be seen from fig. 4.2, after all it is a thermal coefficient and so it is normal for the major effect to come from temperature.

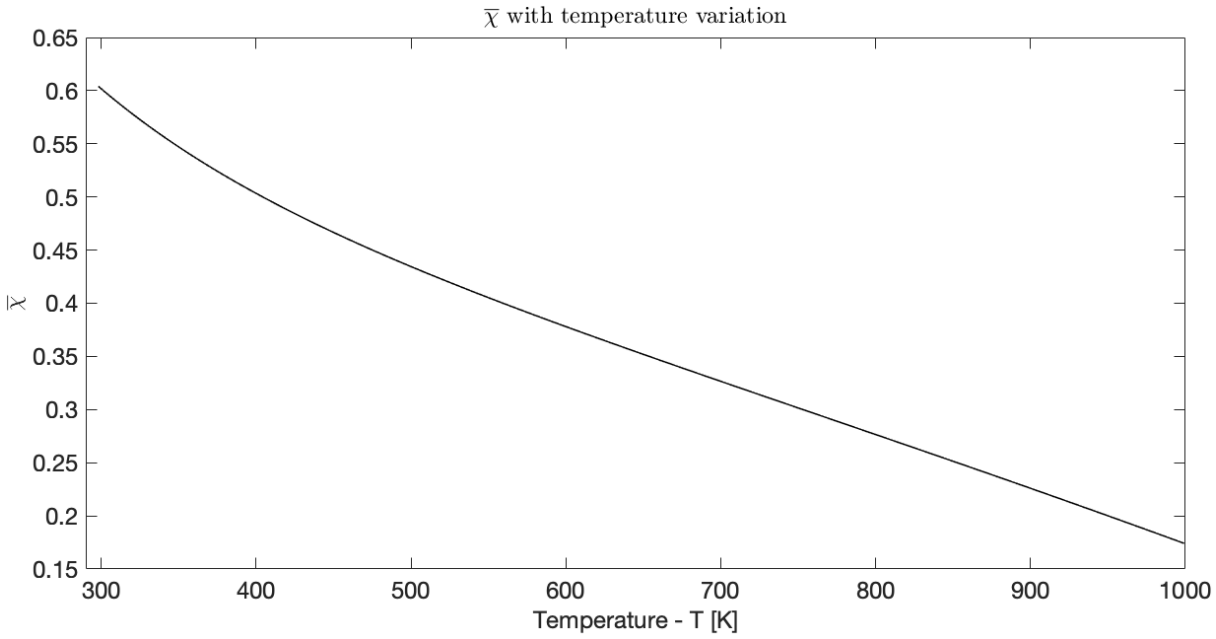

Figure 4.1: Conductivity $\overline{\chi}$ with temperature variation.

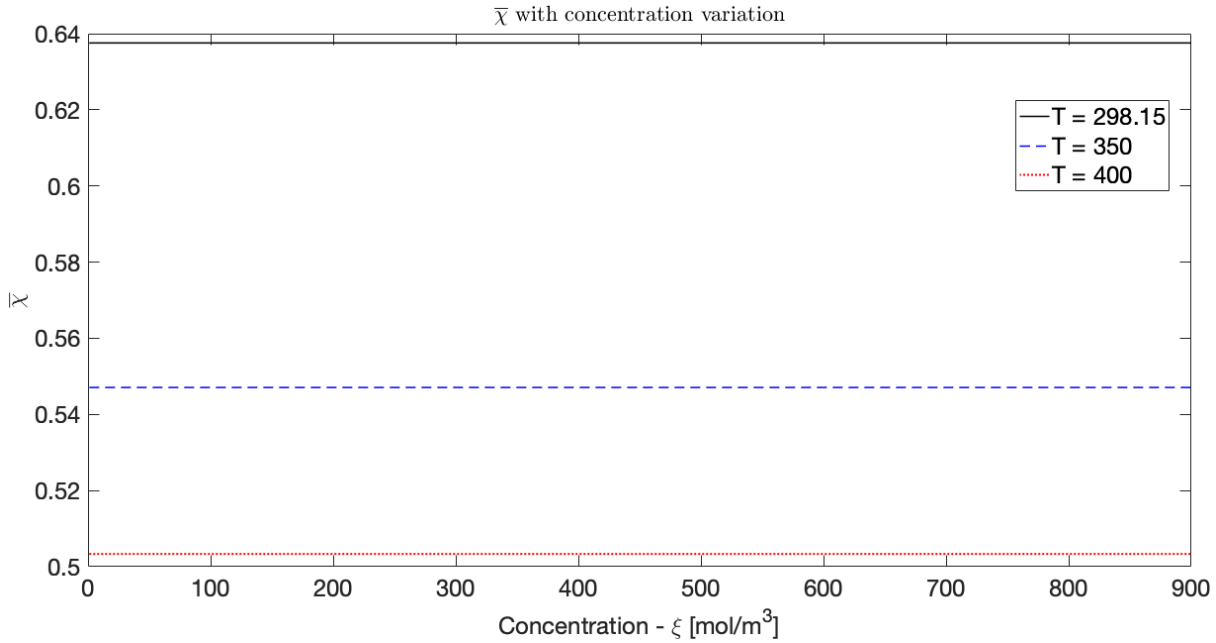

Figure 4.2: Conductivity $\overline{\chi}$ with concentration variation for multiple temperature values in [K].

4.1.2 Mass Diffusion Coefficient - D

The mass diffusion coefficient from eq. (2.89b), also presented in eq. (4.2), depends on the chemical potential derivative, $\frac{\partial \mu}{\partial \xi}$, while this parameter increases with temperature (fig. 3.2a), Γ_{22} from which D

also depends, decreases with temperature (fig. 3.4) and in this case the predominant effect comes from the latter, with the mass diffusion coefficient slightly decreasing with increasing temperature.

$$D \equiv \frac{\Gamma_{22}}{T} \left(\frac{\partial \mu}{\partial \xi} \right)_T . \tag{4.2}$$

Relatively to water flow (fig. 4.4), the mass diffusion coefficient increases with the amount of flow, agreeing with Fick's Law expressed in eq. 2.7b.

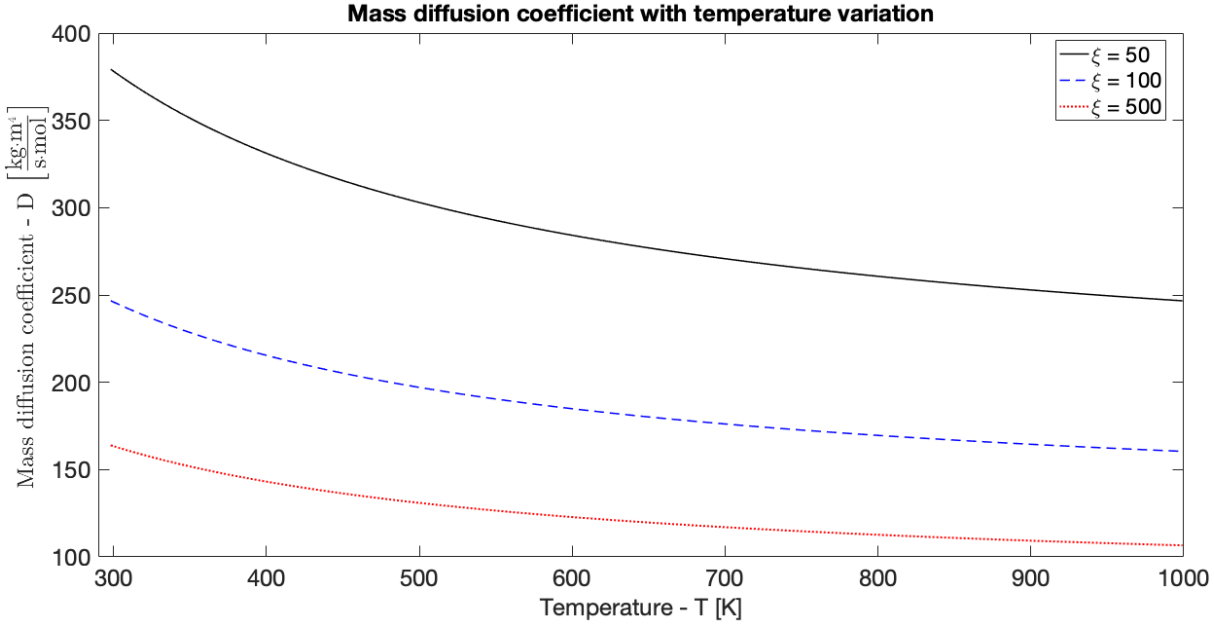

Figure 4.3: Mass diffusion coefficient D with temperature variation for multiple concentration values in [mol/m^3].

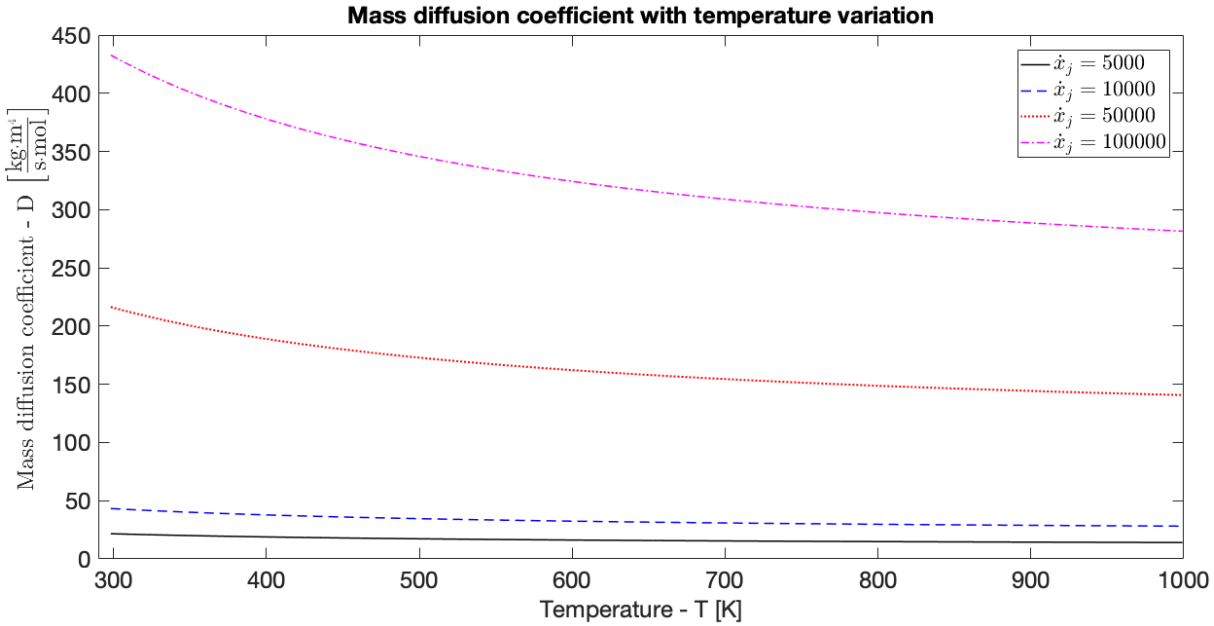

Figure 4.4: Mass diffusion coefficient D with temperature variation for multiple mass flow values in [kg/s].

When analysing eq. (4.2) it is easily observed that the concentration dependence of the mass diffusion

coefficient is a consequence of the fact that the diffusion flow depends on the difference of the chemical potential of the system, it is also expected that this value diminishes with increasing concentration (fig. 4.5), since the higher the molecular density is, the harder it gets for the molecules to flow from one point to another, implying a smaller diffusion rate. Contrary to the thermal conductivity, this is a mass related coefficient, thus being normal to the mass related parameters to have a bigger influence.

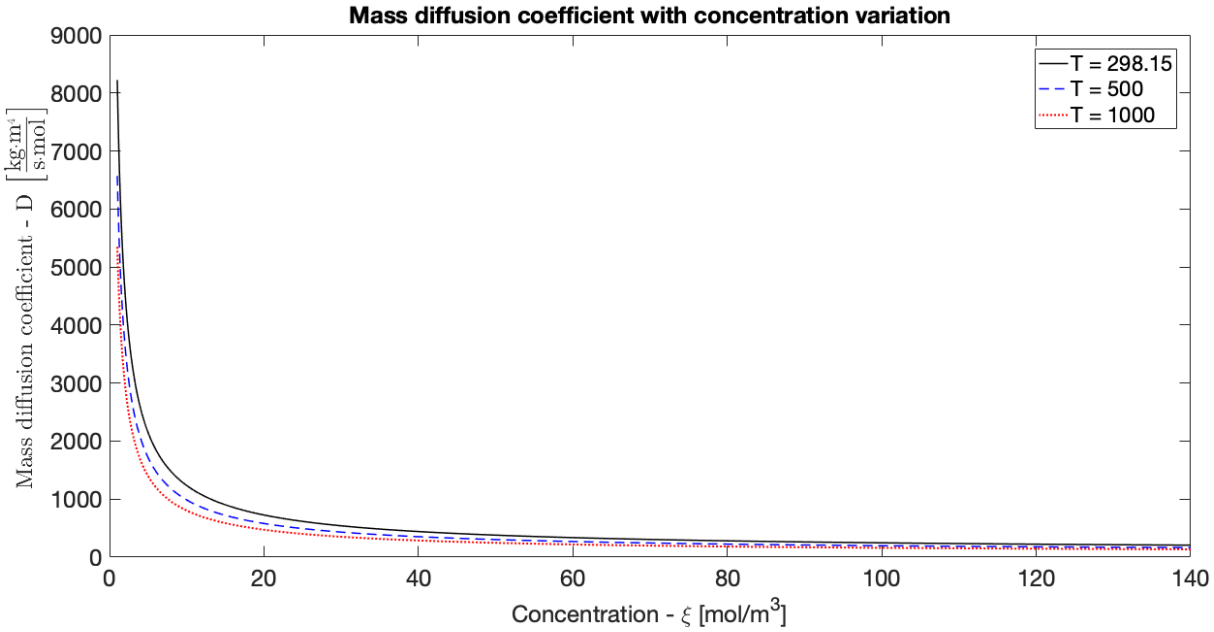

Figure 4.5: Mass diffusion coefficient D with concentration variation for multiple temperature values in [K].

4.1.3 Thermal Cross-coefficient - α

The thermal-cross coefficient (2.89c) and (4.3) as a cross-coupling coefficient accounts for the influence of both temperature and concentration.

$$\alpha \equiv \frac{\Gamma_{12}}{T^2} + \frac{\Gamma_{22}}{T}\left(\frac{\partial \mu}{\partial T}\right)_{\xi}. \tag{4.3}$$

The concentration dependence comes from the logarithmic expression, in eq. (3.5b), and the variation in eq. (3.16), while the temperature dependence is due to Γ_{22} and Γ_{12}, eqs. (3.16) and (3.17) respectively. Being a thermal coefficient, once more, it is expected a substantial part of the effect from the temperature related parameters. In this case there is clearly a parameter with a massive value when comparing with the remaining, Γ_{12} (fig. 3.6), thus being the dominant parameter. As a dominant parameter, α presents the exact same variations as Γ_{12}, this means that the thermal cross-coefficient decreases, in absolute value, with increasing temperature and increases with increasing mass flow quantity (fig. 4.6).

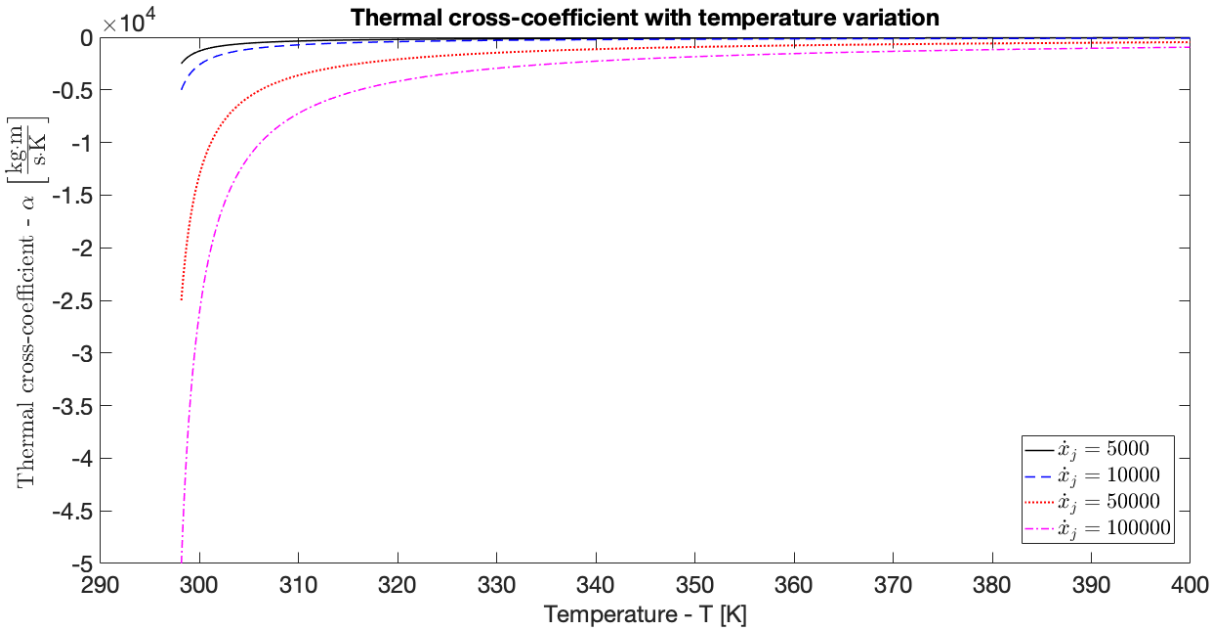

Figure 4.6: Thermal cross-coefficient α with temperature variation for multiple mass flow values in [kg/s].

The temperature has such a considerable impact that the concentration variation is considered negligible (fig. 4.7). Both the kinetic cross-coupling coefficient and the chemical potential have negative values in this way being α also negative.

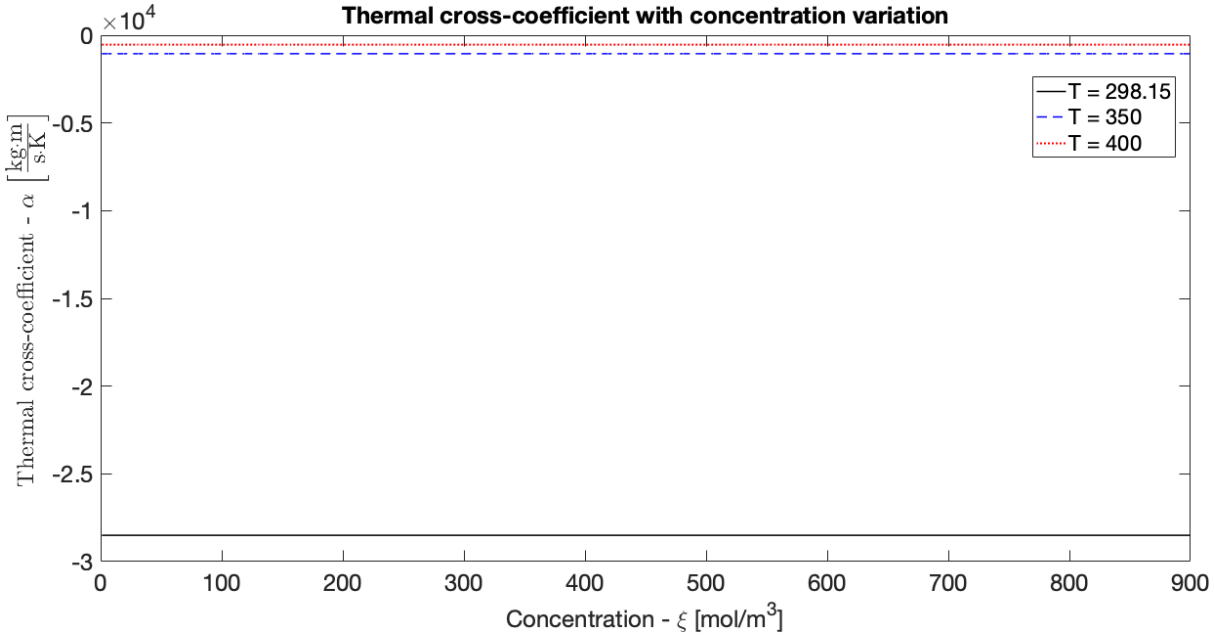

Figure 4.7: Thermal cross-coefficient α with concentration variation for multiple temperature values in [K].

4.1.4 Thermal Conductivity Coefficient - χ

The final form of the thermal conductivity coefficient, formulated in eq. (2.92b) and recalled in eq. (4.4) is presented in figs. 4.8–4.10.

$$\chi = \overline{\chi} + \alpha \frac{\Gamma_{12}}{\Gamma_{22}}. \tag{4.4}$$

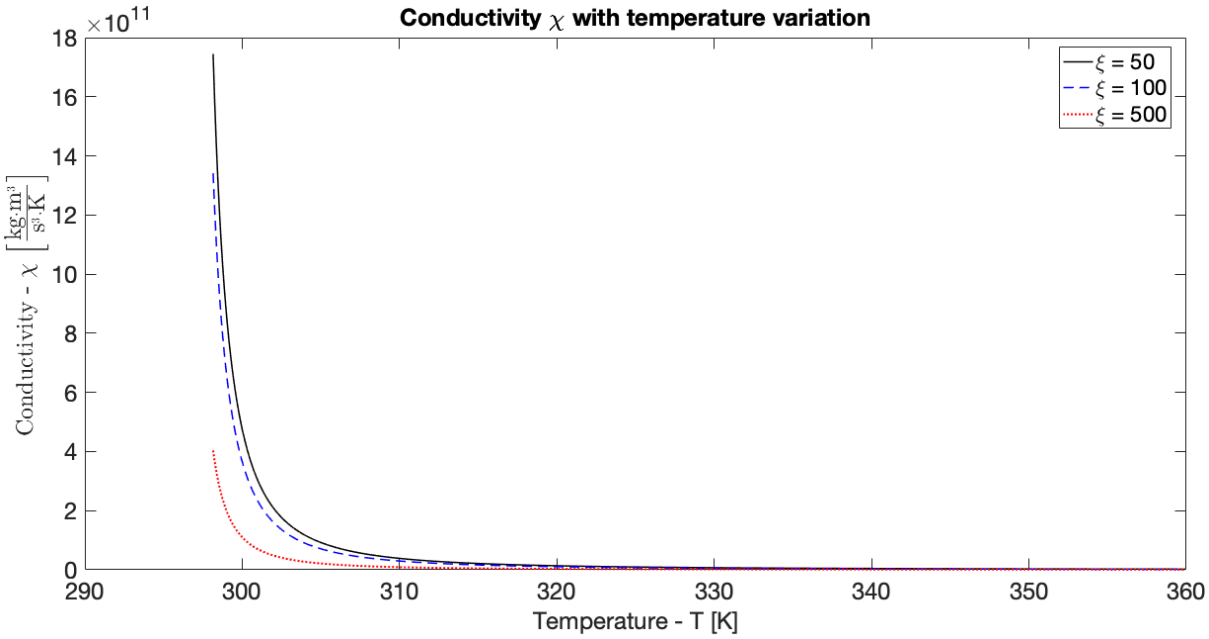

Figure 4.8: Conductivity coefficient χ with temperature variation for multiple concentration values in [mol/m^3].

After analysing the results obtained it is clear that the behaviour of the thermal conductivity is closest from the behaviour of liquids than from gases, this result is due to the fact that the kinetic coefficients were calculated for a water system, instead of a two-phase system. Just as it happens for liquids, in this case, the thermal conductivity also decreases with increasing temperature (fig. 4.8) as a result of the liquid expansion and the molecules moving apart, decreasing the attraction forces. It is also typical of liquids behaviour to achieve approximately constant values at higher temperatures. The dependence on the mass flow (fig. 4.9) comes through the use of the kinetic coefficients, which are proportional to the flow value, hence the conductivity will increase with the increasing of water flow.

Relatively to the concentration (fig. 4.10), the conductivity rely on $\overline{\chi}$ that was proven earlier to have a negligible dependence regarding the concentration, the same happens with α from which χ is also dependent, the other two values in eq. (4.4) are Γ_{12} and Γ_{22}. As seen from eq. (3.17), Γ_{12} does not depend of the concentration, with this the only parameter able to affect the concentration is in fact Γ_{22} through the variation of chemical potential and since this value is in the denominator of eq. (3.17) and is extremely small when compared with the one from the numerator, it will intensely affect the final result. Thus, the results relatively to the decreasing of the conductivity with the increase of concentration, in fig. 4.10 are a reflection of the system chemical potential represented in fig. 3.1b. The enormous values difference between the temperature curves is due to the fact that in fig. 4.8 the conductivity decays

exponentially in just approximately 10 K, presenting only high levels of thermal conductivity for low temperatures.

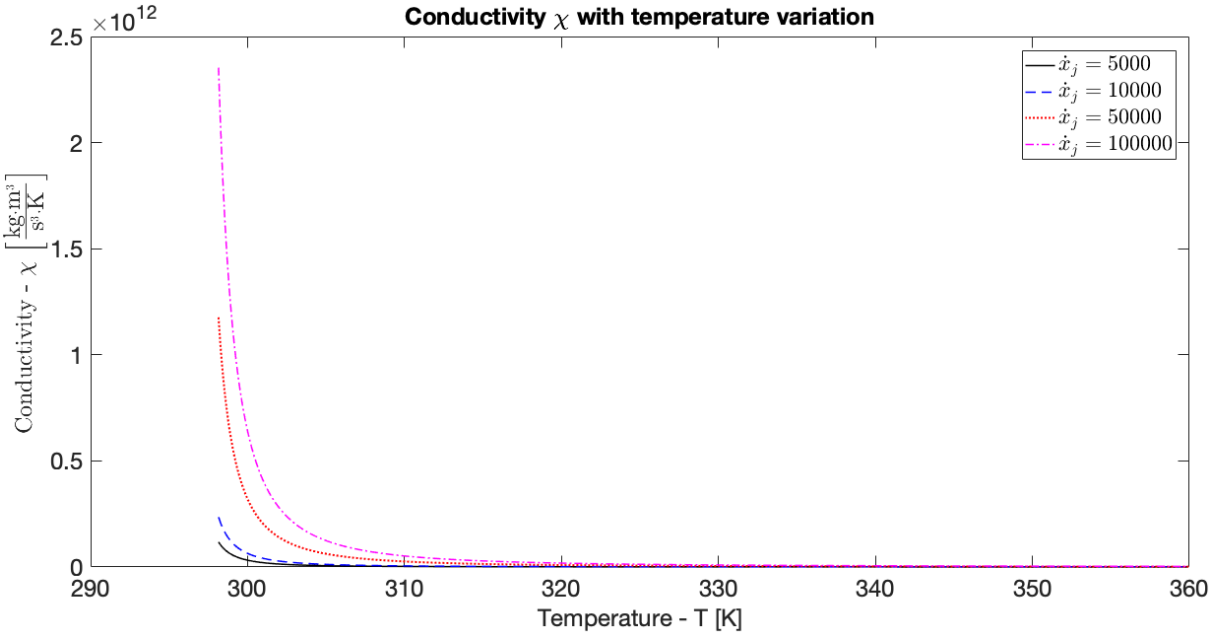

Figure 4.9: Conductivity coefficient χ with temperature variation for multiple mass flow values in [kg/s].

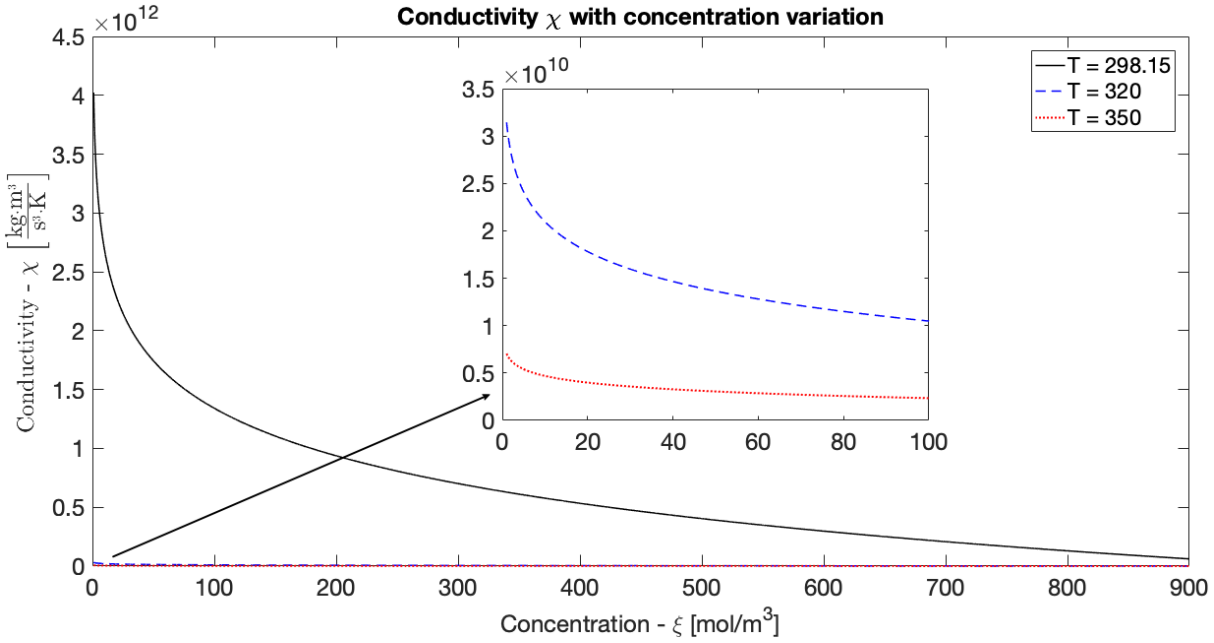

Figure 4.10: Conductivity coefficient χ with concentration variation for multiple temperature values in [K].

4.1.5 Mass Diffusion Cross-coefficient - β

The mass diffusion cross-coefficient (2.92c) and (4.5) is the mass related coefficient and the first result to be aware of is the difference in the order of magnitude relatively to its conjugate, the thermal cross-coefficient. While α is of the order of 10^4, the mass coefficient, β is of the order of 10^{10} a much higher

value. Meaning that in the cross-coupling reaction the mass diffusion is what influences the most.

$$\beta = D\,\frac{\Gamma_{12}}{\Gamma_{22}}. \tag{4.5}$$

In figs. 4.11 and 4.12 it is possible to see the results for temperature variation with different concentrations and mass flows, in an overall observation the behaviour is the same as the thermal cross-coefficient, decreasing values with increasing temperature and for higher mass flows, higher coefficients, seen from an absolute value point-of view. However, the difference between the two cross-coefficients is the influence of the concentration, while on the thermal component the concentration effect was neglected, being this a mass related coefficient it has to take into account the chemical potential variations and hence a concentration contribution (fig. 4.13), nonetheless the effects are bigger for smaller concentrations.

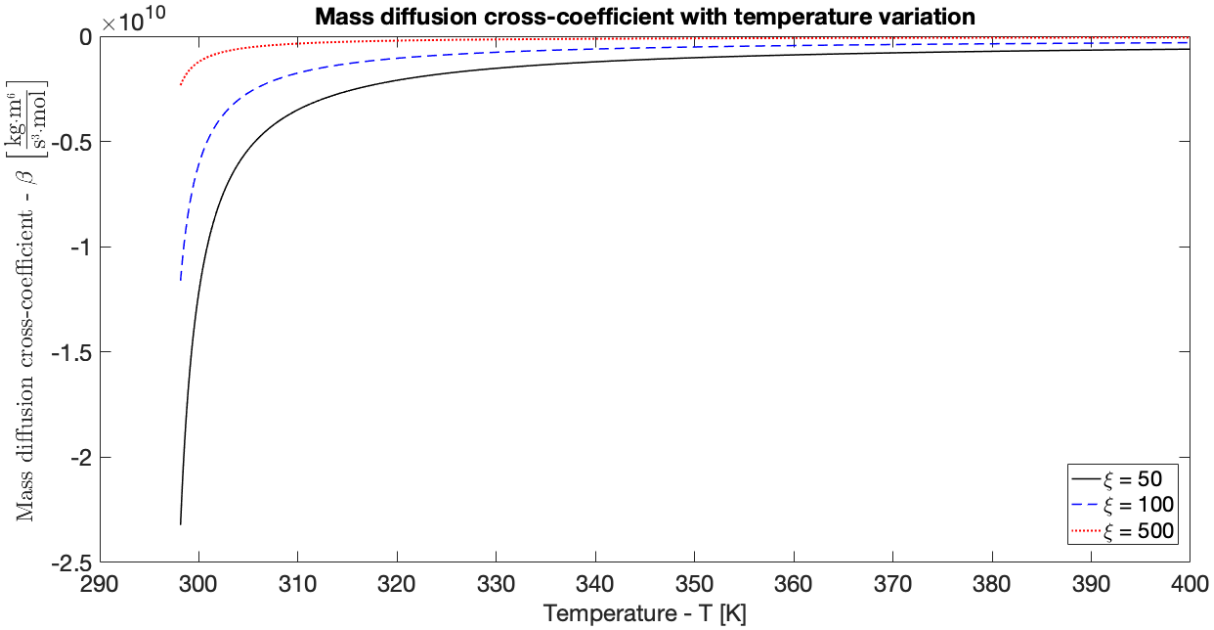

Figure 4.11: Mass diffusion cross-coefficient β with temperature variation for multiple concentration values in [mol/m^3].

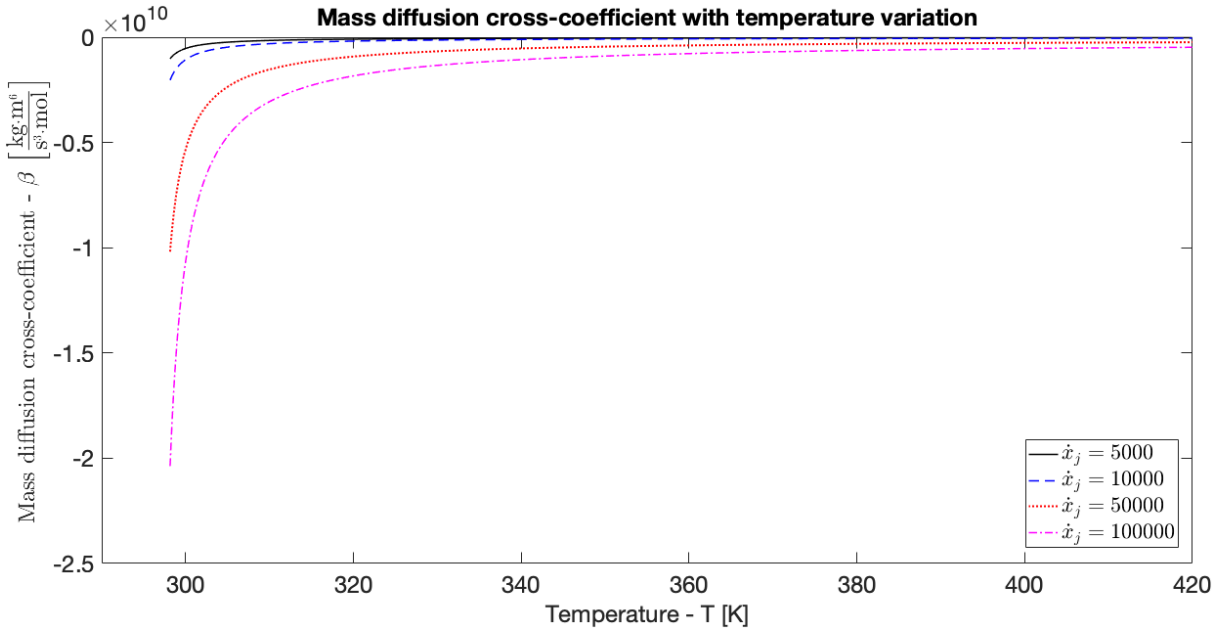

Figure 4.12: Mass diffusion cross-coefficient β with temperature variation for multiple mass flow values in [kg/s].

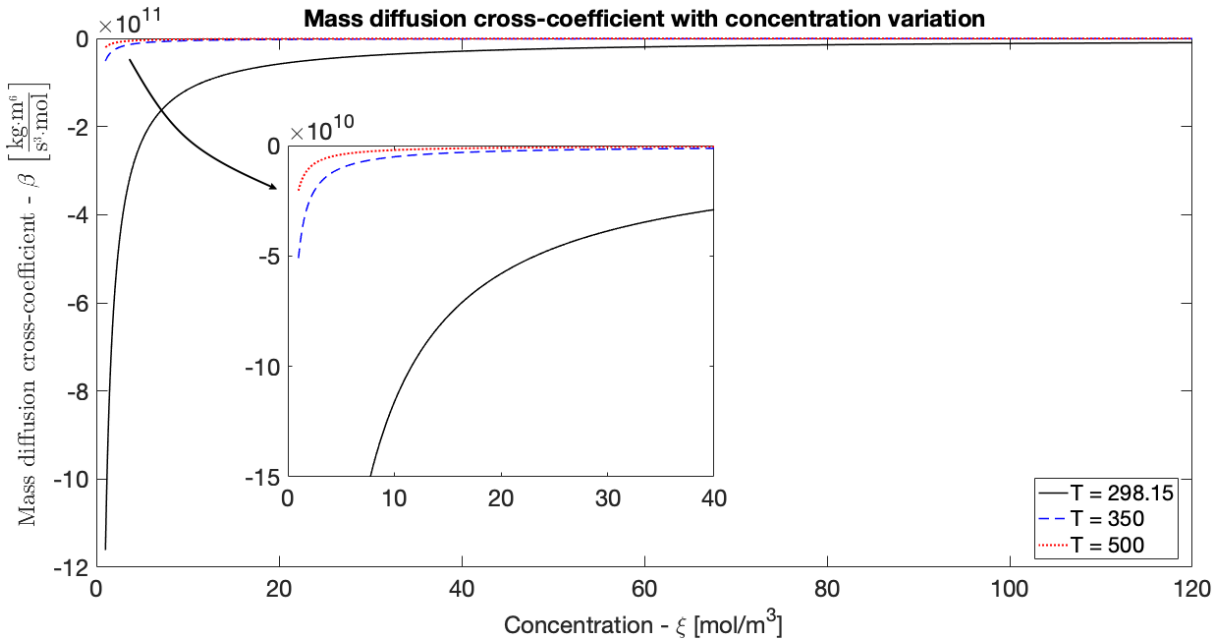

Figure 4.13: Mass diffusion cross-coefficient β with concentration variation for multiple temperature values in [K].

4.2 Acoustic Attenuation

It is known from sections 2.3 and 2.4 that the acoustic attenuation is divided into three components, the thermal damping in eq. (2.42d), the viscous damping, eq. (2.43a) and the mass diffusion damping from eq. (2.43b). For this analysis, the same dampings were parametrized (4.7)–(4.9) by the Doppler shifted

frequency, $\overline{\omega}^2$, in a way of easing the reading of the graphical results.

$$\vartheta = \vartheta_1 + \vartheta_2 + \vartheta_3, \tag{4.6}$$

$$\vartheta_1 = \frac{\varepsilon_1}{\overline{\omega}^2} = \frac{(\gamma - 1)^2 \chi}{2p_0\gamma^2 R}, \tag{4.7}$$

$$\vartheta_2 = \frac{\varepsilon_2}{\overline{\omega}^2} = \frac{1}{2p_0\gamma}\left(\zeta + \frac{4}{3}\eta\right), \tag{4.8}$$

$$\vartheta_3 = \frac{\varepsilon_3}{\overline{\omega}^2} = \frac{\gamma - 1}{2p_0\gamma^2 RT_0}\xi_0\beta. \tag{4.9}$$

The total acoustic attenuation as stated before is calculated through the sum of the three components as shown in eq. (4.6).

4.2.1 Thermal Damping

The thermal damping (4.7) being the temperature related component of the total attenuation is proportional to the thermal conductivity, that in turn depends on the thermal cross-coefficient, in this way having all the temperature related components in its formulation. Being proportional to the thermal conductivity the results of this damping will assume the same behaviour, with a different, smaller, order of magnitude mainly due to the division by the exterior pressure.

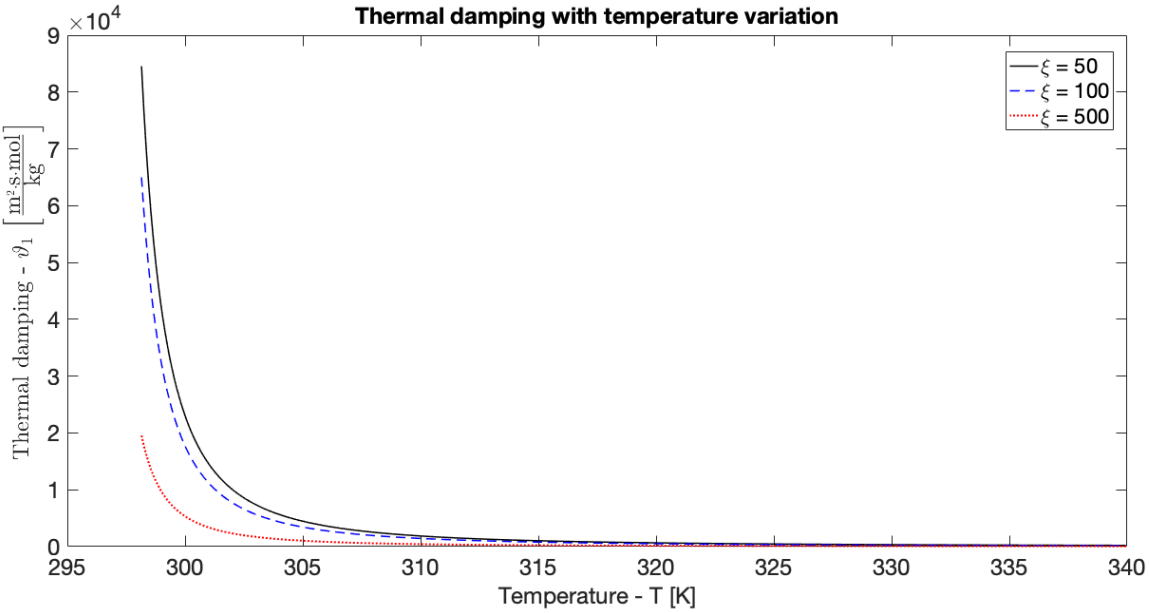

Figure 4.14: Thermal damping ϑ_1 with temperature variation for multiple concentration values in [mol/m^3].

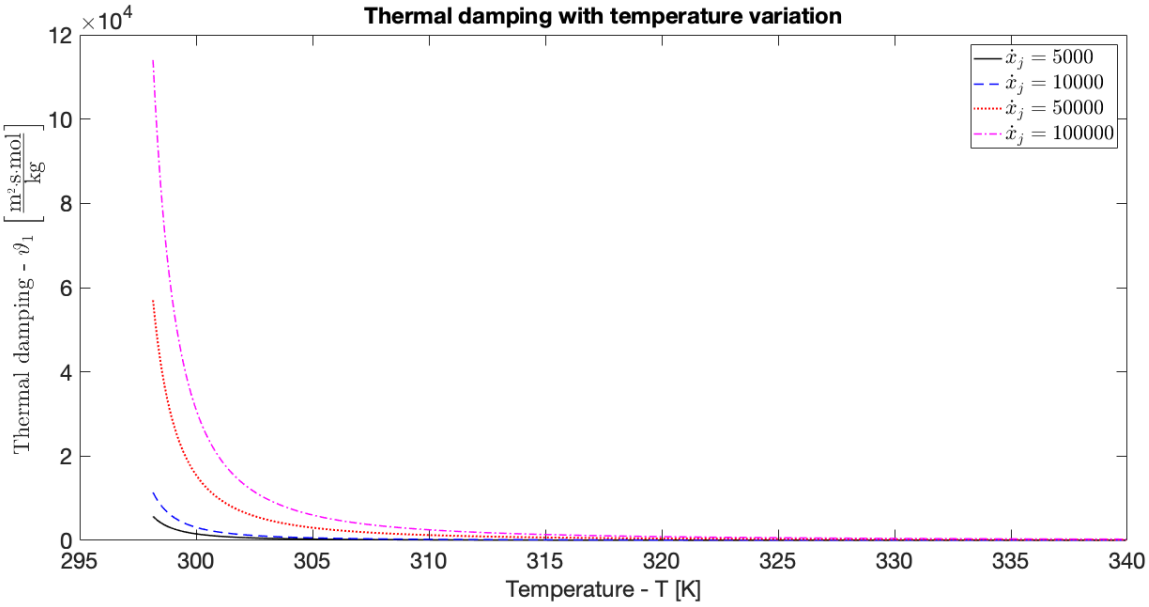

Figure 4.15: Thermal damping ϑ_1 with temperature variation for multiple mass flow values in [kg/s].

In figs. 4.14 and 4.15 it is possible to observe that the attenuation decreases with the increasing of temperature, as was already stated, due to the fact that with increasing temperature the energy of thermal motion loosens the molecules in this way decreasing the attraction forces and hence, the conductivity which induces a decreasing in the attenuation. For higher mass flows a bigger amount of water will be present in the system, thus having more molecules interacting and an increasing capacity of conducting the heat flux.

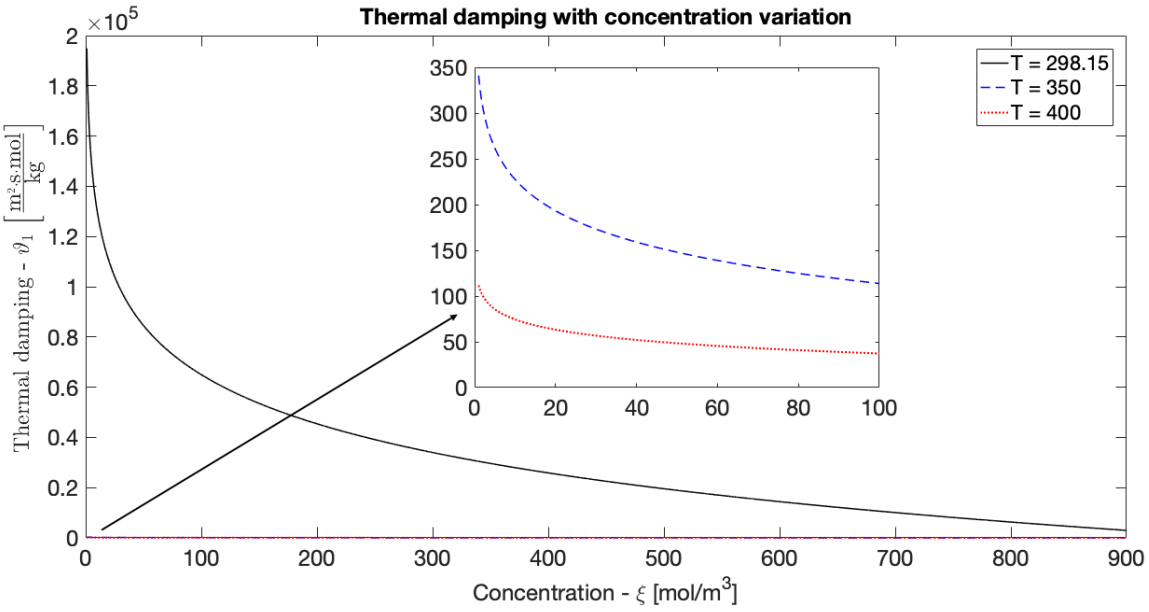

Figure 4.16: Thermal damping ϑ_1 with concentration variation for multiple temperature values in [K].

The variation of the thermal attenuation with regard to concentration (fig. 4.16), is once again, a portrait of the behaviour of the chemical potential, since the thermal conductivity also has components derived from mass diffusion. In cases like this, where it happens multiple irreversible processes, as heat conduc-

tion and mass diffusion, the temperature differences present in the system will cause a degradation of energy by conduction of heat but the second process happening simultaneously will cause an additional degradation of energy making the total rate of increase of the entropy greater than it would be just by heat conduction alone [5].

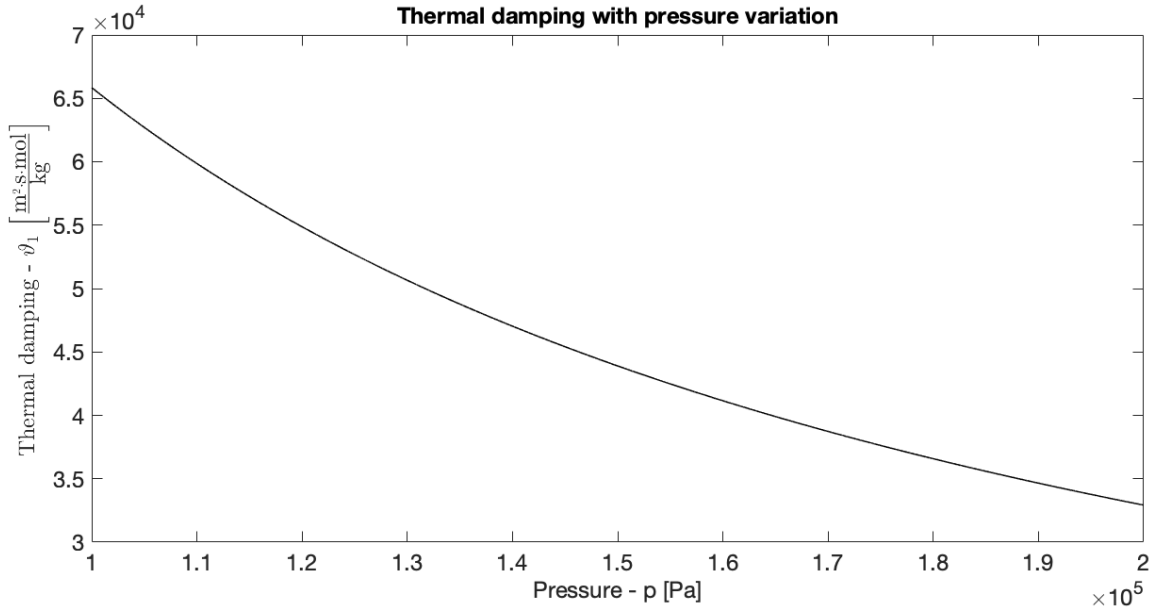

Figure 4.17: Thermal damping ϑ_1 with pressure variation.

The effect of the pressure variation (fig. 4.17) is as expected, since it is present in the denominator of eq. (4.7) it presents an almost inversely proportionality, nonetheless its graphical representation will be presented for all dampings in order to compare the order of magnitude of each one of them.

4.2.2 Viscous Damping

The attenuation owing the viscosity effect of the medium is given by eq. (4.8). This is an attenuation that depends only on the viscosities, shear and bulk, and as analysed in section 3.1.5 although the bulk viscosity presents a higher value comparatively to the shear viscosity, it is still a value on the order of magnitude of 10^{-3} a much smaller value when in comparison, for example, with the thermal conductivity (10^{12}) that is the parameter on which the thermal damping depends. With this, when combining both viscosity effects the values achieved, of the order of 10^{-8} (fig. 4.18) can not be compared with the ones obtained for thermal damping, hence it is completely negligible. Nonetheless, it is relevant to analyse the results obtained for the viscous damping.

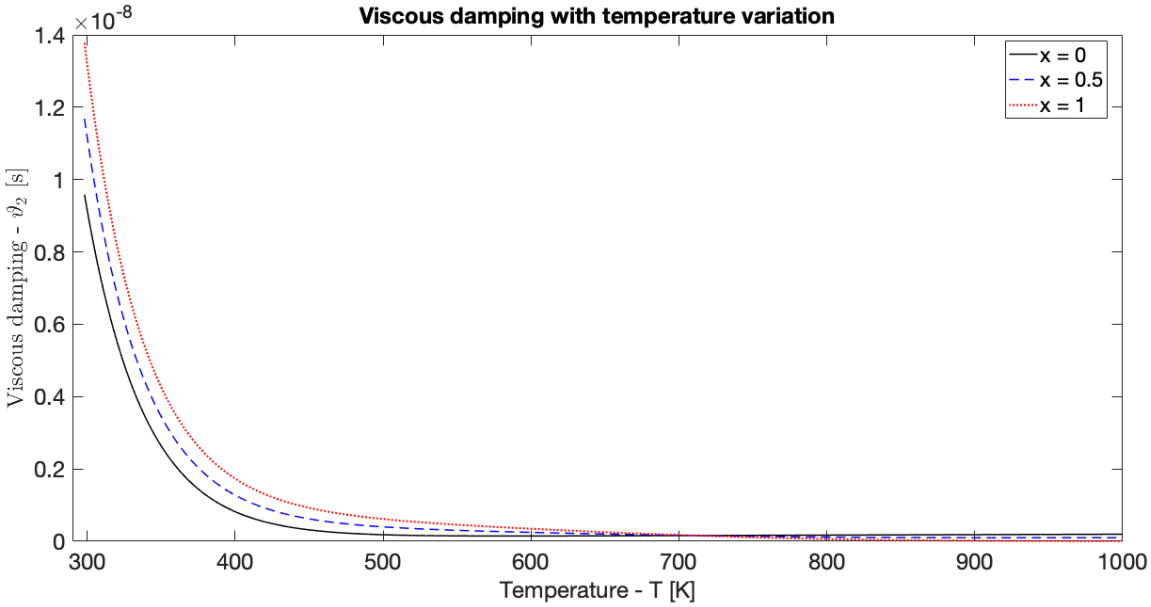

Figure 4.18: Viscous damping ϑ_2 with temperature variation for multiple mass quality values.

When comparing fig. 4.18 with figs. 3.12a and 3.16 it is easy to observe the effect of the bulk viscosity, especially if attending to the black filled curve, represented for a mass quality $x = 0$, where in fig. 3.12a is almost constant and in this case it presents an approximate exponential decay. However, it should be borne in mind, while the shear viscosity is calculated for a two-phase flow, the bulk viscosity was evaluated only for the water component, thus this component is being summed to the entire range of viscosities, this meaning it is also being added when it should only exist air. This explains the major difference between the two curves from both figures stated before, however the value for air bulk viscosity, as in the water case, is still bigger than the shear, as can be seen from the values presented in table B.1 on appendix B, even if in a smaller order of magnitude, it would present the same features. Regarding to temperature variation (fig. 4.18), the viscous attenuation decreases with increasing temperature exhibiting a liquid like behaviour, since when there is an increase in temperature the mean particles have a greater thermal energy being more easy to overcome the attractive forces that are binding them together, implying a decreasing viscosity and so a decreasing power of attenuation.

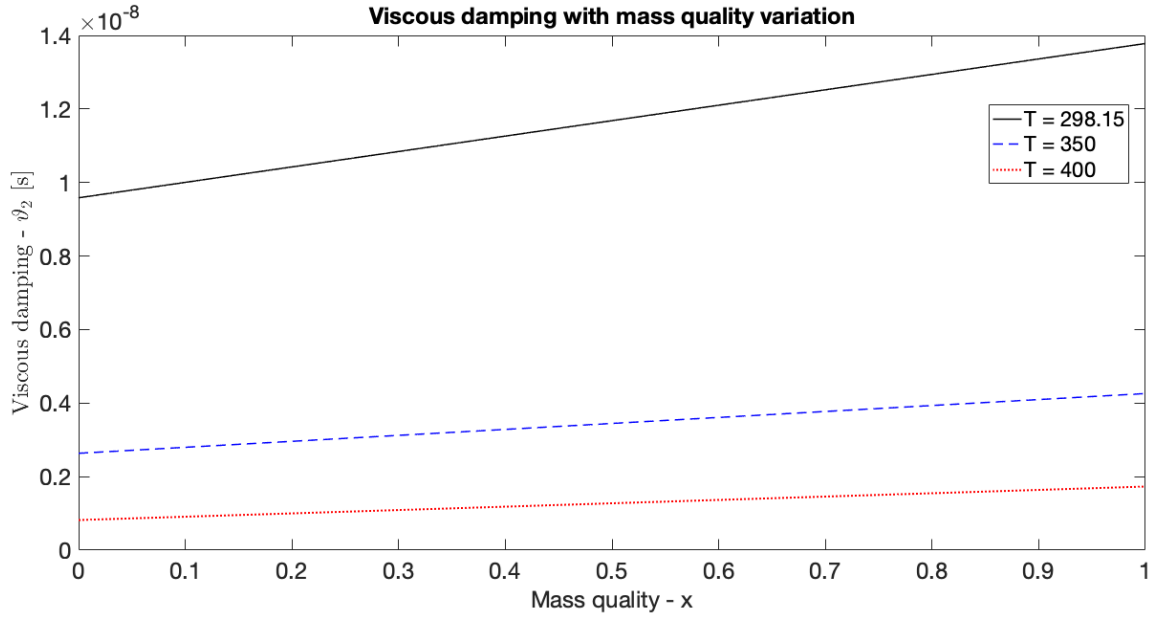

Figure 4.19: Viscous damping ϑ_2 with mass quality variation for multiple temperature values in [K].

It was already discussed how the water presents a higher viscosity value than the air, and so it is expected that when increasing the mass quality, and thus the quantity of water in the system the viscosity also increases leading to an increase of the attenuation (fig. 4.19). When $x = 1$ the attenuation will present a result for a full water medium, in terms of both bulk and shear viscosity. For $x = 0$, while the two-phase shear viscosity presents a full air behaviour, as it should be, the bulk viscosity will add a water component due to the lack of a two-phase model for this parameter. Once again, the pressure variation (fig. 4.20) is presented mainly with a purpose of completeness, since the effect is the same for all the attenuation components.

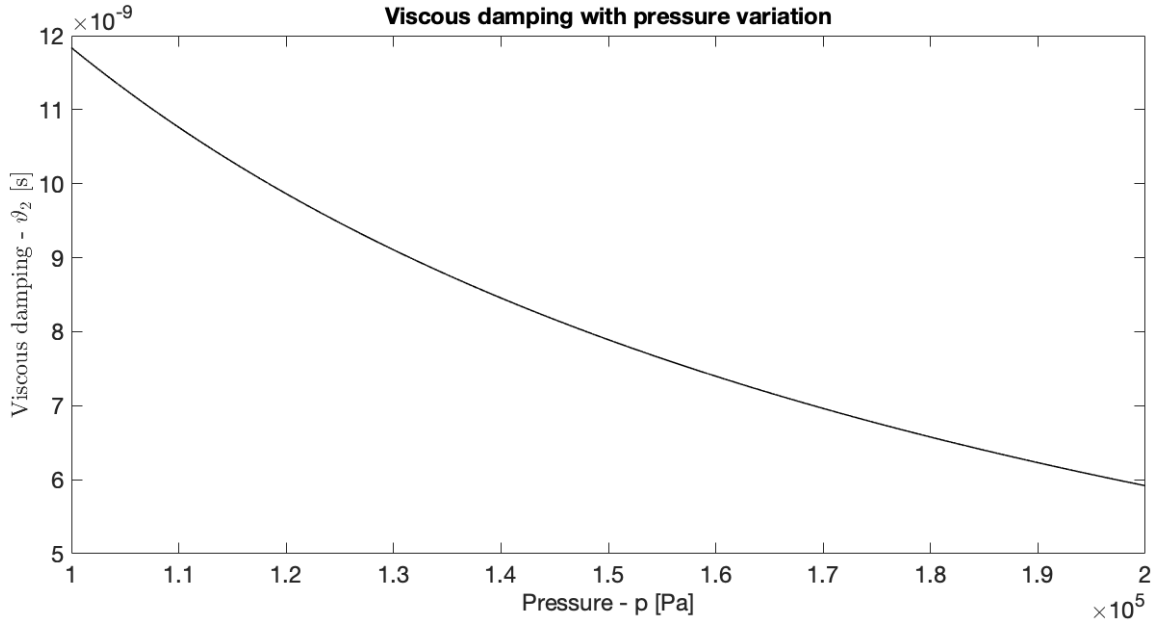

Figure 4.20: Viscous damping ϑ_2 with pressure variation.

4.2.3 Mass Diffusion Damping

The mass diffusion damping, eq. (4.9), is the mass related component of the total acoustic attenuation depending directly on the concentration and the mass diffusion cross-coefficient. The very first result that is important to note is that this damping has a negative value, meaning that instead of contributing to the acoustic attenuation it has in fact an amplification effect, increasing the heat flux instead of decreasing it as it is necessary in an attenuation case. The second result worth mentioning is that, since it depends directly on the concentration it would be expected to have a variation regarding this parameter, however as can be analysed in fig. 4.22 this does not happen and the variation in concentration can actually be neglected. This effect is explained by the fact that both terms, ξ and β cancel due to the existence of opposite gradients of concentration. While the ξ value increase in the direction of the mass flux, within the water spray jet, the mass diffusion cross-coefficient β subsequent from Fourier's law imply a heat flow from higher to lower temperatures, which happens in the opposite direction of the mass flow. The temperature variation effect (fig. 4.21) reproduces the behaviour of the mass diffusion cross-coefficient, it decreases with increasing temperature and increases with the mass flow, in absolute value, since the higher the mass flow, the bigger the amount of water present in the system and thus more mass in which the diffusion process can happen.

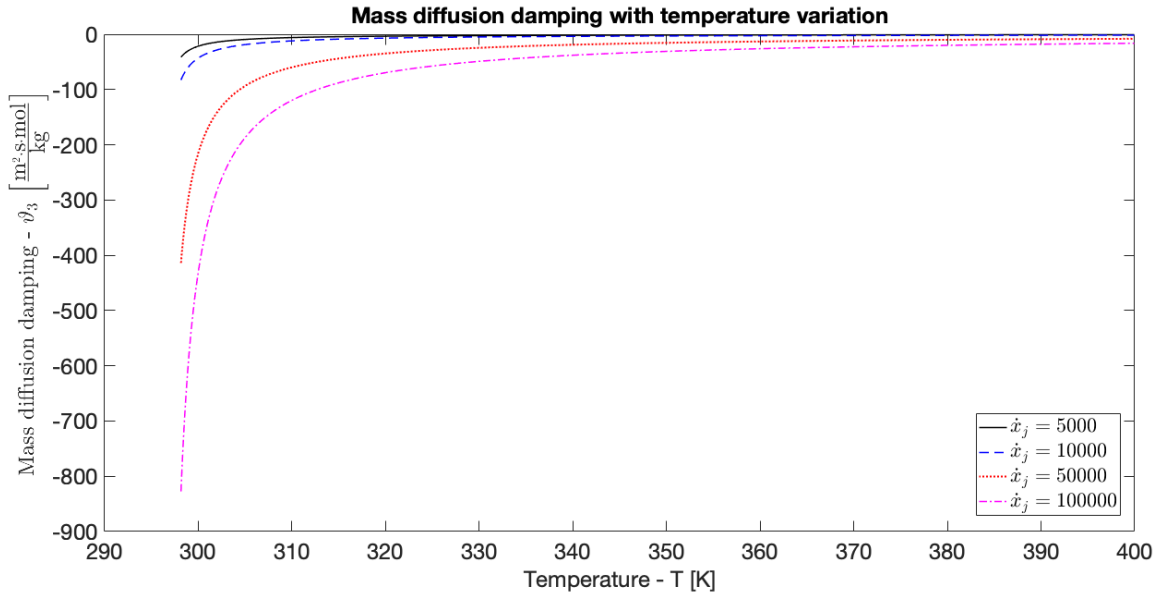

Figure 4.21: Mass diffusion damping ϑ_3 with temperature variation for multiple mass flow values in [kg/s].

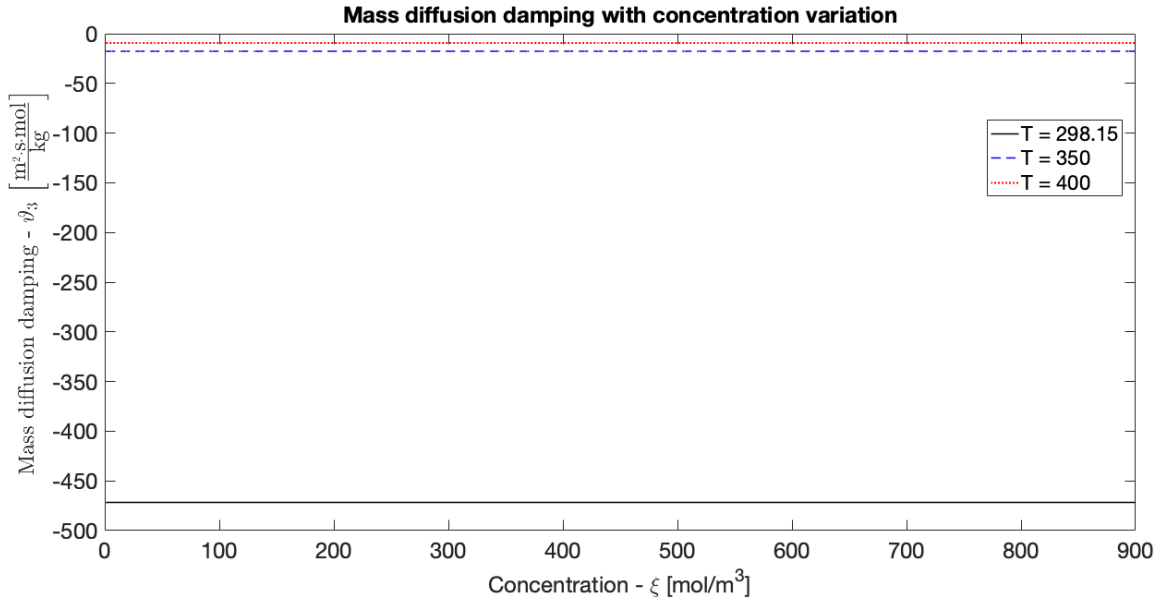

Figure 4.22: Mass diffusion damping ϑ_3 with concentration variation for multiple temperature values in [K].

For the pressure variation (fig. 4.23) it should be kept in mind that the values presented are negative and that seen from an absolute point-of-view the attenuation decays almost linearly with increasing pressure.

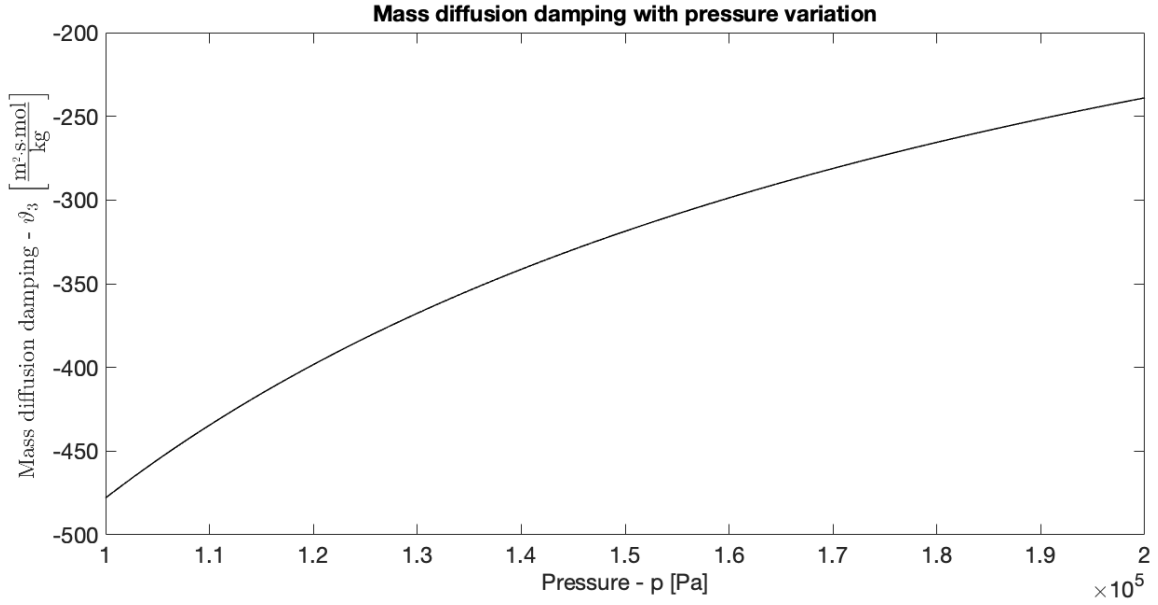

Figure 4.23: Mass diffusion damping ϑ_3 with pressure variation.

4.2.4 Total Damping

The final and most important goal is the analysis of the total acoustic attenuation obtained after implementation of the new theory hereby presented. In order to do so, all the previously calculated dampings, are added as contemplated in eq. (4.6) and all the possible results graphically represented in figs. 4.24–

4.27. The total damping consist of three components: the thermal damping accounts for highest attenuation by a large margin as concerns the order of magnitude of the three dampings, and thus dominates the global attenuation. The viscous damping presented the exact opposite, being the smallest attenuation and in fact able to be neglected. The mass diffusion damping has the opposite effect to attenuation, meaning that is does not contribute to attenuate but instead to amplification.

When analysing fig. 4.24 it is clear that the attenuation with temperature variation is a reproduction of the thermal damping, decreasing with increasing temperature due to the thermal conductivity effect, already established in section 4.1.4. In fig. 4.25 it is actually possible to see the reflection of the mass diffusion contrary damping effect when attending to the available zoom and comparing it with the one from fig. 4.16, showing a slightly decrease in the total attenuation relatively to the thermal damping. The red dotted line is the one where the effect is more easily observed in fig. 4.16 it slightly surpasses 100 where in turn in the fig. 4.25 it achieves this as a maximum value. The mass quality effect (fig. 4.26) is negligible since the viscous attenuation is the only that depends on this parameter and the magnitude of this damping is much smaller when compared with the thermal damping, hence the effect of this damping is not even felt. The pressure, as expected, maintains its approximately inversely proportional effect (fig. 4.27).

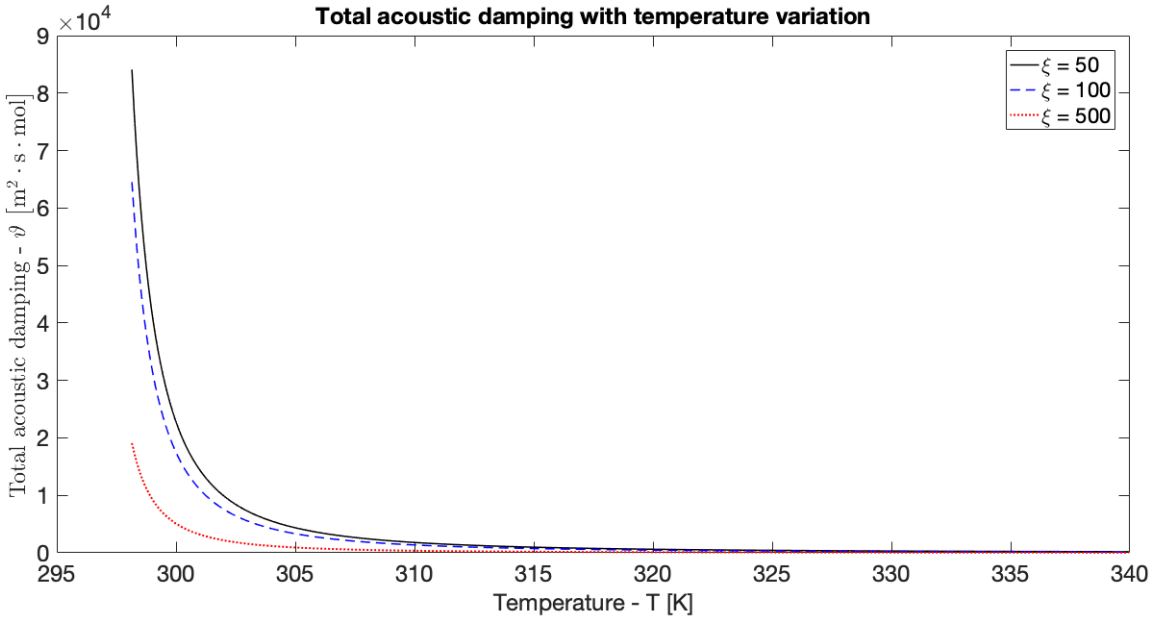

Figure 4.24: Total acoustic damping ϑ with temperature variation for multiple concentration values in [mol/m^3].

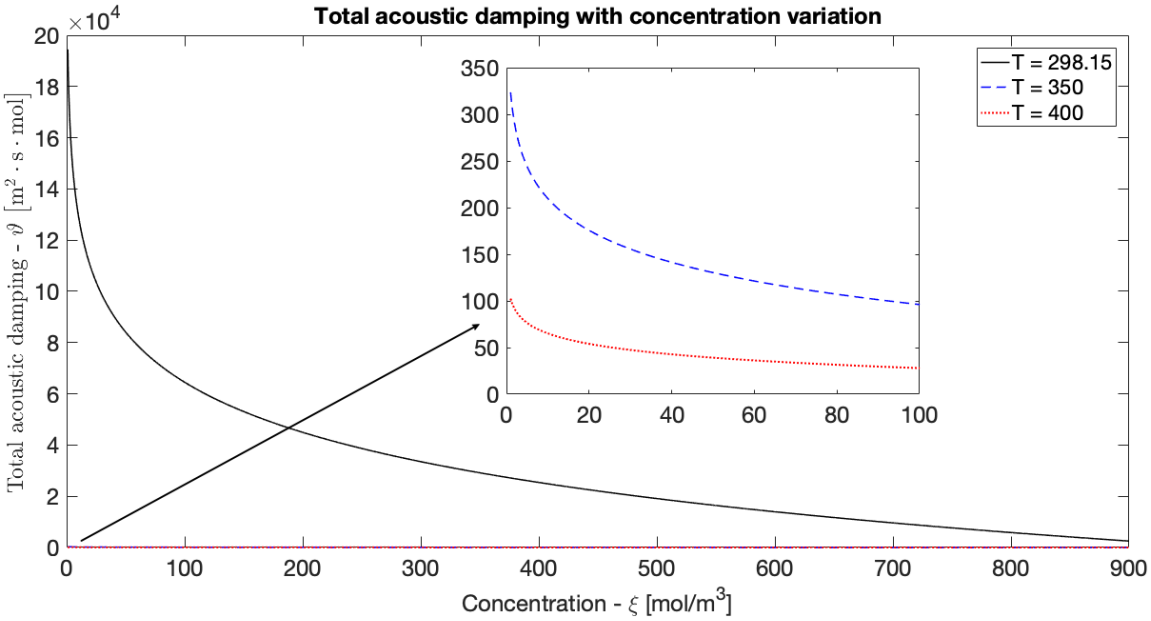

Figure 4.25: Total acoustic damping ϑ with concentration variation for multiple temperature values in [K].

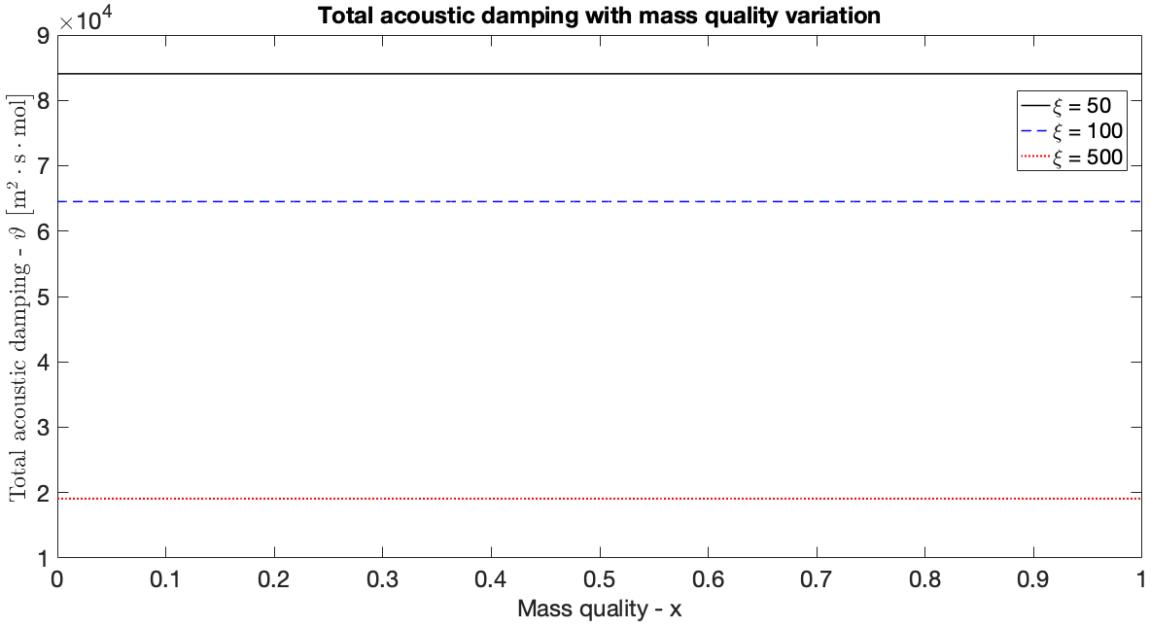

Figure 4.26: Total acoustic damping ϑ with mass quality variation for multiple concentration values in [mol/m^3].

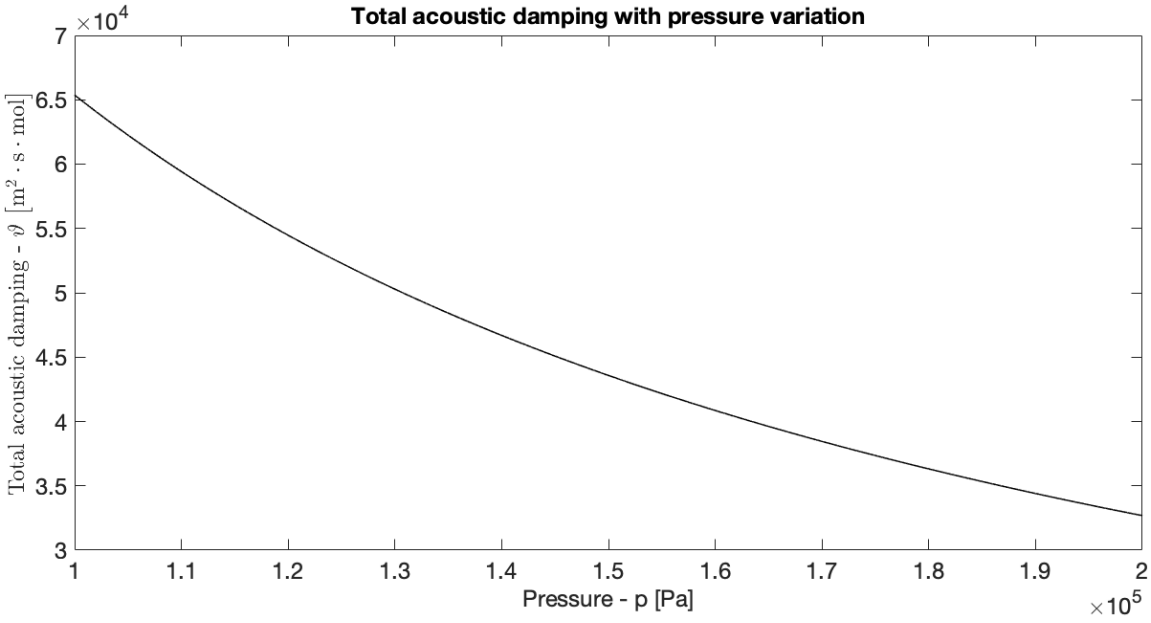

Figure 4.27: Total acoustic damping ϑ with pressure variation.

Table 4.2: Total damping vs. temperature and concentration.

T [ºC] / ξ [mol/m³]	**25**	**50**	**75**	**100**	**150**	**250**	**500**	**1000**
25	1.04×10^5	609.05	175.61	85.53	35.68	14.13	5.26	2.62
50	8.41×10^4	488.03	139.18	67.12	27.54	10.62	3.81	1.88
100	6.45×10^4	367.01	102.75	48.72	19.39	7.13	2.35	1.04
150	5.31×10^4	296.22	81.45	37.95	14.63	5.08	1.50	0.58
200	4.49×10^4	245.99	66.33	30.32	11.25	3.63	0.90	0.25

To complete this chapter, in table 4.2 can be seen the total damping obtained for a combination of temperature and concentration values.

Chapter 5

Conclusions

Lastly, but definitely not less important, this last chapter is destined for the final conclusions regarding the work developed throughout this thesis, as well as some recommendations of improvements that could and should be featured in a future work.

5.1 Achievements

In the first chapter it were established the objectives to be attained with this work (section 1.3), some of them are considered to have been fully achieved, while others were only partially achieved. Based on the objectives pyramid (fig. 1.4) it is presented next, in table 5.1 a status of the proposed objectives all of them implying the calculation for a two-phase flow.

Table 5.1: Objectives achievement.

Objectives	Status
Chemical potential	Achieved
Kinetic coefficients	Partially achieved
Shear viscosity	Achieved
Bulk viscosity	Partially achieved
Thermal conductivity	Achieved
Mass diffusion coefficient	Achieved
Cross-coupling coefficients	Achieved
Total acoustic damping	Achieved

The objectives considered to have been partially achieved is due to the fact that the calculations were not performed for a two-phase flow, but instead only for the liquid phase, as was the case for the kinetic coefficients and bulk viscosity. However, the majority of the objectives proposed are considered to have been fulfilled, it is important to remind that the main goal was not to obtain a definitive theory, but instead a first approach to this new theory in an attempt of understanding its effects and application possibilities.

The major achievement of this thesis is definitely the calculation of the acoustic damping that enabled a deeper understanding on how the various components interact between them and the impact of each in the acoustic attenuation. Concluding, the acoustic attenuation is dominated by the thermal damping which means the heat conduction irreversible process is the one with the biggest impact, while the mass diffusion damping has the opposite effect, the one of sound amplification, which means that the second irreversible process present, the mass diffusion, through the chemical potential differences instead of degrade the energy it will enhance its effect. As concerns to the viscous part, a better understanding on how the bulk viscosity affects a flow comparatively to the shear viscosity, is important and it was established in this work, regarding to the liquid phase, that the bulk viscosity actually has a bigger influence in the medium than its shear counterpart. Nonetheless, this effect does not have an influence in the final result due to the very small magnitude when compared with the thermal damping.

5.2 Future Work

In a posterior work, there are some items to have in mind, specifically,

- the calculation of the kinetic coefficients must be improved allowing inclusion of the gas phase enabling the results for a two-phase flow as it is supposed;
- the bulk viscosity has to be improved in the same way than the kinetic coefficients, because once again it was only calculated for the liquid phase and similarly to the shear viscosity it needs an air component;
- the approximations stipulated in section 1.3 regarding the omission of the less important effects when establishing the basis of the theory, with the six fundamental equations of fluid mechanics, must be considered. Mainly the effects of viscosity, vaporization and chemical reactions that are not considered in the equations of continuity, mass diffusion, heat, momentum, perfect gas state and entropy for an ideal gas that represent the basis of this theory. The inviscid momentum equation could have been replaced by the viscous momentum equation leading to the total acoustic damping in eq. (2.44) where the product of diffusivities is neglected.

Bibliography

[1] Caroline Parsons Lubert. Sixty years of launch vehicle acoustics. *Proceedings of Meetings on Acoustics*, 31(1):040004, 2017.

[2] http://heroicrelics.org/info/apollo-4/sa-501-water-ctrl-sys-test.html.

[3] https://www.nasa.gov.

[4] Tiffany Jeung. Watch nasa shoot olympic pool amounts of water into the air for the sls. https://www.inverse.com/article/51071-nasa-shoots-half-million-gallons-water-for-sls.

[5] Lars Onsager. Reciprocal relations in irreversible processes i. *Phys. Rev.*, 37:405–426, Feb 1931.

[6] L. D. Landau and E. M. Lifshitz. *Fluid Mechanics, Second Edition: Volume 6 (Course of Theoretical Physics)*, volume 6 of *Course of Theoretical Physics*. Pergamon Press, second ed. edition, 1987.

[7] Georg Job and Regina Rüffler. *Physical Chemistry from a Different Angle - Introducing Chemical Equilibrium, Kinetics and Electrochemistry by Numerous Experiments*. Springer International Publishing, Hamburg, Germany, 2016.

[8] Jean-François Dufrêche. Chemical potential - lectures.

[9] Dr. Georg Job. Table of chemical potentials.

[10] Lars Onsager. Reciprocal relations in irreversible processes ii. *Phys. Rev.*, 38:2265–2279, Dec 1931.

[11] Scott C. Doney. Irreversible thermodynamic coupling between heat and matter fluxes across a gas/liquid interface. *J. Chem. Soc., Faraday Trans.*, 90:1865–1874, 1994.

[12] J. W. Cipolla, H. Lang, and S. K. Loyalka. Kinetic theory of condensation and evaporation. ii. *The Journal of Chemical Physics*, 61(1):69–77, 1974.

[13] Young-Ping Pao. Temperature and density jumps in the kinetic theory of gases and vapors. *The Physics of Fluids*, 14(7):1340–1346, 1971.

[14] R. P. Rastogi, R. L. Blokhra, and R. K. Agarwal. Cross-phenomenological coefficients. part 1.—studies on thermo-osmosis. *Trans. Faraday Soc.*, 60:1386–1390, 1964.

[15] R.C. Srivastava and P.K. Avasthi. Non-equilibrium thermodynamics of thermo-osmosis of water through kaolinite. *Journal of Hydrology*, 24(1):111 – 120, 1975.

[16] Donald G. Miller. Thermodynamics of irreversible processes. the experimental verification of the onsager reciprocal relations. *Chemical Reviews*, 60(1):15–37, 1960.

[17] Wolfgang Wagner and Hans-Joachim Kretzschmar. *International Steam Tables*. Springer-Verlag Berlin Heidelberg, second ed. edition, 2008.

[18] David R. Lide. *CRC Handbook of Chemistry and Physics*. CRC Press, Boca Raton, FL, 85th ed. edition, 2005.

[19] C.O. Popiel and J. Wojtkowiak. Simple formulas for thermophysical properties of liquid water for heat transfer calculations (from 0 °c to 150 °c). *Heat Transfer Engineering*, 19(3):87–101, 1998.

[20] W. Kays, M. Crawford, and B. Weigand. *Convective Heat and Mass Transfer*. McGraw-Hill, Singapore, fourth ed. edition, 2005.

[21] A. Kayode Coker. *Ludwig's Applied Process Design for Chemical and Petrochemical Plants*, volume 1, chapter 3 - Physical Properties of Liquids and Gases, pages 103–108. Gulf Professional Publishing, fourth ed. edition, 2007.

[22] Maria Ramires, Carlos Nieto de Castro, Yuchi Nagasaka, Akira Nagashima, Marc Assael, and William Wakeham. Standard reference data for the thermal conductivity of water. *Journal of Physical and Chemical Reference Data*, 24:1377, 05 1995.

[23] M.M. Awad and Y.S. Muzychka. Effective property models for homogeneous two-phase flows. *Experimental Thermal and Fluid Science*, 33(1):106 – 113, 2008.

[24] W.H. McAdams, W.K. Woods, and L.C. Heroman. Vaporization inside horizontal tubes ii-benzene-oil mixtures. *Trans. ASME*, 64(3):193–200, 1942.

[25] A. Cicchitti, C. Lombardi, M. Silvestri, G. Soldaini, and R. Zavattarelli. Two-phase cooling exprimments: pressure drop, heat transfer and burnout measurements. *Energia Nucleare*, 7(6):407–425, 1959.

[26] A. E. Dukler, Moye Wicks III, and R. G. Cleveland. Frictional pressure drop in two-phase flow: Part a: A comparison of existing correlations for pressure loss and holdup and part b: An approach through similarity analysis. *AIChE Journal*, 10(1):38–51, 1964.

[27] D.R.H. Beattie and P.B. Whalley. A simple two-phase frictional pressure drop calculation method. *International Journal of Multiphase Flow*, 8(1):83 – 87, 1982.

[28] S. Lin, C.C.K. Kwok, R.-Y. Li, Z.-H. Chen, and Z.-Y. Chen. Local frictional pressure drop during vaporization of r-12 through capillary tubes. *International Journal of Multiphase Flow*, 17(1):95 – 102, 1991.

[29] M. Fourar and S. Bories. Experimental study of air-water two-phase flow through a fracture (narrow channel). *International Journal of Multiphase Flow*, 21(4):621 – 637, 1995.

[30] William Sutherland. The viscosity of gases and molecular force. *Philosophical Magazine Series 5*, 36(223):507–531, 1893.

[31] Frank M. White. *Fluid Mechanics*. McGraw-Hill, 7th edition edition, 2011.

[32] J. Poiseuille. Recherches expérimentales sur le mouvement des liquides dans les tubes de très petits diamètres. *Compt. Rend.*, 11, 12(961, 1041), 1840, 1841.

[33] K. Hutter, Y. Wang, and I.P. Chubarenko. Chapter 10 - phenomenological coefficients of water. In *Physics of Lakes, Volume 1: Foundation of the Mathematical and Physical Background*, Advances in Geophysical and Environmental Mchanics and Mathematics, chapter Chapter 10 - Phenomenological Coefficients of Water, pages 389–418. Springer-Verlag Berlin Heidelberg, 2011.

[34] Andrei S. Dukhin and Philip J. Goetz. Bulk viscosity and compressibility measurement using acoustic spectroscopy. *The Journal of Chemical Physics*, 130(12):124519, 2009.

[35] Frederike Jaeger, Omar K. Matar, and Erich A. Müller. Bulk viscosity of molecular fluids. *The Journal of Chemical Physics*, 148(17):174504, 2018.

[36] Mel Holmes, Nicholas Parker, and Megan Povey. Temperature dependence of bulk viscosity in water using acousticspectroscopy. *Journal of Physics Conference Series*, 269:012011, 01 2011.

[37] T.A. Litovitz and C.M. Davis. 5 - structural and shear relaxation in liquids. In WARREN P. MASON, editor, *Properties of Gases, Liquids, and Solutions*, volume 2 of *Physical Acoustics*, pages 281 – 349. Academic Press, 1965.

[38] Leonard Hall. The origin of ultrasonic absorption in water. *Phys. Rev.*, 73:775–781, Apr 1948.

[39] Jianfeng Xu, Xiaobin Ren, Wenping Gong, Rui Dai, and Dahe Liu. Measurement of the bulk viscosity of liquid by brillouin scattering. *Appl. Opt.*, 42(33):6704–6709, Nov 2003.

[40] Ziyu Gu and Wim Ubachs. Further validation and refinement of the tenti model for atmospheric lidar backscatter. Technical report, LaserLAB, Vrije Universiteit Amsterdam, 03 2014.

[41] Engineering ToolBox. Air - dynamic and kinematic viscosity, 2003.

Appendix A

Water Data

Table A.1: Water Data [17, 18].

Theoretical data			Experimental data		
Temperature T [°C]	**Thermal Conductivity $\kappa \times 10^{-3}$ [W/m.K]**	**Shear Viscosity $\eta \times 10^{-4}$ [Pa·s]**	**Temperature T [°C]**	**Thermal Conductivity $\kappa \times 10^{-3}$ [W/m·K]**	**Shear Viscosity $\eta \times 10^{-4}$ [Pa·s]**
0	562,0	17,920	0	561,0	17,930
1	564,1	17,914	10	580,0	13,070
2	566,2	17,312	20	598,4	10,020
3	568,2	16,737	30	615,4	7,977
4	570,3	16,192	40	630,5	6,532
5	572,3	15,183	50	643,5	5,470
6	574,3	14,716	60	654,3	4,665
7	576,2	14,272	70	663,1	4,040
8	578,1	13,848	80	670,0	3,544
9	580,0	13,445	90	675,3	3,145
10	581,9	13,060	100	679,1	2,818
11	583,8	12,692			
12	585,6	12,341			
13	587,4	12,005			
14	589,2	11,684			
15	591,0	11,376			
16	592,7	11,081			
17	594,4	10,799			
18	596,1	10,527			
19	597,8	10,267			
20	599,5	10,016			
21	601,1	9,776			
22	602,7	9,544			
23	604,3	9,321			

Continuation of table A.1					
Theoretical data			Experimental data		
Temperature T [°C]	Thermal Conductivity $\kappa \times 10^{-3}$ [W/m.K]	Shear Viscosity $\eta \times 10^{-4}$ [Pa·s]	Temperature T [°C]	Thermal Conductivity $\kappa \times 10^{-3}$ [W/m·K]	Shear Viscosity $\eta \times 10^{-4}$ [Pa·s]
24	605,9	9,107			
25	607,5	8,900			
26	609,0	8,701			
27	610,5	8,509			
28	612,0	8,324			
29	613,5	8,145			
30	615,0	7,972			
31	616,4	7,805			
32	617,8	7,644			
33	619,3	7,488			
34	620,6	7,337			
35	622,0	7,191			
36	623,3	7,050			
37	624,7	6,913			
38	626,0	6,780			
39	627,3	6,652			
40	628,6	6,527			
41	629,8	6,406			
42	631,1	6,289			
43	632,3	6,175			
44	633,5	6,065			
45	634,7	5,958			
46	635,9	5,853			
47	637,9	5,752			
48	638,2	5,654			
49	639,3	5,558			
50	640,5	5,465			
51	641,6	5,375			
52	642,6	5,286			
53	643,7	5,201			
54	644,8	5,117			
55	645,8	5,036			
56	646,8	4,957			
57	647,8	4,880			
58	648,8	4,805			
59	649,8	4,732			
60	650,8	4,660			

Continuation of table A.1					
Theoretical data			Experimental data		
Temperature T [°C]	Thermal Conductivity $\kappa \times 10^{-3}$ [W/m.K]	Shear Viscosity $\eta \times 10^{-4}$ [Pa·s]	Temperature T [°C]	Thermal Conductivity $\kappa \times 10^{-3}$ [W/m·K]	Shear Viscosity $\eta \times 10^{-4}$ [Pa·s]
61	651,7	4,591			
62	652,6	4,523			
63	653,6	4,457			
64	654,5	4,392			
65	655,3	4,329			
66	656,2	4,267			
67	657,1	4,207			
68	657,9	4,149			
69	658,8	4,091			
70	659,6	4,035			
71	660,4	3,981			
72	661,2	3,927			
73	661,9	3,875			
74	662,7	3,824			
75	663,4	3,774			
76	664,2	3,724			
77	664,9	3,678			
78	665,6	3,631			
79	666,3	3,585			
80	667,0	3,540			
81	667,6	3,497			
82	668,3	3,454			
83	668,9	3,412			
84	669,5	3,371			
85	670,1	3,331			
86	670,7	3,291			
87	671,3	3,253			
88	671,9	3,215			
89	672,5	3,178			
90	673,0	3,142			
91	673,5	3,106			
92	674,1	3,071			
93	674,6	3,037			
94	675,1	3,004			
95	675,5	2,971			
96	676,0	2,939			
97	676,5	2,907			

Continuation of table A.1					
Theoretical data			Experimental data		
Temperature T [°C]	Thermal Conductivity $\kappa \times 10^{-3}$ [W/m.K]	Shear Viscosity $\eta \times 10^{-4}$ [Pa·s]	Temperature T [°C]	Thermal Conductivity $\kappa \times 10^{-3}$ [W/m·K]	Shear Viscosity $\eta \times 10^{-4}$ [Pa·s]
98	676,9	2,876			
99	677,3	2,846			
100	677,8	2,816			
102	678,6	2,758			
104	679,3	2,702			
106	680,0	2,648			
108	680,7	2,596			
110	681,3	2,546			
112	681,8	2,498			
114	682,4	2,451			
116	682,8	2,406			
118	683,2	2,362			
120	683,6	2,320			
122	683,9	2,280			
124	684,2	2,240			
126	684,5	2,202			
128	684,6	2,165			
130	684,8	2,129			
132	684,9	2,095			
134	685,0	2,061			
136	685,0	2,029			
138	684,9	1,997			
140	684,9	1,966			
142	684,8	1,937			
144	684,6	1,908			
146	684,4	1,880			
148	684,1	1,853			
150	683,9	1,826			
152	683,5	1,800			
154	683,2	1,775			
156	682,8	1,751			
158	682,3	1,727			
160	681,8	1,704			
162	681,3	1,682			
164	680,7	1,660			
166	680,1	1,639			
168	679,4	1,618			

Continuation of table A.1					
Theoretical data			Experimental data		
Temperature T [°C]	Thermal Conductivity $\kappa \times 10^{-3}$ [W/m.K]	Shear Viscosity $\eta \times 10^{-4}$ [Pa·s]	Temperature T [°C]	Thermal Conductivity $\kappa \times 10^{-3}$ [W/m·K]	Shear Viscosity $\eta \times 10^{-4}$ [Pa·s]
170	678,7	1,598			
172	678,0	1,578			
174	677,2	1,559			
176	676,4	1,540			
178	675,5	1,522			
180	674,6	1,504			
182	673,7	1,486			
184	672,7	1,469			
186	671,7	1,453			
188	670,6	1,436			
190	669,5	1,420			
192	668,3	1,405			
194	667,2	1,390			
196	665,9	1,375			
198	664,7	1,360			
200	663,4	1,346			
202	662,0	1,332			
204	660,7	1,318			
206	659,2	1,305			
208	657,8	1,292			
210	656,3	1,279			
212	654,7	1,266			
214	653,2	1,254			
216	651,5	1,241			
218	649,9	1,229			
220	648,2	1,218			
222	646,4	1,206			
224	644,7	1,195			
226	642,8	1,184			
228	641,0	1,173			
230	639,1	1,162			
232	637,1	1,151			
234	635,2	1,141			
236	633,1	1,131			
238	631,1	1,121			
240	629,0	1,111			
242	626,8	1,101			

Continuation of table A.1					
Theoretical data			Experimental data		
Temperature T [°C]	Thermal Conductivity $\kappa \times 10^{-3}$ [W/m.K]	Shear Viscosity $\eta \times 10^{-4}$ [Pa·s]	Temperature T [°C]	Thermal Conductivity $\kappa \times 10^{-3}$ [W/m·K]	Shear Viscosity $\eta \times 10^{-4}$ [Pa·s]
244	624,6	1,091			
246	622,4	1,082			
248	620,1	1,072			
250	617,8	1,063			
252	615,5	1,054			
254	613,0	1,045			
256	610,6	1,036			
258	608,1	1,027			
260	605,6	1,018			
262	603,0	1,009			
264	600,4	1,001			
266	597,7	0,993			
268	595,0	0,984			
270	592,2	0,976			
272	589,4	0,968			
274	586,6	0,959			
276	583,7	0,951			
278	580,7	0,943			
280	577,7	0,936			
282	574,7	0,928			
284	571,6	0,919			
286	568,5	0,912			
288	565,3	0,904			
290	562,0	0,897			
292	558,7	0,888			
294	555,4	0,881			
296	551,9	0,874			
298	548,5	0,866			
300	545,0	0,859			
305	535,9	0,839			
310	526,5	0,821			
315	516,7	0,802			
320	506,5	0,783			
325	495,8	0,764			
330	484,8	0,744			
335	473,3	0,724			
340	461,4	0,703			

Continuation of table A.1					
Theoretical data			Experimental data		
Temperature T [°C]	Thermal Conductivity $\kappa \times 10^{-3}$ [W/m.K]	Shear Viscosity $\eta \times 10^{-4}$ [Pa·s]	Temperature T [°C]	Thermal Conductivity $\kappa \times 10^{-3}$ [W/m·K]	Shear Viscosity $\eta \times 10^{-4}$ [Pa·s]
345	449,1	0,681			
350	436,5	0,658			
355	423,8	0,632			
360	411,9	0,603			
365	404,0	0,568			

Table A.2: Water bulk viscosity data [34, 36–39].

Bulk Viscosity - $\zeta \times 10^{-3}$ [Pa·s]									
T [°C]	ζ_{Hall}	T [°C]	ζ_{Holmes}	T [°C]	ζ_{Xu}	T [°C]	$\zeta_{Litovitz}$	T [°C]	ζ_{Dukhin}
0	8,0	7	4,50	2	7,60	15	3,09	25	2,43
4	7,0	10	4,03	3	6,50				
5	6,8	15	3,38	4	6,25				
10	6,0	25	2,47	8	4,80				
20	4,7	40	1,84	10	3,85				
30	3,7	50	1,48	15	3,25				
40	2,9	20	2,95						
50	2,4	25	2,25						
60	2,1	30	2,10						
70	1,7	35	2,00						
80	1,4								

.

Appendix B

Air Data

Table B.1: Air Data [40, 41].

Temperature	Shear Viscosity	Temperature	Bulk Viscosity
T [°C]	$\eta \times 10^{-6}$ [Pa·s]	T [K]	$\zeta \times 10^{-5}$ [Pa·s]
0	17,15	253,5	0,970
5	17,40	254,3	0,973
10	17,64	254,8	0,974
15	17,89	276,0	1,038
20	18,13	276,7	1,040
25	18,37	278,0	1,044
30	18,60	297,0	1,099
40	19,07	297,2	1,100
50	19,53	317,7	1,157
60	19,99	318,2	1,159
80	20,88	318,7	1,160
100	21,74	319,2	1,161
125	22,79	337,0	1,210
150	23,80	337,2	1,210
175	24,78	338,2	1,213
200	25,73	338,6	1,214
225	26,66		
250	27,50		
300	29,28		
400	32,50		
412	32,87		
500	35,47		
600	38,25		

Continuation of table B.1			
Temperature	**Shear Viscosity**	**Temperature**	**Bulk Viscosity**
T [ºC]	$\eta \times 10^{-6}$ **[Pa·s]**	**T [K]**	$\zeta \times 10^{-5}$ **[Pa·s]**
700	40,85		
800	43,32		
900	45,66		
1000	47,88		
1100	50,01		